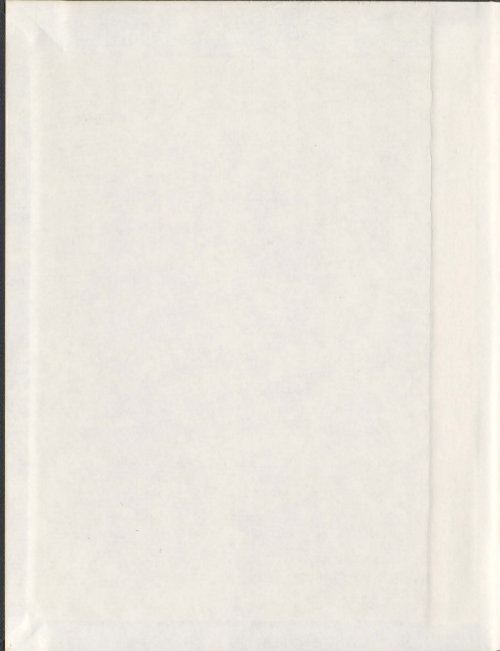


FLUORINATED AND DIMERIC SURFACTANTS IN
MICELLAR ELECTROKINETIC CHROMATOGRAPHY

PRACTICAL APPLICATIONS AND LINEAR
SOLVATION ENERGY RELATIONSHIPS

GEERT VAN BIESEN



001311



**FLUORINATED AND DIMERIC
SURFACTANTS IN MICELLAR
ELECTROKINETIC CHROMATOGRAPHY**

Practical Applications and Linear Solvation Energy Relationships

By © Geert Van Biesen

A thesis submitted to the School of Graduate Studies in partial fulfilment of the requirements for the degree of Doctor of Philosophy

Faculty of Science
Department of Chemistry
Memorial University of Newfoundland

April 2008

Abstract

Micellar electrokinetic chromatography (MEKC) is a form of capillary electrophoresis (CE) that uses a surfactant at a concentration higher than its critical micelle concentration for the separation of analytes. The choice of surfactant can be key to a successful analysis. This is first demonstrated via the application of a relatively volatile surfactant (ammonium perfluorooctanoate - APFOA) for the analysis of *N*-methylcarbamates by MEKC - electrospray ionization - mass spectrometry (MEKC-ESI-MS), circumventing the well-known problem of signal suppression in MS by non-volatile anionic surfactants. An experimental design type of approach is used to optimize the separation voltage, the nebulizer pressure, and the concentrations of APFOA and isopropanol.

The type of surfactant can also have a major impact on the quality of the separation, and surfactants (or more generally, pseudostationary phases - PSPs) are often characterized via linear solvation energy relationships (LSERs). This makes it possible to calculate their system constants, which reflect differences in the properties of the micellar and the aqueous phase with respect to cohesiveness, polarizability, dipolarity, and hydrogen bond accepting and donating ability. This methodology was applied to characterize anionic dimeric surfactants based upon the type (hydrophobic, hydrophilic, fluorinated) and length of the spacer connecting the two amphiphilic moieties. Dimeric surfactants that had spacers with one to six ethylene groups, one to four ethoxy groups, and one to three C_2F_4 groups were synthesized. The system constants of dimeric surfactants with hydrophobic spacers do not depend on the length of the spacer. Compared to sodium dodecylsulfate (SDS), the most commonly used PSP in MEKC, they are slightly more cohesive, interact better with polarizable compounds, and are somewhat better hydrogen

bond acceptors and worse hydrogen bond donors, while there is no difference in dipolarity. Dimeric surfactants with hydrophilic spacers differ from those with hydrophobic spacers in the sense that there is a modest increase in the hydrogen bond accepting ability and a decrease in the hydrogen bond donating ability as the number of ethoxy groups in the spacer increases, while other system constants are the same. Dimeric surfactants with fluorinated spacers have similar selectivity to dimeric surfactants with hydrophobic spacers, although they are somewhat less polarizable, and less able to act as hydrogen bond acceptors. The results are explained in terms of the interphase model of retention, whereby selectivity differences between surfactants are largely shaped by differences in solvation properties of the interphase region and the bulk solution. Although these dimeric surfactants do not show unusual selectivity compared to the wide variety of PSPs already evaluated for MEKC, it is demonstrated that small selectivity differences can be taken advantage of to fine-tune separations.

Acknowledgements

I am indebted to my supervisor, Dr. C.S. Bottaro, for taking me on as a graduate student and letting me pursue my interests, and for helpful advice along the way.

I thank the two supervisory committee members, Drs. P.E. Georghiou and F. Kerton, for reviewing a draft of this thesis, and for their advice.

Drs. Y. Zhao, S. Pansare and P.E. Georghiou are acknowledged for their help with the interpretation of NMR spectra, and for tips on the synthesis of the dimeric surfactants and their intermediates.

I also thank Ms. L. Winsor, Mrs. J. Collins and Dr. C. Schneider for keeping the instruments in C-CART up and running. Mr. P. Hannon, Mrs. L. Thompson and Mr. C. Mitchell are acknowledged for lending me the equipment I needed to do the synthetic work and the physicochemical measurements.

Finally, I thank the Department of Chemistry and the School of Graduate Studies at Memorial University, and the National Sciences and Engineering Research Council (NSERC) of Canada for funding.

Table of Contents

Title	i
Abstract	ii
Acknowledgements	iv
Table of Contents	v
List of Tables	x
List of Figures	xiii
List of Abbreviations	xvi
List of Appendices	xviii
Chapter 1 – Introduction and Overview	1
1.1. A brief history of (capillary) electrophoresis	2
1.2. Advantages and disadvantages of capillary electrophoresis	4
1.3. Capillary electrophoresis theory	7
1.3.1. Introduction	7
1.3.2. Electroosmotic flow and electrophoretic mobility	10
1.3.3. Joule heating	13
1.3.4. Performance criteria and band broadening mechanisms	15
1.3.5. Stacking and sweeping	24
1.4. Micellar electrokinetic chromatography	28
1.4.1. Theory of micellar electrokinetic chromatography	28
1.4.2. Surfactants in micellar electrokinetic chromatography	33
1.4.3. The interphase model of retention	36

1.4.4. Micellar electrokinetic chromatography and mass spectrometry	37
1.5. Linear solvation energy relationships	42
1.5.1. The solvation parameter model	42
1.5.2. Descriptors in LSERs	45
1.5.3. System constants in LSERs	49
1.5.4. Practical LSERs	51
1.6. Thesis objectives	53
1.7. Co-authorship statement	55
1.8. References	56

Chapter 2 - Ammonium Perfluorooctanoate as a Volatile Surfactant for the

Analysis of *N*-Methylcarbamates by Micellar Electrokinetic

Chromatography – Electrospray Ionization Mass Spectrometry	61
Abstract	62
2.1. Introduction	63
2.2. Materials and methods	67
2.2.1. Chemicals	67
2.2.2. Instrumentation	68
2.2.3. Solid Phase Extraction	69
2.3. Results and discussion	70
2.3.1. MEKC-UV experiments	70
2.3.2. MEKC-ESI-MS experiments	74
2.3.2.1 Optimization of the separation	74

2.3.2.2. Optimization of the sensitivity	84
2.3.2.3. Detection limits	88
2.3.3. Analysis of spiked tap water	88
2.4. Concluding remarks	91
2.5. References	92

Chapter 3 - Linear Solvation Energy Relationships of Anionic Dimeric Surfactants in Micellar Electrokinetic Chromatography

1. Effect of the Length of a Hydrophobic Spacer	95
Abstract	96
3.1. Introduction	97
3.2. Experimental	102
3.2.1. CE instrument and conditions	102
3.2.2. Solutes	103
3.2.3. Calculations	105
3.2.4. Synthesis and analysis of dimeric surfactants	106
3.3. Results and discussion	109
3.3.1. Analysis and CMCs of dimeric surfactants	109
3.3.2. Linear solvation energy relationships	112
3.4. Conclusion	121
3.5. Acknowledgements	121
3.6. References	122

**Chapter 4 - Linear Solvation Energy Relationships of Anionic Dimeric
Surfactants in Micellar Electrokinetic Chromatography**

II. Effect of the Length of a Hydrophilic Spacer	125
Abstract	126
4.1. Introduction.....	127
4.2. Experimental	130
4.2.1. CE instrument and conditions	130
4.2.2. Solutes	131
4.2.3. Calculations.....	131
4.2.4. Synthesis and analysis of dimeric surfactants.....	133
4.3. Results and discussion	136
4.3.1. Analysis and CMCs of dimeric surfactants.....	136
4.3.2. Linear solvation energy relationships	137
4.4. Conclusions.....	145
3.5. Acknowledgements.....	146
4.6. References.....	146

**Chapter 5 - Linear Solvation Energy Relationships of Anionic Dimeric
Surfactants in Micellar Electrokinetic Chromatography**

III. Effect of Fluorination	149
Abstract	150
5.1. Introduction.....	151
5.2. Experimental	154

5.2.1. CE instrument and conditions	154
5.2.2. Solutes	155
5.2.3. Calculations	156
5.2.4. Synthesis and analysis of fluorinated dimeric surfactants	156
5.3. Results and discussion	158
5.3.1. Analysis and CMCs of dimeric surfactants.....	158
5.3.2. Linear solvation energy relationships	159
5.4. Conclusions.....	165
5.5. Acknowledgements.....	166
5.6. References.....	166
5.7. Addendum.....	169
5.7.1. Synthesis of a dimeric surfactant with fluorinated chains	169
5.7.2. Application of dimeric surfactant II in MEKC.....	175
5.7.3. References	175
Chapter 6 – Conclusions	178
References.....	187
Appendices	189

List of Tables

Chapter 1

Table 1.1: Common acronyms used by CE practitioners	4
Table 1.2: Rough guide to detection limits in CE.....	6
Table 1.3: Properties of some common surfactants	35
Table 1.4: Common surfactants and their system constants	51

Chapter 2

Table 2.1: Conditions and instrumental settings used to optimize the separation of the N-methylcarbamate mixture	75
Table 2.2: Factors that influence the separation, and the levels at which they were studied in the experimental design.....	78
Table 2.3: Optimized responses in the experimental design.....	80
Table 2.4: Comparison between predicted and experimental values for resolutions, migration time of last analyte, and current.....	83
Table 2.5: Conditions and instrumental settings used to optimize the sensitivity	85
Table 2.6: Detection limits for the 10 N-methylcarbamates.....	89
Table 2.7: Recovery of the 10 N-methylcarbamates from tap water	90

Chapter 3

Table 3.1: Solutes and their descriptors.....	104
Table 3.2: Cross-correlation matrix of the descriptors of the 36 solutes	105

Table 3.3: Summary of NMR and MS data, and CMC of dimeric surfactants.....	110
Table 3.4: System constants and regression statistics for the LSERs of SDS and dimeric surfactants.....	114
Table 3.5: Methylene selectivity, electrophoretic mobility and efficiency of SDS and dimeric surfactants.....	119
 Chapter 4	
Table 4.1: Solutes and their descriptors.....	132
Table 4.2: Cross-correlation matrix of the descriptors of the 41 solutes.....	133
Table 4.3: ¹ H-NMR and ESI-MS data, and CMCs of dimeric surfactants.....	136
Table 4.4: System constants and regression statistics for the LSERs of SDS and dimeric surfactants.....	138
Table 4.5: Methylene selectivity and electrophoretic mobility of SDS and dimeric surfactants.....	145
 Chapter 5	
Table 5.1: ¹ H-NMR and ESI-MS data, and CMCs of dimeric surfactants with fluorinated spacers.....	158
Table 5.2: System constants and regression statistics for the LSERs of SDS, LPFOS, and dimeric surfactants.....	159
Table 5.3: Average system constants of the three dimeric surfactants with fluorinated spacers using a bootstrapping procedure.....	161

Table 5.4: Methylene selectivity and electrophoretic mobility of SDS and PSPs

Ia-c..... 165

Chapter 6

Table 6.1: Principal components analysis of 55 PSPs and 11 dimeric surfactants..... 184

List of Figures

Chapter 1

Fig. 1.1: The electrical double layer at the surface of the inner wall of a fused-silica capillary	10
Fig. 1.2: Temperature profile as a result of current flow through a capillary	14
Fig. 1.3: Peak distortion due to electrophoretic dispersion.....	21
Fig. 1.4: Sweeping in a homogeneous electric field	27
Fig. 1.5: Schematic principle of MEKC	29
Fig. 1.6: Schematic of the structure of a micelle, and its surroundings.....	37
Fig. 1.7: Schematic of the CE-ESI-MS interface, and the tip of the sprayer.....	39
Fig. 1.8: Model of the solvation process.....	43

Chapter 2

Fig. 2.1: Electropherogram of the N-methylcarbamate mixture (20 mg/L in water/ACN 99:1). BGE: 40 mM SDS and 10 mM NH ₄ Ac	71
Fig. 2.2: Electropherogram of the N-methylcarbamate mixture at 20 mg/L. BGE: 50 mM APFOA at pH 9.0. a) sample in water/ACN 99/1, 30 kV applied; b) sample in BGE, 24 kV applied	72
Fig. 2.3: UV spectra of a) 100 mM SDS and b) 100 mM APFOA.....	73
Fig. 2.4: Extracted Ion Electropherogram of the N-methylcarbamate mixture. BGE: 50 mM APFOA at pH 9.0. 24 kV applied	76

Fig. 2.5: Extracted Ion Electropherogram of the N-methylcarbamate mixture. BGE: 50 mM APFOA at pH 9.0/IPA 98/2. 30 kV applied	77
Fig. 2.6: Separation dashboard showing the influence of each of the factors.....	81
Fig. 2.7: Extracted ion electropherogram of the N-methylcarbamate mixture	84
Fig. 2.8: Comparison of the S/N of the 10 N-methylcarbamates under different conditions.....	87
Fig. 2.9: SIM electropherogram of 25 mL tap water spiked with 10 N- methylcarbamates at the 10 µg/L level after SPE.....	90

Chapter 3

Fig. 3.1: General schematic structures of dimeric and trimeric surfactants.....	98
Fig. 3.2: Synthetic pathway to the dimeric surfactants used in this project.....	106
Fig. 3.3: Conductance vs. concentration plots for determination of the CMC	111
Fig. 3.4: Selectivity plots of IIIb vs. SDS and IIIe vs IIIa	116
Fig. 3.5: Separation of a homologous series of alkyl benzoates with (a) SDS and (b) dimeric surfactant IIIa	120

Chapter 4

Fig. 4.1: Synthetic pathway to the dimeric surfactants for this project	134
Fig. 4.2: Selectivity plots of IIIe vs. SDS and IIIe vs. IIIa	142
Fig. 4.3: Electropherograms of a mixture of phenol, benzyl alcohol, toluene, methyl benzoate, geraniol and 1-nitronaphthalene with SDS, IIIa , IIIe and IIIe	144

Chapter 5

Fig. 5.1: Structures of dimeric surfactants with fluorinated spacers and fluorinated chains	154
Fig. 5.2: Plots of experimental vs. predicted log <i>k</i> values for (a) Ia , (b) Ib and (c) Ic	160
Fig. 5.3: Selectivity plot of dimeric surfactant Ia vs. SDS	164
Fig. 5.4: Reactions for the synthesis of dimeric surfactant II	172
Fig. 5.5: Neg. ESI-MS spectra of reaction mixture after (a) 1 hr and (b) 5 hrs.	173
Fig. 5.6: ¹ H-NMR spectrum of dimeric surfactant II	174
Fig. 5.7: Electropherogram with 2 mM II in 20 mM Na ₂ HPO ₄ at pH 7 as BGE	175
Fig. 5.8: UV spectra of (a) 20 mM G12 and (b) 20 mM G49.....	176
Fig. 5.9: Electropherogram with 20 mM G49 in 20 mM Na ₂ HPO ₄ at pH 7 as BGE	177

Chapter 6

Fig. 6.1: Scores plot of PC2 vs. PC1.....	185
Fig. 6.2: PC1 and PC2 loading plot	187

List of Abbreviations

¹H-NMR: proton nuclear magnetic resonance

ACN: acetonitrile

APFOA: ammonium perfluorooctanesulfonate

BGE: background electrolyte

CE: capillary electrophoresis

CMC: critical micelle concentration

CZE: capillary zone electrophoresis

DAD: diode array detector (or detection)

EIE: extracted ion electropherogram

EOF: electroosmotic flow

ESI-MS: electrospray ionization – mass spectrometry (or spectrum)

FASS: field amplified sample stacking

GC: gas chromatography

GE: gel electrophoresis

HBA: hydrogen bond acceptor(s)

HBD: hydrogen bond donor(s)

HPLC: high performance liquid chromatography

ID: internal diameter

IEF: isoelectric focussing

IPA: isopropanol

LSERS: linear solvation energy relationships

LVSS: large volume sample stacking

MEKC: micellar electrokinetic chromatography

MeOH: methanol

MS: mass spectrometry (mass spectrometer, mass spectrum, or mass spectra)

MW: molecular weight

NHB: non-hydrogen bonding solute(s)

OD: outer diameter

PAGE: polyacrylamide gel electrophoresis

PCA: principal components analysis

PSP: pseudostationary phase

RSD: relative standard deviation

S/N: signal to noise ratio

SDS: sodium dodecylsulfate

SIM: selected ion monitoring

SPE: solid phase extraction

THF: tetrahydrofuran

UV-vis: ultraviolet-visible

List of Appendices

Appendix 1:

ESI-MS and structures of <i>N</i> -methylcarbamates.....	190
--	-----

Appendix 2:

¹ H-NMR spectra of dimeric surfactants and intermediate products of Chapter 3	194
--	-----

Appendix 3:

ESI-MS of dimeric surfactants of Chapter 3.....	220
---	-----

Appendix 4:

¹ H-NMR spectra of dimeric surfactants and intermediate products of Chapter 4	225
--	-----

Appendix 5:

ESI-MS of dimeric surfactants of Chapter 4.....	244
---	-----

Appendix 6:

CMC determinations of dimeric surfactants of Chapter 4	248
--	-----

Appendix 7:

Electropherograms of LSER mixtures	252
--	-----

Appendix 8:

¹ H-NMR spectra of dimeric surfactants and intermediate products of Chapter 5	259
--	-----

Appendix 9:

ESI-MS of dimeric surfactants of Chapter 5.....	277
---	-----

Appendix 10:

CMC determinations of dimeric surfactants of Chapter 5	281
--	-----

Appendix 11:

System constants of PSPs.....	284
-------------------------------	-----

Chapter 1

Introduction and Overview

1.1. A brief history of (capillary) electrophoresis

The theoretical foundations of electrophoresis go back as far as the 19th century, with contributions from prominent scientists such as M. Faraday (electrolysis), J.W. Hittorf (ion transport numbers), and F. Kohlrausch (independent migration of ions) [1-3]. Tiselius described the very first application of electrophoresis in free solution as a separation technique in his PhD dissertation on the separation of blood plasma proteins (1930) [1-4]. He already realized that Joule heating (Section 1.3.3) caused severe band broadening, and in later experiments he cooled the electrophoresis cell with cold water. In subsequent years, the problem of band broadening was partly circumvented by using paper or high viscosity media such as cellulose acetate, agarose, and polyacrylamide. This so-called 'slab gel electrophoresis' (GE, or PAGE if the gel is polyacrylamide), and modified forms such as sodium dodecylsulfate – PAGE (SDS-PAGE) and isoelectric focusing (IEF) quickly became instrumental in the analysis of proteins and nucleic acids, and greatly advanced the understanding of biochemical processes and the composition of organisms. These techniques are still widely used to date, and continue to be developed [5], but suffer from drawbacks such as the lack of complete automation, lengthy separations, and elaborate staining/destaining procedures. Note that the analysis of small ions (MW <1000) by these techniques is impractical because of diffusion during fixing [1].

At the end of the 1960s, Hjertén recognized that Joule heating was greatly reduced in narrow diameter glass tubes (3 mm ID). Rotating the capillaries also smoothed out convective gradients, thereby further decreasing band broadening [1-3,6]. When the technology to make even narrower capillaries (<500 µm ID) became widely available in

the 1970s, their superior heat dissipation (Section 1.3.3) was such that higher field strengths could be applied without the need for rotation. R. Virtanen [7] succeeded in separating Li^+ , Na^+ and K^+ via what is now called capillary electrophoresis (CE), and noted the importance of the influence of the electroosmotic flow (EOF) on the electrophoretic behaviour of the analytes. However, it was not until Jorgenson and Lukacs published their work on the separation of fluorescent derivatives of amino acids, dipeptides and amines [8] that the tremendous potential of CE was recognized. They used 75 μm ID glass capillaries and took advantage of the electroosmotic flow (EOF) to analyze both positive and negative ions in a single run, and obtained efficiencies in excess of 400,000 plates. They also made significant contributions to the development of the theory, relating efficiency (N) and resolution (R_s) in CE to instrumental parameters. This proved to be the start of a very successful era in CE, with adaptations of GE and IEF to the capillary format, and the development of micellar electrokinetic chromatography (MEKC) by S. Terabe in 1984 [9] (Section 1.4), which greatly expanded the application of CE to neutral compounds as well as ionic species. In 1988, the first commercial CE instrument became available (most researchers built their own CE instruments up to then, since the basic set-up is relatively simple). Numerous other developments have taken place over the course of the subsequent years: coupling to MS, NMR, and inductively coupled plasma – MS, advances in column technology, development of stacking protocols, use of cyclodextrins, chip based systems, etc., and the field of CE has matured into the recognized and established technique it is today. There are a bewildering number of acronyms for different modes of CE, and the ones that are most often used are given in

Table 1.1. The basic theory behind CZE and MEKC is described to some extent in Sections 1.3 and 1.4, but discussion of the rest of the techniques is beyond the scope of this work.

Table 1.1: Common acronyms used by CE practitioners

CE	Capillary Electrophoresis Used as a general description of all capillary electromigration techniques, or specifically for CZE
CZE	Capillary Zone Electrophoresis (Section 1.3)
MEKC	Micellar Electrokinetic Chromatography (Section 1.4)
MEEKC	Microemulsion Electrokinetic Chromatography Similar in many respects to MEKC, but a microemulsion instead of micelles is used
CEC	Capillary Electrochromatography Electroosmosis is used to move the BGE through a packed or wall-coated capillary
CGE	Capillary Gel Electrophoresis Ions are separated based upon size/shape in a gel-filled capillary; used for macromolecules
CIEF	Capillary Isoelectric Focussing Separation of amphoteric analytes in order of their isoelectric points
CITP	Capillary Isotachopheresis Separation of ions in order of their electrophoretic mobility in a discontinuous buffer system

1.2. Advantages and disadvantages of capillary electrophoresis

CE is an enormously versatile technique. It can be applied to the separation of charged and uncharged molecules; from small metal cations and inorganic anions, to organic molecules, proteins, DNA and even whole cells [6]. These can be analyzed using the same capillary, only changing the composition of the background electrolyte (BGE). This is different from HPLC¹, where several (expensive) columns may be needed for different types of analytes. This is particularly the case for enantiomeric separations, where CE is quickly becoming the method of choice [10]. The resolving power of CE is also superior to that of HPLC, because of the plug-like flow profile and the absence

¹ CE is most often compared to HPLC, since this is also a liquid based technique.

(ideally) of dispersion effects due to flow non-uniformity (Section 1.3.4) [5]. Multiplexing, i.e. using several capillaries simultaneously within a single instrument, is another advantage of CE, and allows for a tremendous increase in sample output. Typically, 96 capillaries are used, and this set up was a significant contributor to the timely conclusion of the Human Genome Project [1,10]. From an environmental point of view, CE is also superior to HPLC since it requires almost no organic solvents. Most CE separations take place in an aqueous medium, sometimes with a small percentage of an organic solvent as a modifier. In addition, the absolute amount of liquid required for a typical CE analysis (a few mLs) is much smaller than for HPLC (tens or hundreds of mLs, rinsing of the column included¹).

There is no such thing as 'the ideal separation technique', and CE does have a number of shortcomings. One of the main disadvantages of CE compared to HPLC is its relatively high concentration detection limit (although the mass detection limit is low), especially when using a UV-vis detector. This is first of all because the amount of sample injected is typically in the nL range, while it is in the μL range for HPLC. Secondly, since detection is on-column, the path length is short and equal to the diameter of the column. This is typically between 25 – 100 μm , while in HPLC UV detectors this is often 1 cm [2,5]. Stacking and sweeping (Section 1.3.5), and the use of capillaries with extended light path (~ three fold increase in sensitivity) or with a Z-shaped section at the detector (~ten fold increase in sensitivity) have come some way in alleviating this concern, but liquid core waveguides seem to be the most promising new development [11]. Of course,

¹ All comparisons between HPLC and CE in this section are for a standard HPLC configuration with a 250 x 4.6 mm column; microbore and nanobore LC, which are not widespread technologies at this time, are not considered here.

other types of detectors are used as well, and often provide better sensitivity than UV-vis (Table 1.2).

Table 1.2: Rough guide to detection limits for CE (adapted from [5])

Detection Mode	Typical Detection Limits	
	Mass (mole)	Concentration (M)
Absorption (UV-vis)	$10^{13} - 10^{16}$	$10^3 - 10^8$
Indirect		$10^5 - 10^7$
Fluorescence	$10^{15} - 10^{17}$	$10^5 - 10^{10}$
Laser Induced	$10^{18} - 10^{21}$	$10^{10} - 10^{16}$
Indirect	$10^{15} - 10^{17}$	$10^5 - 10^7$
Chemiluminescence	$10^{13} - 10^{17}$	$10^9 - 10^{10}$
Conductivity	$10^{15} - 10^{16}$	$10^4 - 10^8$
Amperometry	$10^{18} - 10^{20}$	$10^5 - 10^8$
Potentiometry		$10^7 - 10^8$
MS	$10^{16} - 10^{17}$	$10^8 - 10^{10}$

The small amounts of sample (nLs) introduced into the capillary, and the dimensions of the capillary itself are such that interfacial forces play a large part in the relatively poor injection precision in CE (~2% RSD [12]). Siphoning and droplet formation, movement of sample on the outside of the capillary, and evaporation during vial change, can all affect injection volume [5]. Ubiquitous injection occurs if the capillary is in contact with the sample for more than a few seconds, simply by diffusion of analytes into the capillary, and is more important for low molecular weight analytes, because of their higher diffusion coefficients [2]. The use of internal standards sometimes, but not always, offers improvement [12].

Shifting migration times due to changes in the EOF can also be a matter of concern, and depend on the reproducibility of the surface chemistry of fused silica, and still poorly understood properties of sample matrix and BGE [5]. Proper capillary

conditioning procedures between sample injections can be elaborate, and decrease sample throughput. CE practitioners, therefore, often prefer using electrophoretic mobility (Section 1.3.2), which is independent of the EOF, to migration time [13].

It was thought by some that CE would replace high performance liquid chromatography (HPLC) over time, but this has not happened so far [5,10]. HPLC has proven to be a very robust and reliable technique that most analytical labs are very familiar with. Therefore, in the situation where CE is an alternative to HPLC instead of an improvement, the incentive for investment in a CE instrument and training of personnel is not really there. The commercial success of CE, judged by the number of instruments being sold, is therefore modest compared to that of HPLC and GC. Still, many industries (especially biotechnical and pharmaceutical) and government agencies (e.g. environmental and forensic) have adopted CE methods, and CE continues to progress to the forefront of analytical chemistry [10].

1.3. Capillary electrophoresis theory

CE theory has been addressed in many excellent textbooks, e.g. [2,3,5,6,14,15]. In the context of the introduction to a thesis, only the basic principles can be presented here, and this section is not meant to be a comprehensive overview.

1.3.1. Introduction

Separation in CE is based upon the differential migration of analytes in an electric field. In the ideal situation of a homogenous electric field applied to an electrolyte

solution at infinite dilution (i.e. no ionic interactions, and complete dissociation), an ion is accelerated by the electrostatic force F according to Eq.1:

$$F = qE \quad (\text{Eq. 1})$$

q : charge of the ion (product of the number of elementary charges and the charge on an electron) (C)

E : the electric field strength ($\text{V}\cdot\text{m}^{-1}$).

This force is opposed by the viscous force in solution, which for a spherical particle is given by Stokes' law:

$$F = 6\pi\eta r v_{ep} \quad (\text{Eq. 1.2})$$

η : viscosity of the solution (Pa·s)

r : hydrodynamic radius of the ion (m)

v_{ep} : electrophoretic velocity of the ion ($\text{m}\cdot\text{s}^{-1}$).

Note that the hydrodynamic radius of the ion is the radius of the solvated (hydrated) ion. This radius is larger than the crystallographic radius, which can be found tabulated in many textbooks [16,17].

A steady state condition is obtained very soon after the application of the electric field whereby the opposing forces cancel one another:

$$qE = 6\pi\eta r v_{ep}. \quad (\text{Eq. 1.3})$$

The constant migration velocity of the ion is then calculated from:

$$v_{ep} = qE / 6\pi\eta r. \quad (\text{Eq. 1.4})$$

The electrophoretic mobility, μ_{ep} ($m^2 \cdot V^{-1} \cdot s^{-1}$), is the velocity of the ion independent of the electric field strength:

$$\mu_{ep} = q / 6\pi\eta r = v_{ep} / E. \quad (\text{Eq. 1.5})$$

For a given ion, μ_{ep} only depends on the viscosity of the solution; and the effect of temperature on μ_{ep} finds its origin almost entirely in the change of viscosity with temperature. As a rule of thumb, the mobility increases approximately 2% per one degree Kelvin [3].

Equations 1.1 - 1.5 are applicable to spherical particles in infinitely dilute solutions only. For non-spherical species, a 'shape factor' can be taken into account (Table 22.3 in [17]). Furthermore, CE is often performed with solutions of moderate to high ionic strength, and multiple ionic species are present. This strongly affects the mobility of analyte ions, since they are surrounded by a diffuse cloud of oppositely charged counter-ions (Debye-Hückel theory [17]). With an electric field applied, this cloud of counter-ions will migrate in the opposite direction of the sample ion, exerting an additional viscous force opposing the motion of the analyte ion [3,5,17] (Stokes' law assumes movement in a stationary environment [3]). In addition to this so-called electrophoretic or retardation effect, there is also a relaxation effect. Since the cloud of oppositely charged counter-ions cannot instantly adjust to the moving ion, it is incompletely formed in front of the moving ion, and incompletely decayed behind the ion. The net effect is the displacement of the centre of charge of the ion cloud a short distance behind the moving ion. Since they are of opposite charge, their Coulomb interaction slows down the moving analyte ion [3,5,17]. Friedl et. al [18] derived an

empirical correction for this effect of ionic strength on ion mobility for electrolyte concentrations of 1 – 100 mM, and $z = 1 - 6$:

$$\mu_{ep} = \mu_0 \exp[-0.77 (zI)^{1/2}] \quad (\text{Eq. 1.6})$$

I: ionic strength: $1/2 \cdot \sum c_i z_i^2$ (no units).

1.3.2. Electroosmotic flow and electrophoretic mobility

The weakly acidic silanol groups on the inside wall of the capillary are exposed to the BGE, and under normal conditions ($\text{pH} > 3$), the capillary wall acquires a negative charge. Cations in solution adsorb onto the silica wall by electrostatic attraction to balance this surface charge (Fig. 1.1), and form an immobile layer (Stern layer). Not all of the surface charge can be neutralized by cations in the Stern layer, and the remaining charge is neutralized by more mobile, solvated cations in the diffuse part of the double layer.

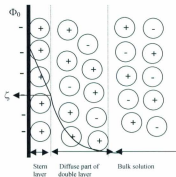


Fig. 1.1: The electrical double layer at the surface of the inner wall of a fused-silica capillary and variation of the potential with distance from the wall (adapted from [17]). See text for explanation.

layer. The charge separation between the capillary wall and the solution causes an electric potential Φ at the interface. Within the Stern layer, Φ decreases linearly with distance from the capillary wall, reaches a value denoted as the ζ potential (typically < 100 mV [5]) at the start of the diffuse part of the double layer, and then drops exponentially. The diffuse part of the double layer is typically ~ 10 nm for solutions with an ionic strength of 1 mM, to < 1 nm for an ionic strength of 1 M [19]. The application of an electric field causes cations to move towards the cathode (and anions towards the anode). Since there is a predominance of cations in the diffuse part of the double layer, and because of their strong association with water molecules, there is a net flow of liquid towards the cathode. The flow profile is virtually flat across the capillary diameter (except very close to the capillary wall). This is in contrast to the pressure induced parabolic flow profile encountered in HPLC, and explains in large part the much higher resolving power of CE. This bulk flow of liquid is called the electroosmotic flow (EOF), and its velocity v_{eo} is given by [5]:

$$v_{eo} = \frac{\epsilon\zeta E}{\eta} = \mu_{eo}E \quad (\text{Eq. 1.7})$$

ϵ : permittivity of the solution ($F \cdot m^{-1}$) (also reported as $\epsilon_r \epsilon_0$, where ϵ_r is the relative permittivity, and ϵ_0 is the permittivity of vacuum)

ζ : potential at the start of the diffuse part of the double layer (V)

η : viscosity of the solution (Pa-s).

The magnitude of v_{eo} depends on the surface charge density at the capillary wall, the ionic strength, dielectric constant and viscosity¹ of the solution, and the magnitude of the

¹ Temperature indirectly affects v_{eo} by changes in viscosity of the solution.

applied electric field [5]. A plot of v_{eo} vs. pH has a sigmoidal shape and shows that v_{eo} is minimal at pH <3, increases with increasing pH and levels off around pH 8. Under normal CE operation (i.e. basic BGE, injection at the anode), the presence of the EOF almost always allows for anions and cations to be analyzed in a single run, since v_{eo} is higher than the v_{ep} of anions (which migrate in opposite direction to v_{eo} – cations migrate in the same direction as v_{eo}).

The electrophoretic mobility as defined in equation 1.5 can be determined experimentally from an electropherogram according to:

$$\mu_{app} = v_{app} / E = (L_d/t_m) / (V/L) \quad (\text{Eq. 1.8})$$

μ_{app} : apparent or observed mobility ($\text{m}^2 \cdot \text{V} \cdot \text{s}^{-1}$)

v_{app} : apparent or observed velocity ($\text{m} \cdot \text{s}^{-1}$)

t_m : migration time (time for ion to reach the detector) (s)

L_d : length of capillary to the detector (m)

L : total length of the capillary (m)

V : applied voltage (V).

Apparent mobility/velocity is used here since it is the sum of EOF and electrophoretic mobility/velocity¹:

$$v_{app} = v_{eo} + v_{ep} \quad (\text{Eq. 1.9})$$

$$\mu_{app} = \mu_{eo} + \mu_{ep} \quad (\text{Eq. 1.10})$$

To cancel out the effect of the EOF, we derive equation 1.11 from equations 1.8 and 1.10:

$$\mu_{eff} = (L_d L / V) [(1/t_m) - (1/t_{eo})] \quad (\text{Eq. 1.11})$$

¹ Note that these are vector quantities and are summed with respect to their signs.

t_{eo} : migration time of EOF marker.

A neutral solute, such as acetone or benzyl alcohol [3], that does not interact with the capillary wall can be used as EOF marker¹. The effective electrophoretic mobility is characteristic of the ion (i.e. is independent of the system properties), and is a much more reliable parameter for solute identification than migration time [13].

1.3.3. Joule heating

It was already realized from the earliest electrophoresis experiments that Joule heating was an important contributor to zone broadening (Section 1.1). Joule heating is the phenomenon that heat is generated when a current flows through a conductor, and in CE this is caused by the loss of kinetic energy by colliding ions. The power P ($J\cdot s^{-1}$ or W) generated can be calculated as [3]:

$$P = Vi = Ri^2 \quad (\text{Eq. 1.12})$$

V : potential (V)

i : current (A)

R : resistance (Ω).

If the capillary is cooled by forced air convection (as in most instruments), a rule of thumb is that a power of 0.1 W increases the temperature in the capillary by 0.6 K [3]. It was shown previously (Sections 1.3.1 and 1.3.2) that temperature has an effect on the mobility of both ions and the EOF. However, the main problem with heat generation in

¹ For MEKC (Section 1.4), an additional requirement is that the EOF marker does not partition into the micelles. Samples are often dissolved in methanol or another organic solvent, and the small disturbance in the baseline (caused by a change in refractive index) when the organic solvent zone passes the detector can be used as EOF marker.

capillaries is that while the heat is generated uniformly across the capillary, heat dissipation only occurs through the capillary walls. A parabolic temperature gradient develops across the capillary (Fig. 1.2), resulting in a similar migration velocity profile due to a viscosity gradient. In MEKC (Section 1.4), a temperature gradient also causes changes in retention factors.

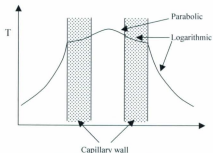


Fig. 1.2: Temperature profile as a result of current flow through a capillary (not to scale - adapted from [20]).

Joule heating depends on both the applied voltage, and the current in the capillary (Eq. 1.12). For reasons explained in the next section, it is advantageous to apply as high a voltage as possible. Using small diameter capillaries minimizes the current ($i \sim$ cross sectional area), while at the same time the increase in surface-to-volume ratio allows for a better heat dissipation. It can be shown that the temperature gradient is proportional to ID^2 [2,20], and it was not until the technology for making small diameter capillaries ($<100 \mu\text{m}$) became available that the full potential of CE became clear. The fused-silica capillary itself has a high resistance and does not contribute significantly to the current. The ionic strength of the BGE, however, is another important factor in Joule heating

because higher ionic strengths draw higher currents. The need for a BGE arises first of all from the fact that a solution is needed that can conduct electricity. A buffer is used as BGE to prevent severe pH changes due to electrolysis of water at the cathode and anode (at the cathode OH^- is produced, while at the anode, H^+ is produced). A fairly large excess of BGE ions is needed relative to analyte ions in order not to distort the electric field too much, since this leads to asymmetric peak shapes (Section 1.3.4) [2]. If the ionic strength of the BGE is not too high, the effect of Joule heating in capillaries with an ID $< 100 \mu\text{m}$ can be virtually eliminated [2]. A simple experiment can determine the voltage that can be applied to a capillary of a given length, filled with a BGE of a specific ionic strength, without the negative effects of excessive Joule heating. A plot of current vs. voltage (an Ohm plot) [6] is linear ($i = V/R$), until the increase in temperature of the BGE due to Joule heating noticeably decreases the resistance of the BGE, from which point on the plot deviates from linearity. The maximum voltage that can be applied corresponds to the voltage just before where the deviation from linearity begins.

1.3.4. Performance criteria and band broadening mechanisms

CE has often been critically acclaimed because of its high efficiency. This is partly due to the flat flow profile of the EOF (Section 1.3.2), and partly due to the absence of peak broadening mechanisms that are of concern in chromatography. The Van Deemter equation, which relates plate height to column characteristics and flow rate [5,19], is composed of three terms:

$$H = A + B/u + (C_s + C_m)u \quad (\text{Eq. 1.13})$$

H: plate height (m)

A: contribution from Eddy diffusion (multiple paths) (m)

B: contribution from longitudinal diffusion ($m \cdot L \cdot s^{-1}$)

C_s, C_m : contributions from resistance to mass transfer in stationary and mobile phases, resp. ($m \cdot s \cdot L^{-1}$)

u: flow rate ($L \cdot s^{-1}$).

For CZE, the A- and C-terms are zero, because there is no packing and no stationary phase, respectively. In the ideal case, only longitudinal diffusion causes peak broadening.

Zone broadening by diffusion can be described using the Einstein equation [3]:

$$\sigma^2 = 2Dt_m \quad (\text{Eq. 1.14})$$

σ^2 : spatial variance (m^2) of the Gaussian peak^{1,2}

D: diffusion coefficient ($m^2 \cdot s^{-1}$).

Longitudinal diffusion will be more severe for solutes with high diffusion coefficients (low MWs) and when migration times are longer. An increase in temperature also increases σ^2 because of the temperature dependence of D.

Combining equations 1.8 and 1.14, we find:

$$\sigma^2 = 2D(L_d/\mu_{app}) / (V/L). \quad (\text{Eq. 1.15})$$

Using expressions for plate height H (Eq. 1.16) and plate number N (Eq. 1.17) [3,19], we can derive an expression for the theoretical efficiency in CZE (Eq. 1.18):

$$H = \sigma^2 / L_d \quad (\text{Eq. 1.16})$$

¹ In an electropherogram, the x-axis is time and consequently the variance of a peak is temporal variance. Spatial variance can be calculated by multiplying temporal variance by the square of the peak velocity [3].

² In these and all other calculations, we assume Gaussian peaks. Corrections for fronting or tailing peaks taking into account asymmetry factors can be found in [2].

$$N = L_d / H \quad (\text{Eq. 1.17})$$

$$N = (L_d / L)(\mu_{app} V / 2D) = (L_d / 2D)E\mu_{app} \quad (\text{Eq. 1.18})$$

The efficiency will be higher if a strong electric field (E) is applied, and if the mobility of the ions (μ_{app}) is high. High values for both these variables minimize the time an ion spends in the capillary, and therefore minimize longitudinal diffusion. Macromolecules, with their small diffusion coefficients, are especially suited for CE separations because of their highly efficient separations. From the second part of equation 1.18, one might be tempted to draw the conclusion that increasing L_d also increases N (as in chromatography). This is true only to the extent that E can be held constant, and herein lies the catch. In practice, the only way to increase L_d is by increasing the total length of the capillary (L) because for commercial instruments the distance from the capillary outlet to the detector is fixed (8.5 cm for the Agilent^{3D} system). Increasing L means that the applied voltage V has to be increased as well in order to keep E constant, and the limit of 30 kV¹ on most instruments is reached very quickly.

Equation 1.17 is found in some textbooks [5,14,19], while in others [2,3,6] a slightly different expression is found:

$$N = \mu_{app} V / 2D. \quad (\text{Eq. 1.19})$$

In the derivation of this formula, the difference between L and L_d is neglected, as in the original publication by Jorgenson and Lukacs [8], but it leads to similar considerations as above. This was also pointed out in [22]. Equations 1.18 and 1.19 predict plate numbers

¹ At higher voltages, electrical breakdown of the fused-silica and arcing will occur. Ultra-high voltages (120 kV) can be applied if the capillary is protected via electrical shielding [21].

>500,000 for low-mass ions, and $> 10^6$ for macromolecules [5], much higher than typical HPLC plate numbers, which are in the ten thousands.

Optimizing a separation implies separating the different species present in a sample, and while a high efficiency is desirable, it is not sufficient. The resolution R_s (dimensionless) expresses how well two peaks are separated from one another [5]:

$$R_s = \Delta t / 2(\sigma_1 + \sigma_2) \quad (\text{Eq. 1.20})$$

Δt : difference in migration time between both peaks (s)

σ_1, σ_2 : standard deviations of peak 1 and 2, respectively (s).

For symmetrical peaks of equal height, an R_s of ~ 1.5 is required for baseline separation [5]. Equation 1.20 applies to both chromatography and CE, and can be related to instrumental CE parameters [3] via:

$$R_s = 0.177 \cdot (\mu_2 - \mu_1) \cdot [(L_d/L) \cdot (V/D(\mu_{av} + \mu_{co}))]^{1/2} \quad (\text{Eq. 1.21})$$

μ_1, μ_2 : effective mobilities of species 1 and 2, respectively ($\text{m}^2 \cdot \text{V}^{-1} \cdot \text{s}^{-1}$)

μ_{av} : average effective mobility ($\text{m}^2 \cdot \text{V}^{-1} \cdot \text{s}^{-1}$).

Equation 1.21 again takes into account the factor L_d/L , as in equation 1.15, which is omitted in many textbooks [2,3,6]. The resolution is directly proportional to the difference in electrophoretic mobilities between the two species, and inversely proportional to the square root of their average apparent mobility ($\mu_{av} + \mu_{co}$). While a high apparent mobility is required for good efficiency (Eq. 1.18 or 1.19), it is unfavourable for obtaining good resolution simply because there is not enough time for the two species to separate from one another [2]. The resolution becomes maximal when $\mu_{av} \approx -\mu_{co}$, but this is at the expense of the analysis time (which is infinite if $\mu_{av} = -\mu_{co}$), and these conditions

are only necessary for the most extreme separations (e.g. separations of isotopes [23]). The application of a high voltage is advantageous since the resolution increases with the square root of the voltage; but this is only up to the point where Joule heating becomes a factor in band broadening.

This section so far has been concerned with efficiency and resolution from a theoretical point of view, under the assumption that longitudinal diffusion is the only factor contributing to peak broadening. The theoretical efficiency (Eq. 1.18) and resolution (Eq. 1.21) are unobtainable, however, since other peak broadening mechanisms have to be taken into account. Although these can never be totally eliminated, it is possible to minimize their effects by selecting appropriate working conditions. Kuhn and Hoffstetter-Kuhn [3] present a comprehensive overview, which is briefly summarized below. The total peak variance σ_t^2 is given by:

$$\sigma_t^2 = \sigma_D^2 + \sigma_A^2 + \sigma_j^2 + \sigma_E^2 + \sigma_i^2 + \sigma_w^2. \quad (\text{Eq. 1.22})$$

The variances due to longitudinal diffusion (σ_D^2) and Joule heating (σ_j^2) were addressed previously (Eq. 1.14 and Section 1.3.3, respectively).

The variance due to adsorption (σ_A^2) finds its origin in the interaction of the fused-silica wall with analytes, if the kinetics of this adsorption process are slow. For linear adsorption isotherms, where the distribution coefficient between solution and capillary wall is independent of the concentration of the analyte, peak shapes stay symmetrical and only peak broadening is observed. However, convex adsorption isotherms are more common in adsorption processes, and here peak tailing is observed because adsorbed analyte molecules will lag behind analyte molecules in solution. Ion-pairing (cations with

the negatively charged capillary wall), polar and hydrophobic interactions can be especially severe for large molecules with multiple binding sites (e.g. proteins, DNA fragments) [6]. Adjusting the pH of the BGE such that analytes carry a negative charge, or that the capillary wall carries no charge ($\text{pH} < 3$) eliminates coulombic interaction, but these conditions may not be optimal for separation. Alternatively, capillary wall coating can be considered [5]. Dynamic surface treatment relies on the physical adsorption of additives (alkylamines, diamines, ionic polymers etc.) on the capillary wall, and requires occasional regeneration or addition of the additive to the BGE. Covalent bonding of the silanol groups with for instance organotrialkoxysilanes or ω -iodoalkylammonium salts forms a chemically bonded layer. This type of capillaries generally has a longer lifetime and requires less maintenance, but they are more difficult to prepare and column reproducibility may not be optimal. Besides for preventing analyte-capillary interactions, capillary wall coating is also used for EOF control.

The variance due to electrophoretic dispersion (σ_E^2) is unique to electrophoretic separation techniques and causes triangular peak shapes. It finds its origin in the distortion of the electric field in the sample zone by analyte ions, whenever the analyte has a different mobility than the co-ion (i.e. the BGE ion with the same charge as the analyte) and the concentration of the analyte is not negligible compared to the BGE concentration [3,5,6]. Since sample ions partially replace BGE ions, the BGE concentration in the sample zone is always less than outside the sample zone. Therefore, it is mainly the mobility of the sample ions that determines the conductivity of the sample zone. For instance, if the mobility of the analyte is lower than the co-ion mobility, then

the conductivity in the sample zone is lower than in the BGE. The electric field strength across the sample zone will then be higher than in the BGE. Analyte ions at the front edge of the sample zone that enter the BGE (by diffusion or convection) are subjected to a lower electric field strength, are slowed down, and the sample zone quickly catches up with them; the frontal boundary will therefore be sharpened (Fig. 1.3). Sample ions at the rear boundary that enter the BGE are also slowed down, are not able to catch up with the sample zone, and are permanently slowed down relative to the sample zone. This results in a diffuse rear boundary ('tailing'). If the conductivity in the sample zone is higher than in the BGE, the opposite peak shape (diffuse rear, sharp front - 'fronting') is observed.

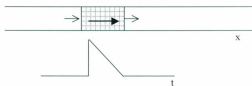


Fig. 1.3: Peak distortion due to electrophoretic dispersion when the conductivity of the sample zone is lower than that of the BGE. The peak is tailing since the sharpened front of the sample zone reaches the detector first, followed by the more diffuse rear. Arrow in bold depicts velocity of the sample zone; smaller arrows depict the velocity of sample ions just outside the sample zone.

The effect is more severe the higher the sample concentration relative to the BGE concentration, and a rule of thumb for preventing this phenomenon is that the sample concentration should be <1% of the BGE concentration. In this case, the field strength can be considered constant over the entire length of the capillary. Decreasing the sample concentration is often not desirable because it increases the detection limit, but one can also increase the BGE concentration. This, however, can lead to excessive Joule heating.

Since electrodispersion also depends on the difference between the mobilities of BGE co-ion and analyte, matching the mobility of analyte and BGE co-ion is also recommended. In general, sample analytes will have a range of mobilities, so for some of them, peak broadening will be unavoidable. If sufficient resolution is built into the method, this may not compromise quantitation [6].

An important contributor to peak variance is the length of the injection plug (σ_i^2) [2,3,5,6]. The technique for introducing the sample into the capillary is most often hydrodynamic injection¹. With the inlet of the capillary in the sample, a carefully controlled pressure is applied to the sample vial for a certain amount of time. The amount of sample injected can be calculated using the Poiseuille equation [3]:

$$V = \Delta P(ID^4)\pi t / 8\eta L \quad (\text{Eq. 1.23})$$

V: volume of sample injected (m^3)

ΔP : applied pressure (Pa)

ID: internal diameter of capillary (m)

t: time that pressure is applied (s)

η : viscosity of the sample (Pa·s)

L: total length of the capillary (m).

Typical injection volumes are in the nL range, with lengths, calculated by dividing by the cross-sectional area of the capillary ($ID^2\pi$), in the order of a few mm.

The contribution of the injection to the peak variance is [3]:

$$\sigma_i^2 = l^2 / 12 \quad (\text{Eq. 1.24})$$

¹ Electrokinetic injection introduces the sample via the application of an electric field, but is not considered here.

l : length of the injection plug (m).

Typical injection lengths should be less than 1% of the capillary length in order to maintain a high efficiency, but stacking and sweeping procedures (Section 1.3.5) allow for much longer injection plugs.

The final contribution to peak variance is given by σ_w^2 , the variance due to the detection system. For on-column detection, for instance UV-Vis, fluorescence, and conductimetric detection, the cell is part of the capillary itself, and introduces no extra band broadening. For off-column detection, for instance potentiometric and amperometric detection, the dead-volume introduced by fittings and connectors has to be kept as small as possible.

Although CE is a highly efficient technique, and a lot of separations are quite straightforward, there are a large number of variables to be considered when efficiency and/or resolution have to be optimized. The task of optimization can look daunting, considering that BGE concentration, composition, pH, voltage, temperature, type and concentration of organic modifier or complexing agent, injection protocol etc. can all to some extent affect resolution and efficiency. For complicated separations, an experimental design type of approach (Chapter 2) can be extremely helpful in finding the right conditions.

1.3.5. Stacking and sweeping

The relatively poor concentration detection limits of CE have already been mentioned (Section 1.2), and some form of sample concentration is usually necessary to

overcome this limitation. Although off-column pre-concentration is an option, for instance by solid phase extraction (SPE), but CE is particularly suited for on-column pre-concentration. There are a number of procedures collectively called 'stacking', but the sheer number of procedures, terms and acronyms in the literature [24-27], is somewhat confusing. In general, stacking is any procedure that transforms a long sample zone into a short one. This is done by either an electrophoretic mechanism (i.e. governed by local conductivity and concentration of charged species), or by chromatographic effects (i.e. physisorption). The latter is usually called 'sweeping', and is used in MEKC (Section 1.4). Stacking results in an increase in signal to noise ratio (S/N), with enhanced detection limits. In addition, more sample can be introduced into the capillary without losing separation efficiency, because the length of the injected sample plug is compressed.

The simplest situation is encountered for so-called field-amplified sample stacking (FASS), originally described by a model developed by Burghi and Chien [28]. It entails dissolving the sample in a lower concentration of buffer than is used for the BGE. The ratio of the electric field strength in the sample plug (E_1) and in the BGE (E_2) can then be described by:

$$E_1 / E_2 = C_{b2} / C_{b1} = \gamma \quad (\text{Eq. 1.25})$$

C_{b1} , C_{b2} : concentration of buffer in sample plug and in BGE, respectively.

If γ is large, the sample ions experience a strong electric field and will move rapidly towards the boundary with the BGE (cations in the direction of the cathode, anions in the

direction of the anode)¹, where they are slowed down. Under steady-state conditions, the ion fluxes through the boundaries have to be conserved, where:

$$c_{i1}v_{i1} = c_{i2}v_{i2} \quad (\text{Eq. 1.26})$$

c_{i1} , c_{i2} : concentration of species i in sample plug and BGE, respectively
(mol·L⁻¹)

v_{i1} , v_{i2} : electrophoretic velocity of species i in sample plug and BGE,
respectively (m·s⁻¹).

Using equations 1.5 and 1.25, equation 1.26 can be rearranged as:

$$c_{i2}/c_{i1} = v_{i1}/v_{i2} = \mu_i E_1 / \mu_i E_2 = E_1/E_2 = C_{b2}/C_{b1} = \gamma. \quad (\text{Eq. 1.27})$$

Thus, the concentration of sample ions migrating into the BGE is enhanced by a factor γ . Because of conservation of mass, the length of the sample plug has to decrease by the same factor:

$$x_{i2} = l/\gamma \quad (\text{Eq. 1.28})$$

x_{i2} : plug length of species i in BGE (m)

l : original sample plug length (m).

A large concentration ratio between BGE and sample concentration is clearly preferred, since this increases the amount of stacking. There is, however, a practical limit to this process. It was found experimentally that for samples dissolved in very dilute buffers or in pure water, the laminar flow generated during the stacking process increases zone broadening again [28]. An optimal value for γ is approximately ten, i.e. the sample buffer concentration should be ten times less than the BGE buffer. This gives an increase in

¹ Note that there is no charge separation since there is influx of BGE ions into the sample zone as well.

detection limits of one order of magnitude. Removing the sample buffer from the capillary by applying a high voltage with reversed polarity (large volume sample stacking – LVSS), much larger sample volumes can be loaded and concentration factors of several hundred times are possible [29].

Many more stacking procedures have been described in the literature, often with two orders of magnitude or more increase in detection sensitivity (see [24-27] for reviews). FASS and LVSS can be applied to MEKC (Section 1.4) as well, whereby the sample is dissolved in a BGE with a lower concentration of surfactant (but still above the critical micelle concentration – CMC) than in the separation BGE. The most powerful preconcentration technique in MEKC, however, is sweeping, which specifically refers to the situation where the sample does not contain a PSP. We will only describe the simplest form of sweeping of neutral analytes in a zero EOF environment, as originally published by Quirino and Terabe [30]. In their own words, sweeping is ‘the picking and accumulating of analytes by the pseudostationary phase (PSP) that fills the sample zone during application of voltage’. The principle behind this technique is based upon physisorption and is dependent on the affinity of the analytes for the PSP, but the process would not be possible without electrophoresis, which induces the movement of the charged PSP into the sample zone. Briefly, the sample is prepared in a buffer with the same conductance as the BGE (such that the electric field after loading the sample is homogenous), and since the EOF has to be suppressed, this is a low pH (<2.5) buffer. The capillary is initially filled with the BGE, containing an anionic PSP. After hydrodynamically loading a long sample plug (Fig. 1.4A), and replacing the sample vial with a BGE vial, a reversed voltage is applied (cathode at inlet, anode at outlet) (Fig.

1.4B). PSP micelles from the inlet vial then enter the capillary and 'sweep' the neutral analyte molecules, greatly enhancing their concentration in a narrow zone (the dark area in Fig. 1.4B). At the same time, a PSP vacancy develops at the anodic end of the sample zone, where PSP ions are replaced by BGE ions. When PSP micelles reach the end of the sample zone (Fig. 1.4C), the separation by EKC begins. Since the migration velocity of the neutral analytes is less than that of the PSP¹, they will never reach the vacancy zone, which constantly moves towards the anode. It can be shown [32] that the length of the zone into which an analyte is compressed, is:

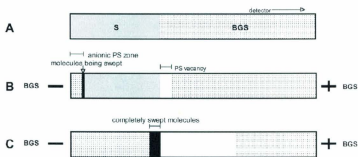


Fig. 1.4: Sweeping in a homogeneous electric field. Grey area: sample zone; dotted area: BGE with PSP; black area: swept analytes; white area: PSP vacancy (reprinted with permission from [31]).

$$l_{\text{sweep}} = l / (1 + k) \quad (\text{Eq. 1.29})$$

l_{sweep} : length of compressed zone (m)

l : length of original sample zone (m)

k : retention factor (see Section 1.4; Eq. 1.31).

¹ The analytes spend part of their time in the BGE and part of their time associated with the PSP. Being neutral, they only have a directed velocity towards the anode when they are associated with the micelles, thus they move slower than the PSP.

This leads to an increase in the concentration of the analytes of:

$$C_{\text{sweep}} = C_{\text{inj}}(1 + k) \quad (\text{Eq. 1.30})$$

C_{sweep} : concentration of analytes in compressed zone (M)

C_{inj} : concentration of analytes in original sample zone (M).

The stronger the interaction of the analytes with the PSP, the shorter the compressed zone, and the higher their concentration will be. Concentration factors of up to 5,000 have been reported [30].

1.4. Micellar electrokinetic chromatography

1.4.1. Theory of micellar electrokinetic chromatography

Introduced in 1984 by S. Terabe [9,33], MEKC was the first addition to what is now becoming a large family of electrokinetic chromatography (EKC) techniques. These are based on a combination of electrophoresis and interactions of analytes with additives that form a dispersed phase moving at a different velocity than the analytes [15]. Either the additive or the analytes are charged, or both. In MEKC, the additive is a surfactant at a concentration above its CMC¹, and in the vast majority of applications, it is the surfactant that is charged. The development of MEKC was revolutionary in that it allowed neutral solutes to be separated via CE, although it is often useful for charged analytes as well. It is truly a hybrid between CE and chromatography, and the only distinguishing feature from CZE is the addition of a surfactant at a concentration higher than its CMC to the BGE (i.e. the same type of instrument and capillary are used as in CZE). In the situation where the surfactant carries a negatively charged head group, and

¹ Other types of EKC make use of microdroplets, vesicles, dendrimers, dissolved polymers etc. [15].

normal polarity is applied (i.e. anode at inlet, cathode at outlet), the effective electrophoretic velocity of the micelles is towards the inlet (Fig. 1.5).

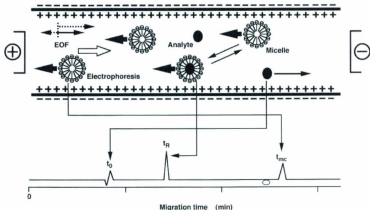


Fig. 1.5: Schematic principle of MEKC. t_0 : migration time of unretained solute (EOF marker); t_R : migration time of analyte; t_{mic} : migration time of micellar marker (reprinted with permission from [34]).

In most circumstances, however, there is a strong EOF that will push the micelles towards the outlet. They effectively can be regarded as a phase that moves in the same direction as the EOF, but at a lower velocity. The term pseudostationary phase (PSP) is often used as a general term for the dispersed phase in EKC because it moves through the capillary, in contrast to the truly stationary phase in conventional chromatography. Depending on the affinity of the analytes towards the PSP, they will spend part of the time in the BGE, and part of the time associated with the PSP. When they are in the BGE, they move towards the outlet at the speed of the EOF, because neutral analytes are not affected by the electric

field. Associated with the PSP, however, they move slower because of the slower speed of the PSP relative to the EOF. With respect to EKC, with a negatively charged PSP and with normal polarity applied, we can distinguish between three types of solutes. Solute that have no affinity for the PSP move with the EOF and can be used as so-called EOF markers (e.g. methanol, dimethylsulfoxide, thiourea etc.). These types of analytes will be the first to reach the detector. Solute that have very limited solubility in water (mainly hydrophobic solute) will be associated with the PSP during the entire analysis, and will have the longest migration time. Their migration time corresponds to the time it takes for the PSP ions that are at the inlet of the capillary at the start of the analysis, to reach the detector. These solute are known as PSP markers (micelle markers in MEKC), for instance dodecanophenone and Sudan III. All other solute have migration times somewhere in between the migration time of the EOF marker and the PSP marker; closer to t_0 if they have a limited affinity for the PSP, closer to t_{mc} if they have a stronger affinity for the PSP. Consequently, separations are constrained to occur within this time frame (the migration time window), and this defines the peak capacity of the system [5]. In chromatography, with the exception of size-exclusion chromatography, no such restriction exists; solute in principle can have an infinite elution time when they bond permanently to the stationary phase. Thanks to the high efficiency of EKC, a reasonable peak capacity is often obtainable, even with a narrow migration time window.

It is possible to derive an equation for the retention factor k of an analyte in terms of t_0 (migration time of an unretained solute), t_m (migration time of analyte) and t_{mc}

(migration time of a micelle marker). We will limit ourselves to neutral analytes here¹ [14]. The retention factor k is defined in the same manner as in chromatography [5,19]:

$$k = n_{mc}/n_{aq} = \beta K \quad (\text{Eq. 1.31})$$

n_{mc} : number of moles of analyte in the micellar phase (moles)

n_{aq} : number of moles of analyte in the aqueous phase (moles)

β : phase ratio (V_{mc} / V_{aq}), with V_{mc} and V_{aq} the volumes of the micellar phase and the aqueous phase, respectively

K : distribution coefficient: concentration of the analyte in the micellar and aqueous phase, respectively.

Therefore;

$$1 + k = (n_{aq} + n_{mc}) / n_{aq} \quad (\text{Eq. 1.32})$$

and:

$$1 / (1 + k) = n_{aq} / (n_{aq} + n_{mc}) \quad (\text{Eq. 1.33})$$

$$k / (1 + k) = n_{mc} / (n_{aq} + n_{mc}). \quad (\text{Eq. 1.34})$$

Equations 1.33 and 1.34 represent the fractions of the analyte in the aqueous phase and the PSP, respectively, and these are equivalent to the time the analyte spends in those phases [14,19]. The apparent velocity of an analyte, taking into account the time it spends in both phases, can be written as:

$$v_{app} = [1 / (1 + k)] v_{co} + [k / (1 + k)] v_{mc} \quad (\text{Eq. 1.35})$$

or (see Eq. 1.8):

$$(L_d / t_m) = [1 / (1 + k)] (L_d / t_0) + [k / (1 + k)] (L_d / t_{mc}). \quad (\text{Eq. 1.36})$$

¹ The interested reader is referred to [2] for a detailed description of the derivation of formulas for k and R_f for ionized analytes.

After rearranging, we find:

$$k = (t_m - t_0) / \{ [1 - (t_m/t_{mc})] t_0 \}. \quad (\text{Eq. 1.37})$$

This expression is similar to the expression for k in chromatography [19]:

$$k = (t_m - t_0) / t_0 \quad (\text{Eq. 1.38})$$

but is corrected for the fact that the PSP moves through the capillary. In fact, equation 1.38 is the special case where t_{mc} in equation 1.37 is infinite (i.e. for a stationary phase).

For the resolution R_s of neutral analytes, we first consider an equation that is often used in chromatography [2,5,35]:

$$R_s = (\sqrt{N}/4) [(\alpha - 1)/\alpha] [k_2/(k_2 + 1)] \quad (\text{Eq. 1.39})$$

k_1, k_2 : retention factors of analyte 1 and 2

α : selectivity factor ($= k_2/k_1$).

The first term shows that the resolution is proportional to the square root of the efficiency of the system; doubling the column length increases the resolution only by a factor of 1.4. A better approach for maximizing the resolution is choosing the conditions such that the selectivity factor is large; although eventually this effect levels off for $\alpha > 10$. Increasing k_2 is another way of increasing the resolution, but again this effect levels off eventually ($k_2 \approx 10$). The ideal range for k_2 is between 2 and 10, because at higher values analysis times become excessively long [5].

In MEKC, the resolution equation is very similar, but again corrected for the fact that the PSP moves through the capillary [2,5]:

$$R_s = (\sqrt{N}/4) [(\alpha - 1)/\alpha] [k_2/(k_2 + 1)] [1 - (t_0/t_{mc})] [1 + (k_1 t_0/t_{mc})]^{-1} \quad (\text{Eq. 1.40})$$

With t_{mc} approaching infinity (stationary phase), equation 1.39 is obtained. The same strategy as above can be used for optimization, but increasing the length of the capillary increases N (and R_s) only if the field strength does not decrease (Eq. 1.18). Increasing the phase ratio is an effective way of increasing the retention factors (see Eq. 1.31). However, large retention factors are to be avoided because then the product of the last two terms becomes almost zero. The best resolution is obtained for a value k_{opt} of [2]:

$$k_{opt} = (t_{mc} / t_0)^{1/2} \quad (\text{Eq. 1.41})$$

Note that the efficiency N in equation 1.40 can be calculated according to equation 1.19. The diffusion coefficient D in that case is a weighted average of the diffusion coefficients in the aqueous and micellar phase [5]:

$$D = [1 / (1 + k)] D + [k / (1 + k)] D_{mc}$$

D_{mc} : micelle diffusion coefficient ($\text{m}^2\text{-s}^{-1}$); usually an order of magnitude less than D

1.4.2. Surfactants in micellar electrokinetic chromatography

Surfactants are amphiphilic molecules; they contain both a hydrophobic and a hydrophilic moiety in their structure. The hydrophobic part is a hydrocarbon or fluorocarbon chain, or a steroidal structure, while the hydrophilic part can be anionic (e.g. sulphate, sulfonate, carboxylate), cationic (quaternary ammonium group) or non-ionic (polyoxyethylene). The latter are only useful for the separation of ionic analytes, but are often added to ionic surfactants to modify their selectivity (Section 1.5). At a concentration higher than their CMC, surfactants form micelles, with (in an aqueous environment) an inner core consisting of the hydrophobic part and an outer shell

consisting of the polar head groups at the micelle-water interface. Micelles are very dynamic entities, with the lifetime of a single monomer within a micelle on the order of 10 μ s, while micelles themselves exist on the millisecond timescale [36]. The driving force for their formation is the favourable free energy change that accompanies the packing of the hydrophobic moieties into a central core, surrounded by the polar head groups [37]:

$$\Delta G^{\circ} = RT(1 + \beta) \ln(\text{CMC}) \quad (\text{Eq. 1.42})$$

β : fraction of the charges of the micellized univalent surfactant ions
neutralized by micelle-bound univalent counterions

CMC: critical micelle concentration ($\text{mol}\cdot\text{L}^{-1}$).

This favourable free energy change is counteracted by electrostatic repulsion between the head groups, or in the case of non-ionic surfactants, steric repulsion. The balance between these opposing forces determines CMC, size, shape¹, and aggregation number of the micelle [5,38], and is for instance influenced by the ionic strength and pH of the medium.

The original experiments by Terabe [9] were performed using sodium dodecylsulfate (SDS), and to date, this is by far the most widely used surfactant in MEKC. The CMCs and aggregation number of SDS and some other commonly used surfactants are shown in Table 1.3. In order to keep the current (i.e. Joule heating) within reasonable limits, charged surfactants need to have a relatively low CMC, preferably <10 mM, so that a range of concentrations can be explored to optimize retention factors. Other requirements that impose practical limits on the surfactants used in MEKC are that they

¹ Micelles are usually spherical in aqueous solutions in the range of 1 – 10 times the CMC. At higher concentrations, rod-like or dumbbell-like shapes, which can better pack head groups, are formed [5].

need to be available in pure form, dissolve well in aqueous solutions, and be stable under the conditions for MEKC [5]. They also need to have a low UV-absorbance, because of the widespread use of UV-vis detection. In addition, the Krafft point¹ should be below room temperature.

Table 1.3: Properties of some common surfactants used in MEKC (adapted from [5])

Surfactant	CMC in water (mM)	Aggregation number
Sodium dodecylsulfate (SDS)	8.1	62
Sodium dodecanesulfonate	7.2	54
Lithium perfluorooctanesulfonate (LPFOS)	6.7	-
Sodium cholate	13-15	2-4
Sodium deoxycholate	4-6	4-10
Tetradecyltrimethylammonium bromide (TTAB)	3.5	75
Polyoxyethylene [23] dodecanol (Brij 35)	0.09	-

Cationic surfactants such as TTAB (Table 1.3) have the interesting property that they reverse the EOF, and this usually means that the polarity has to be reversed as well (cathode at the inlet, anode at the outlet) in order for analytes to reach the detector. The reversal is due to the adsorption of micelles (with positively charged head groups) to the capillary wall, or by the adsorption of a bilayer of surfactant molecules.

While selectivity in MEKC can be manipulated by the addition of organic solvents (such as methanol or acetonitrile), cyclodextrins, or urea, the most important variable seems to be choice of surfactant [5,15,39]. This is discussed in greater detail in Section 1.5.

¹ The Krafft point is the temperature at which the solubility of the surfactant is equal to its CMC, i.e. below this temperature no micelles can be formed.

1.4.3. The interphase model of retention

The interaction of solutes and micelles has been an active area of research (see [40,41], and references herein). An exact theory of solubilization has proven difficult to formulate, because micelles have too small an aggregation number to be considered a bulk phase, have a large surface-to-area ratio, and are structurally heterogeneous. In general, solutes can be either in a 'dissolved' state in the micelle core (especially at high solute concentration), or in an 'adsorbed' state at the micellar surface. In MEKC, with its low solute concentrations, there is a lot of experimental evidence that the sorption properties of micelles can be explained by assuming either an average or a single sorption environment [5,39,42], and this environment is considerably more polar than would be expected given the hydrocarbon core of micelles. Conceptually, the interphase model [5,39] is often invoked to explain selectivity differences between different types of surfactants (Section 1.5). The interphase is the region that surrounds the core of the micelle, and contains the hydrated polar head groups and probably also the first few segments of the hydrocarbon chain (Fig. 1.6). It also holds components of the BGE, and associated water molecules. The composition of the interphase region is probably not homogeneous, and solute molecules may experience a range of microenvironments. Indeed, individual micelles are only moderately larger than the solutes being separated, and there is an averaging effect when macroscopic properties (such as the retention factor) are determined. The boundaries of the interphase region are not well defined and may change as the composition of the BGE is changed. In essence, according to this model, retention in MEKC is a consequence of differences in solvation properties of the

bulk electrolyte solution and the interphase. One could even go as far as stating that the micelle core does not play a role in retention, beyond stabilizing the micelle structure [5].

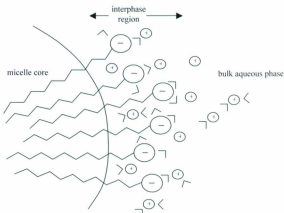


Fig. 1.6: Schematic of the structure of a micelle, and its surroundings; the boundaries of the interphase are not well defined (adapted from [42]).
◻ : water molecule

1.4.4. Micellar electrokinetic chromatography and mass spectrometry

UV-vis detection is the most widely used type of detection in CE, because of its straightforward application, and its usefulness for a large number of different types of compounds. However, detection limits are relatively poor, and almost no structural information is conveyed by UV-vis spectra. In these respects, MS is superior to UV-vis detection, with, if not unambiguous identification of analytes, at least labelling them with a (pseudo-) molecular mass. Further structural information can be acquired via MS/MS experiments, with for instance a triple quadrupole, an ion trap or a quadrupole-time-of-flight MS. An additional advantage of MS over UV-vis is that unresolved compounds can

also be identified and quantified, if they have different (pseudo-) molecular masses [15]. It is therefore not surprising that the coupling of CE and MS was attempted relatively soon after the development of CE [43]. In analogy to HPLC, electrospray ionization (ESI) was, and still is, the most common ionization technique¹, but atmospheric pressure chemical ionization (APCI) and atmospheric pressure photoionization (APPI) have also been applied [15].

Normally, in CE, the voltage is applied between the inlet and the outlet vial. However, in CE-MS there is no outlet vial since the liquid exiting the capillary outlet has to be sprayed into the MS. In order to maintain a closed electric circuit, the voltage is either applied via a conducting sheath liquid (coaxial liquid sheath flow interface), a sheathless interface, or a liquid-junction interface [45-47]. The sheath flow interface is by far used most often, and is described in some detail below. An excellent overview of recent developments in other interfaces for liquid-phase separations/MS techniques is given by Gelpi [48].

The coaxial liquid sheath flow interface typically consists of three coaxial capillaries (Fig. 1.7b). The inner capillary is the CE capillary, and contains the BGE and solutes. The CE capillary is inside a stainless steel capillary through which the sheath liquid flows, and which is connected to ground potential. The sheath liquid is delivered by a pump (usually via a splitter to generate the low flow), and mixes with the BGE in the Taylor cone [46]. The stainless steel capillary, in turn, is inside a third capillary through which an inert gas can be administered to facilitate spray formation. The whole unit, with

¹ Strictly speaking, ESI, unlike APCI and APPI, is not an ionization technique, since ions are simply transferred from the solution to the gas phase [44].

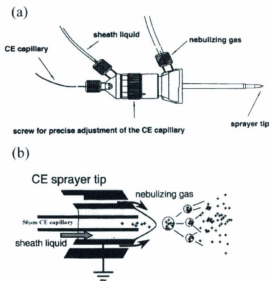


Fig. 1.7: Schematic of the CE-ESI-MS interface (a), and the tip of the sprayer (b) (reprinted with permission from [49]).

connections, is called the CE-ESI-MS interface (Fig. 1.7a). The flow of the sheath liquid is typically in the low μLs per minute, and is several times higher than the EOF (typically in the hundreds of nLs per minute), so the eluate is diluted considerably. This unfortunately leads to somewhat poorer detection limits, and some band-broadening because of diffusion [47,50,51]. Besides its role in maintaining a closed electric circuit, the sheath liquid also aids in maintaining a stable electrospray, since normally the flow through the CE capillary is too low to sustain a stable spray with an 'ordinary' sprayer tip (with a tapered capillary and/or a small diameter sprayer tip, it is possible to maintain a

stable electrospray with flows in the hundreds of nLs (or less) range). The composition (type and percentage of organic modifier, pH, ionic strength) and flow rate of the sheath liquid have to be adjusted to optimize ESI-MS sensitivity (see also Chapter 2) and this makes method optimization that much more complicated. On the other hand, the sheath liquid to some extent provides a means to overcome limitations in the compatibility of the BGE with the electrospray process. In general, a BGE with a non-volatile buffer at high ionic strength has to be avoided, because ion-pairing reduces the intensity of signals, and because of the build-up of salts in the MS [44,52]. High electrolyte content also interferes with the stability of the Taylor cone [53]. BGEs with volatile buffer components (ammonium acetate, -formate, or -carbonate) are often used as alternatives to BGEs with sodium phosphate and sodium tetraborate, although they may not always be optimal for the separation [54].

There are numerous successful applications of CZE-ESI-MS [50,55-58], and this is essentially now an established technique. Coupling of MEKC to ESI-MS has proven to be more difficult because of the non-volatile PSP (e.g. SDS), which severely suppresses analyte signals [15,52,53,59], and causes extra signals in the mass spectra (often in the region of interest) [60]. Rundlett and Armstrong [53] describe the ability of anionic surfactants, such as SDS, to quench signals in positive ESI mode with a modified aerosol ionic redistribution model. Surfactants in a droplet preferentially position themselves at the liquid/gas interface, with their hydrophobic tails towards the gas phase, and their hydrophilic head groups anchored in the aqueous phase, where they attract the oppositely charged analytes. From pictures of droplets undergoing fission, it appears that offspring droplets are formed from surface layers of the parent droplets [44,53], and these are

consequently enriched in surfactant and analytes. The surfactant interferes with the transfer of cationic analytes from the electrospray droplets to the gas phase due to Coulombic attractions between the oppositely charged analytes and the surfactant. Evidence for this model comes from the observation that analyte signals are detected much better in ESI-MS when surfactants with low surface activities (for instance polymeric surfactants), and non-ionic surfactants are used, and the fact that cationic surfactants do not suppress the signals of cationic analytes [53].

Despite the reported problems, some authors do not seem to be discouraged from using direct MEKC-ESI-MS for certain applications, although this requires daily cleaning of the ion source [59]. More often, these problems are circumvented as best as possible by several approaches. The initial solution was to prevent the PSP from entering the MS, via the partial filling technique or by using reverse migrating micelles, and these techniques (which are described in some detail in Chapter 2) still find application [61,62]. Other ionization techniques such as APCI [63] and APPI [64] seem to be more compatible with the BGEs commonly used in CE, but developments in this area are still in their infancy, and no clear improvements over ESI have been demonstrated yet. An interface consisting of a low-flow sheath liquid with a bevelled capillary tip, combining the versatility of the sheath-flow liquid and the sensitivity of the sheathless interface, has provided better performance than the classical sheath-flow liquid interface [54]. With the smaller sprayer orifice (75 μm), smaller droplets are initially formed in the ESI process, which results in a higher sensitivity and a better tolerance to salts [65]. Finally, 'MS-friendly' surfactants (i.e. surfactants that are more compatible with the electrospray process and do not

precipitate in the entrance to the MS) are another alternative, and this is the topic of Chapter 2.

1.5. Linear Solvation Energy Relationships

The concept of linear solvation energy relationships (LSERs) was developed in the mid 1980s in order to better understand the types and relative importance of the various physicochemical forces that determine retention and selectivity in chromatography and EKC. An excellent discussion of the theory and practice of LSERs, and their complicated historical roots can be found in reference 66, and this paper is the basis for much of this section.

1.5.1. The Solvation Parameter Model

Retention of neutral solutes in chromatography and EKC is determined by the forces between uncharged molecules (solutes and solvent), collectively called van der Waals interactions, which are in the order of $0 - 10 \text{ kJ}\cdot\text{mol}^{-1}$ [66]. Dispersion or London forces determine the ability of molecules to interact through instantaneous dipoles (also called 'polarizability'). Dipole-dipole or Keesom forces are the interactions between the electric fields of molecules with a charge separation, and dipole-induced dipole forces or Debye forces are interactions between the permanent electric field of one molecule and the polarizability of another molecule. Finally, hydrogen bond interactions take place between hydrogen atoms covalently bound to an electronegative element (principally oxygen, nitrogen or fluorine) and lone pair electrons on nearby electronegative elements (mainly oxygen, nitrogen, fluorine, or in some cases the π electrons of aromatic rings).

All these forces contribute to the free energy of transfer of a solute between two condensed phases.

In chromatography and EKC, the solvation parameter model views the transfer of a solute into a solvent in three steps (Fig. 1.8) [5,66,67]. In the first step, a cavity of suitable size is created in the solvent. This requires disrupting intermolecular interactions between solvent molecules and is therefore always energetically unfavourable. The larger the solute's size, and the stronger the intermolecular interactions in the solvent, the more energy this requires. In a second step, the solute is inserted in the cavity, and the solvent molecules are reorganized into the positions they will adopt when the solute is in equilibrium with the solvent. The free energy change for this step is approximately zero,

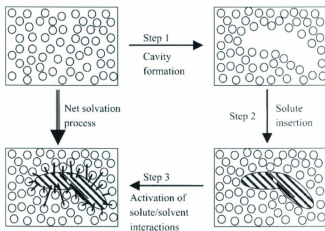


Fig. 1.8: Model of the solvation process (reprinted with permission from [66]). See text for explanation.

and can be neglected¹. In the third and final step, the solute-solvent van der Waals interactions are set up, all of which are exergonic. When the transfer occurs between two condensed phases, the Gibbs free energy of transfer is equivalent to the difference in Gibbs free energy of cavity formation and solute-solvent interactions in the two phases.

For practical purposes, it is necessary to move from a qualitative model to a quantitative one. The LSER model describes the contribution of all the interactions by the sum of a series of product terms, each consisting of a solute factor ('descriptor') and a complementary solvent factor ('system constant'). The general LSER equation, applicable in liquid-liquid² systems, such as HPLC and EKC, is:

$$\log k = c + eE + sS + aA + bB + vV. \quad (\text{Eq. 1.43})$$

Most often, the retention factor k is used as the independent variable, but other free energy related solute properties (distribution constant, adjusted retention time etc.) can be used as well. Note that since the interactions are free energy related and are summed, one has to take the logarithm of the solute property. The descriptors V , E , S , A and B have evolved over a number of years [66], but are now well established. They are related to measures of the solute's molecular volume, polarizability in excess of that of a comparable sized *n*-alkane, dipolarity, hydrogen bond donating and accepting ability, respectively. Unfortunately, some of the descriptors account for more than one type of interaction (Section 1.5.2). The system constants c , v , e , s , a and b reflect the properties of

¹ Entropy and enthalpy changes for reorganizations may be large, but compensate one another. It is analogous to the melting of a solid [67].

² For GC, the vV term is replaced by a lL term, where L is the logarithm of the retention of a solute on a hexadecane column [5,39,67]

the solvent into which the solute is being transferred, and are determined via multiple linear regression (Section 1.5.3).

1.5.2. Descriptors in LSERs

The five descriptors used in LSERs of condensed phases are now considered in some more detail. They find their origins in the development of solvent descriptors, used to correlate and rationalize the effects of solvents on reaction rates and equilibria. Kamlett, Taft and Abboud [68-70] developed the solvatochromically¹ derived scales of solvent dipolarity/polarizability, hydrogen bond donor acidity and hydrogen bond acceptor basicity in the mid 1970s. Quantifying these effects led to the following general equation [71]:

$$Y = Y_0 + s(\pi^* - d\delta) + a\alpha + b\beta \quad (\text{Eq. 1.44})$$

Y : solvent dependent property (e.g. log of reaction rate, shift of wavelength of absorbance peak of a probe solute)

$\delta, \pi^*, \alpha, \beta$: solvent dependent descriptors; measures of solvent polarizability, polarity/polarizability, hydrogen bond donating and accepting ability, respectively

Y_0, s, d, a, b : constants determined via multiple linear regression; solute dependent.

After the amendment of Eq. 1.44 for gas-liquid partition equilibria with a term accounting for a cavity formation process [71], it was rationalized that a similar equation could be

¹ The scales were based upon the effect of solvent on the frequency of maximum absorbance of a selected set of solutes. There were a number of such solvatochromic scales being developed at the time, but the one mentioned here was the most general and useful [66].

used for the study of solute effects. In essence, the fundamental concept was inverted. The values for the solvent descriptors were used as *initial* estimates of a solute's interaction (i.e. the solvent is now used as a solute) with chromatographic phases, and were soon applied in the correlation with HPLC retention data [72]. The main reason that these values were only *initial* estimates, is that variables characterizing a bulk liquid (i.e. a solvent, as in the solvatochromically derived scales) cannot necessarily be used to characterize the same species when present as separate molecules (i.e. as a solute, as in a chromatography). This is particularly pertinent for solvents that self-associate via hydrogen bonds.

McGowan's characteristic volume (V)¹ is used as a measure of a solute's volume [73,74]. This measure of volume is strongly correlated with the intrinsic volume of a molecule as determined by X-ray diffraction, but is much easier to calculate. It can be calculated for any molecule with a given structure, using atomic volumes and the total number of bonds [5,73,74]. Unfortunately, there is a strong correlation between V and the polarizability of a molecule. The larger a molecule, the greater its tendency to engage in London type interactions [66,75], and within a homologous series, molecular volume is linearly correlated with molecular polarizability (see below). It does not seem possible to separate these effects [75], so the volume descriptor V invariably also contains a contribution from polarizability.

The excess molar refraction, E , is an indication of a solute's polarizability, in excess of that of a comparable sized (hypothetical) n-alkane. It is a measure of a solute's

¹ The calculated volume is actually divided by 100 to put it on the same scale as the other descriptors; likewise, calculated E values are divided by 10.

interaction through polarizable electrons (non-bonding and π -bonding electrons). The molar refraction of a solute X (MR_X) can be calculated via [75]:

$$MR_X = V[(\eta^2 - 1) / (\eta^2 + 2)] \quad (\text{Eq. 1.44})$$

V : McGowan's characteristic volume ($\text{cm}^3\text{-mol}^{-1}$)

η : refractive index of the pure liquid at 298 K

As already pointed out, there is a linear correlation between molar volume and polarizability, for that reason MR_X cannot be used as a system descriptor¹. For n-alkanes, this relationship is:

$$(MR_X)_{\text{alkane}} = 2.83195V - 0.52553. \quad (\text{Eq. 1.45})$$

The excess molar refraction E is now calculated as:

$$E = (MR_X) - 2.83195V + 0.52553 \quad (\text{Eq. 1.46})$$

and this 'filters out' the inherent polarizability due to size. Software is available to calculate E [66,75], but since E is very much an additive property, addition of fragment values can also be used.

The dipolarity, S , is in fact a blend of the ability of a solute to engage in dipole-dipole and dipole-induced dipole interactions, and polarizability [66,67]. These values were originally obtained via gas chromatographic measurement of retention factors on polar stationary phases [67,71].

Scales of hydrogen bond acidity (A) and basicity (B) were originally developed using the logarithm of equilibrium constants of 1:1 hydrogen bond complexes between a series of solutes and a set of strong hydrogen bond donors and acceptors in an inert polar

¹ If descriptors are correlated, the statistical programme used to determine the system constants by multiple linear regression cannot disentangle the contribution of each type of interaction to $\log k$ (See Section 1.5.4).

solvent [66,76]. Empirically, it was then found that solutes with multiple donor or acceptor sites deviated from the equations, and adjustments had to be made. This was done by back-calculation: a correlation was established first for solutes with single hydrogen bond donor or acceptor sites, and A and B values of solutes with multiple sites were then adjusted so they would fit the equations. Testimony to the fact that this was done with great care and that they reflect real ability to interact chemically comes from the fact that these scales have also been successfully used to fit thermodynamic data unrelated to their original development [66].

While the V and E descriptors can be calculated from the structure of the solute, the other descriptors are determined experimentally. This is done by first determining the system constants (c, v, e, s, a, b values) of a large number of chromatographic phases with equation 1.43, using existing solute parameters. For any new solute, equation 1.43 is then rearranged as:

$$\log k - c - eE - vV = sS + aA + bB. \quad (\text{Eq. 1.47})$$

The left hand side of this equation is known, and so are the $s, a,$ and b coefficients. In principle, measuring the retention factor of the solute in three different systems is sufficient to solve equation 1.47 for $S, A,$ and B . For statistical reasons, it is recommended to overdetermine the system by using more $\log k$ values, preferably from systems that differ greatly in their chemistry [66,75].

Examples of solute descriptors can be found in Tables 3.1 and 4.1. Note that V and E have units of $\text{cm}^3 \cdot \text{mol}^{-1}$, while the other descriptors are dimensionless; it is customary to report these values without any units at all.

1.5.3. System Constants in LSERs

The system constants are a function of the solvents between which the solutes are partitioned. In MEKC, the partitioning is between an aqueous phase and a micellar phase. They are determined using multiple linear regression of some 20 – 40 $\log k$ determinations of solutes with known descriptors (Section 1.5.4), and reflect differences in solute interactions in the two phases with respect to ease of cavity formation (plus some polarizability effects - v system constant), interaction with solutes through n -bonding and π -bonding electrons (e system constant), ability to engage in dipole-type interactions (plus some polarizability effects - s system constant), and hydrogen bond accepting (a system constant) and donating (b system constant) ability [5,66]. The interpretation of the e system constant is somewhat difficult; it has contributions from the phase ratio (the higher the surfactant concentration, the more positive e is), and also accounts for residual polarizability effects not included in the LSER model [66]. It is therefore usually not included in the evaluation of PSPs based upon system constants. Note that the A and B descriptors are a solute's ability to act as a hydrogen bond donor and acceptor, respectively, and that the a and b system constants are the complementary properties of the solvent to act as a hydrogen bond acceptor and donor, respectively. It is important to stress that these system constants reflect *differences* between the two phases. A small value for a particular system constant does not necessarily mean that that type of interaction is not important in those solvents, but rather that *they are of approximately the same value in both solvents*.

A small selection of surfactants and their system constants is shown in Table 1.4. In general, the v system constant is large and positive, and thus contributes to retention of the solute in the micellar phase. This means that it is energetically more favourable for a solute to create a cavity in the micellar phase than in the aqueous phase, and this agrees well with our chemical intuition: the van der Waals bonds holding micelles together are easier to break than the strong hydrogen bonds of the aqueous phase. The b system constant is also often large, but negative. Here we see that the micellar phase is always a worse hydrogen bond donor than the aqueous phase¹. The a system constant is generally small for anionic surfactants (and typically larger for cationic surfactants), and can be both positive or negative. The s system constant is always negative: dipole-type interactions are favoured with the aqueous phase over the micellar phase. Lastly, the e system constant is small and usually positive, indicating that the micellar phase is usually slightly more polarizable than the aqueous phase. The conditions under which the system constants are determined (e.g. concentration of surfactant, concentration and type of buffer) seem to have little impact on the obtained values (except for e - see previous page) [15,77]. It is evident from Table 1.4 that there is a limited variation in selectivity, although a notable exception is LPFOS. Clearly, a more varied collection of surfactants would be desirable from the point of view of method development [39], and synthesis and evaluation of novel PSPs is an ongoing area of research [39,78,79].

¹ The hydrogen bond donating properties of most PSPs are attributed to bound water molecules in the interphase. This is discussed in more detail in Chapter 4.

Table 1.4: Common surfactants and their system constants. Standard errors are 0.04 – 0.16. There is some disagreement on the system constants for LPFOS (see Chapter 5).

	<i>e</i>	<i>s</i>	<i>a</i>	<i>b</i>	<i>v</i>	Ref
SDS (50 mM)	0.24	-0.30	-0.18	-1.85	2.98	[80]
Sodium cholate (75 mM)	0.63	-0.47	0	-2.29	2.74	[39]
Sodium deoxycholate (75 mM)	0.66	-0.47	0	-2.47	2.67	[39]
Sodium parmitoylsarcosinate (40 mM)	0.42	-0.45	0.48	-2.58	3.11	[80]
Sodium N-dodecanoyl-N-methyltaurine	0.72	-0.50	0.22	-2.58	3.07	[39]
TTAB (10 mM)	0.30	-0.20	0.87	-2.71	2.99	[80]
LPFOS (40 mM)	-0.68	0.46	-0.80	-0.61	2.36	[80]
	-0.11	-0.24	-0.88	-0.46	1.97	[81]

1.5.4. Practical LSERS

Determining the system constants of a PSP starts with selecting 20 – 40 solutes with known descriptors. To date, descriptors are available for about 4,000 compounds, and there are a few large compilations available [5]. The selection, however, is not at random. Besides some pragmatic considerations (price, availability, absorption in the UV region if detection is via UV-vis), the solutes should show a wide variety in descriptor values for the model to be statistically and chemically valid [5,15,66,82]. There should also not be any significant cross-correlation between system descriptors (See footnote on p. 65, and Tables 3.2 and 4.2). The solutes are dissolved, 4-10 per vial plus a micelle marker (the solvent can usually be used as EOF marker), at a concentration of ~ 500 mg·L⁻¹, and are run in a BGE with a suitable PSP concentration. There are no strict rules for how many solutes can be added together, but the main concern here is to avoid co-migration and allow for unambiguous identification of the solutes. If identification is via UV-vis spectrophotometry, a spectral database is definitely helpful in the identification. From the measured migration time, EOF time and micelle marker time, and with equation 1.37, the retention factor can be determined for each solute. This leads to 20 – 40

equations of the form of equation 1.43, where the appropriate $\log k$ values and values of the descriptors are filled in for each solute. The system constants are now determined via multiple linear regression, and the statistics of the analysis are evaluated. Generally, the program that performs the regression will report the correlation coefficient, the standard error of the fit, the F-statistic, and standard errors in the system constants. No absolute rules exist for deciding whether a good fit has been obtained, but one reference lists an F statistic >150 , correlation coefficient >0.97 and a standard error of the fit <0.1 as acceptable [15]. Often, the program will also identify outliers, solutes that do not fit the equation very well, and it is common practice to remove these to improve the statistics [66,79]. Most of the time, it is not possible to identify any causes for a solute being an outlier. We can only point out that the LSER model, just like any model, is an incomplete description of the real world. Notable shortcomings of the model are the fact that polarizability effects are distributed over the V , S and E descriptors, and the lack of a descriptor taking into account the shape of the solute [66,83]. The latter would be necessary to rationalize enantiomeric separations, and differences in retention for positional isomers. Besides an evaluation of the statistical aspects, the model should also make sense from a chemical point of view. This is discussed in more detail in Chapters 3-5.

1.6. Thesis Objectives

The development and evaluation of new PSPs continues to be of interest in EKC, and it is the aim of this thesis to make a contribution to this field, both from a practical and a theoretical point of view.

The first chapter deals with a practical application of an MS-friendly surfactant (the ammonium salt of perfluorooctanesulfonate - APFOA) in MEKC-ESI-MS. Originally proposed by Ishihama et al. [84], who performed some preliminary experiments, and studied in more detail by Petersson et al. [52], the use of APFOA in MEKC-ESI-MS could prove to be a very simple solution to some of the problems that have held back the routine application of MS in MEKC (Section 1.4.4). To date, however, no real practical applications, other than Petersson's et al. [52] experiments on pharmaceuticals, have been published. Given the potential importance of APFOA for MEKC-ESI-MS, we wanted to explore its usefulness in a more elaborate procedure for the analysis of *N*-methylcarbamates in drinking water.

The other chapters are devoted to the synthesis and evaluation of anionic dimeric surfactants in MEKC. With very few exceptions [79,85,86], these types of surfactants so far have eluded the attention of separation scientists. Given their interesting properties (Chapter 3), this is somewhat surprising, and they certainly require a closer look with respect to their applicability to MEKC. Their main distinguishing feature from 'traditional' surfactants is the spacer, which connects the two amphiphilic moieties at the level of the head groups, or very close to the head groups. With reference to Fig. 1.6, one can easily imagine that the spacer resides in the interphase, where extensive interaction with solutes takes place (Section 1.4.3). This opens up some interesting avenues for

modifying their selectivity, without interfering too much with the micelle-forming properties, which in large part depend on the hydrophobic chains. Depending on the length and the nature (i.e. the presence of specific functional groups) of the spacer, one could expect the interaction with certain types of solutes to be either enhanced or attenuated. Thus, the hypothesis was that the spacer in dimeric surfactants influences the selectivity. The goal was to synthesize dimeric surfactants with hydrophobic, hydrophilic and fluorinated spacers of various lengths, and determine their selectivity via LSERs to test this hypothesis. It was not expected to see very different selectivity between dimeric surfactants with hydrophobic spacers (aliphatic chain) of various lengths, but they could serve as a baseline reference to which dimeric surfactants with spacers of similar length but with functional groups could be compared. It was expected that the hydrogen bond accepting properties of dimeric surfactants with hydrophilic spacers (polyethoxy chain) would be enhanced, although it was not possible to make any quantitative predictions. This could be interesting, because in general anionic surfactants used in MEKC have little hydrogen bond accepting abilities. Therefore, surfactants with enhanced hydrogen bond accepting abilities could find practical utility. Fluorinated spacers were selected because the only fluorinated surfactant evaluated via LSERs, LPFOS, has very different selectivity from other surfactants used in MEKC (Table 1.4). Although some of this different selectivity (i.e. cohesiveness) can be attributed to fluorination of the hydrophobic chain, the question remained what the effect of a fluorinated spacer on the selectivity would be. Finally, a dimeric surfactant with an aliphatic spacer and fluorinated long chains was also to be synthesized. Some of the dimeric surfactants with hydrophobic and hydrophilic spacers that are reported here have been synthesized before. However,

the types of dimeric surfactants with fluorinated spacers synthesized here, to the best of our knowledge, have not been synthesized before.

1.7. Co-authorship Statement

Chapters 2-4 were published in peer-reviewed journals with G. Van Biesen as first author and Dr. C. S. Bottaro as corresponding author, while Chapter 5 (except for Section 5.7) at the time of writing has been submitted for review. It is therefore appropriate to clarify both authors' contributions to these manuscripts.

The first author proposed the ideas of using APFOA for the analysis of *N*-methylcarbamates by MEKC-ESI-MS (Chapter 2), and of determining the effect of the spacer on the selectivity of dimeric surfactants in MEKC (Chapters 3-5). Dr. C. S. Bottaro suggested using an experimental design for optimization of the instrumental parameters (Chapter 2).

All experimental work was performed by the first author. This includes the synthesis and purification of dimeric surfactants (and intermediate products), their analysis (¹H-NMR, ESI-MS, CMC determination), and all CE analysis. The first author also performed all data analysis with some input from Dr. C. S. Bottaro in the interpretation of ¹H-NMR spectra.

Finally, the first author prepared all manuscripts and replies to reviewers, with editing by Dr. C. S. Bottaro.

1.8. References

- [1] H.J. Issaq, *J. Liq. Chromatogr. Relat. Technol.* 25 (2005) 1153
- [2] P. Camilleri (Ed.), *Capillary electrophoresis – theory and practice*, CRC Press (1998)
- [3] R. Kuhn, S. Hoffstetter-Kuhn, *Capillary electrophoresis: principles and practice*, Springer-Verlag (1993)
- [4] O. Vesterberg, *J. Chromatogr.* 480 (1989) 3
- [5] C.F. Poole, *The essence of chromatography*, Elsevier (2003)
- [6] R. Weinberger, *Practical capillary electrophoresis*, Academic Press, San Diego, CA (2000)
- [7] R. Virtanen, *Zone electrophoresis in a narrow-bore tube employing potentiometric detection – a theoretical and experimental study*, *Acta Polytechnica Scandinavia* 123 (1974)
- [8] J.W. Jorgenson, K.D. Lukacs, *Anal. Chem.* 53 (1981) 1298
- [9] S. Terabe, K. Otsuka, K. Itchikawa, A. Tsuchiya, T. Ando, *Anal. Chem.* 56 (1984) 111
- [10] K.D. Altria, D. Elder, *J. Chromatogr. A* 1023 (2004) 1
- [11] T. Dallas, P.K. Dasgupta, *Trends Anal. Chem.* 10 (2004) 385
- [12] J.P. Schaeper, M.J. Sepaniak, *Electrophoresis* 21 (2000) 1421
- [13] C.M. Boone, G. Manetto, F. Tagliaro, J.C.M. Waterval, W.J.M. Underberg, J-P. Franke, R.A. de Zeeuw, K. Ensing, *Electrophoresis* 23 (2002) 67
- [14] N.A. Guzman (Ed.), *Capillary Electrophoresis Technology*, *Chromatographic Science Series Volume 64*, Marcel Dekker Inc., New York (1993)

- [15] U. Pyell (Ed.), *Electrokinetic Chromatography – Theory, Instrumentation & Applications*, Wiley, West Sussex, England (2006)
- [16] D.R. Lide (Ed.), *CRC Handbook of Chemistry and Physics*, 84th Edition (2003-2004), CRC Press (2003)
- [17] P. Atkins, J. de Paula, *Physical Chemistry*, Seventh Ed., W.H. Freeman and Company, New York (2002)
- [18] W. Friedl, J.C. Reijenga, E. Kenndler, *J. Chromatogr. A* 709 (1995) 163
- [19] D.C. Harris, *Quantitative Chemical Analysis*, Sixth Ed., W.H. Freeman and Company, New York, 2003
- [20] J.H. Knox, *Chromatographia* 26 (1988) 329
- [21] K.M. Hutterer, J.W. Jorgenson, *Anal. Chem.* 71 (1999) 1293
- [22] X. Huang, W.F. Coleman, R.N. Zare, *J. Chromatogr.* 480 (1989) 95
- [23] C.A. Lucy, T.L. McDonald, *Anal. Chem.* 67 (1995) 1074
- [24] M.Urbánek, L. Krivánková, P. Boček, *Electrophoresis* 24 (2003) 466
- [25] R.-L. Chien, *Electrophoresis* 24 (2003) 486
- [26] D.M. Osbourn, D.J. Weiss, C.E. Lunte, *Electrophoresis* 21 (2000) 2768
- [27] Z. Malá, L. Krivánková, P. Gebauer, P. Boček, *Electrophoresis* 28 (2007) 243
- [28] D.S. Burghi, R.-L. Chien, *Anal. Chem.* 63 (1991) 2024
- [29] D.S. Burghi, R.-L. Chien, *Anal. Chem.* 64 (1992) 1046
- [30] J. P. Quirino, S. Terabe, *Science* 282 (1998) 465
- [31] J. P. Quirino, J.-B. Kim, S. Terabe, *J. Chromatogr. A* 965 (2002) 357
- [32] J. P. Quirino, S. Terabe, *Anal. Chem.* 71 (1999) 1638
- [33] S. Terabe, K. Otsuka, T. Ando, *Anal. Chem.* 57 (1985) 834

- [34] T. Watanabe, S. Terabe, *J. Chromatogr. A* 880 (2000) 311
- [35] J.P. Foley, *Analyst* 116 (1991) 1275
- [36] G.L. McIntyre, *Crit. Rev. Anal. Chem.* 21 (1990) 257
- [37] R. Zana, *Langmuir* 12 (1996) 1208
- [38] C.F. Poole, S.K. Poole, *J. Chromatogr. A* 792 (1997) 89
- [39] C.F. Poole, S.K. Poole, *J. Chromatogr. A* 792 (1997) 89
- [40] P. Mukerjee, J.-S. Ko, *J. Phys. Chem.* 96 (1992) 6090
- [41] M. Aamodt, M. Landgren, B. Jönsson, *J. Phys. Chem.* 96 (1992) 945
- [42] M.D. Trone, M.G. Khaledi, *Anal. Chem.* 71 (1999) 1277
- [43] J.A. Olivares, N.T. Nguyen, C.R. Yonker, R.D. Smith, *Anal. Chem.* 59 (1987) 1230
- [44] P. Kebarle, L. Tang, *Anal. Chem.* 65 (1993) 972
- [45] A. von Brocke, G. Nicholson, E. Bayer, *Electrophoresis* 22 (2001) 1251
- [46] P. Schmitt-Koppling, M. Frommberger, *Electrophoresis* 24 (2003) 3837
- [47] S.A. Shamsi, B.E. Miller, *Electrophoresis* 25 (2004) 3927
- [48] E. Gelpi, *J. Mass Spectrom.* 37 (2002) 241
- [49] S.A. Shamsi, *Electrophoresis* 23 (2002) 4036
- [50] J. Zheng, M.W. Jann, Y.Y. Hon, S.A. Shamsi, *Electrophoresis* 25 (2004) 2033
- [51] Y.-R. Chen, M.-C. Tseng, Y.-Z. Chang, G.-R. Her, *Anal. Chem.* 75 (2003) 503
- [52] P. Petersson, M. Jörntén-Karlsson, M. Stålebro, *Electrophoresis* 24 (2003) 999
- [53] K.L. Rundlett, D.W. Armstrong, *Anal. Chem.* 68 (1996) 3493
- [54] M.-C. Tseng, Y.-R. Chen, G.-R. Her, *Anal. Chem.* 76 (2004) 6306
- [55] Z. Cai, E.N. Fung, A.K. Sinhababu, *Electrophoresis* 24 (2003) 3160

- [56] S. Xia, L. Zhang, P. Tong, M. Lu, W. Liu, G. Chen, *Electrophoresis* 28 (2007) 3268
- [57] E.D. Lee, W. Mück, J.D. Henion, T.R. Covey, *Biol. Mass. Spectrom.* 18 (2005) 253
- [58] H.L. Cheng, M.-C. Tseng, P.-L. Tsai, G.-R. Her, *Rapid Commun. Mass Spectrom.* 15 (2001) 1473
- [59] G.W. Somsen, R. Mol, G.J. de Jong, *J. Chromatogr. A* 1000 (2003) 953
- [60] H. Ozaki, S. Terabe, *J. Chromatogr. A* 794 (1998) 317
- [61] L.K. Amundsen, J.T. Kokkonen, S. Rovio, H. Siren, *J. Chromatogr. A* 1040 (2004) 123
- [62] M. Frommberger, P. Schmitt-Koppling, F. Menzinger, V. Albrecht, *Electrophoresis* 24 (2003) 3067
- [63] Y. Tanaka, K. Otsuka, S. Terabe, *J. Pharm. Biomed. Anal.* 30 (2003) 1889
- [64] R. Mol, G.J. de Jong, G.W. Somsen, *Anal. Chem.* 77 (2005) 5277
- [65] R. Juraschek, T. Dülcks, M. Karas, *J. Am. Soc. Mass Spectrom.* 10 (1999) 300
- [66] M. Vitha, P.W. Carr, *J. Chromatogr. A* 1126 (2006) 143
- [67] M.H. Abraham, C.F. Poole, S.K. Poole, *J. Chromatogr. A* 842 (1999) 79
- [68] M.J. Kamlet, J.L. Abboud, R.W. Taft, *J. Am. Chem. Soc.* 99 (1977) 6027
- [69] M.J. Kamlet, R.W. Taft, *J. Am. Chem. Soc.* 98 (1976) 377
- [70] R.W. Taft, M.J. Kamlet, *J. Am. Chem. Soc.* 98 (1976) 2886
- [71] J. Li, Y. Zhang, A.J. Dallas, P.W. Carr, *J. Chromatogr. A* 550 (1991) 101
- [72] P.C. Sadek, P.W. Carr, R.M. Doherty, M.J. Kamlet, R.W. Taft, M.H. Abraham, *Anal. Chem.* 57 (1985) 2971

- [73] D.E. Leahy, P.W. Carr, R.S. Pearlman, R.W. Taft, M.J. Kamlet, *Chromatographia* 21 (1986) 473
- [74] M.H. Abraham, J.C. McGowan, *Chromatographia* 23 (1987) 243
- [75] M.H. Abraham, A. Ibrahim, A.M. Zissimos, *J. Chromatogr. A* 1037 (2004) 29
- [76] M.H. Abraham, *Chem. Soc. Rev.* (1993) 73
- [77] S.K. Poole, C.F. Poole, *Analyst* 122 (1997) 267
- [78] S. Schulte, C.P. Palmer, *Electrophoresis* 24 (2003) 978
- [79] C. Akbay, R.A. Agbaria, I.M. Warner, *Electrophoresis* 26 (2005) 426
- [80] M.D. Trone, M.G. Khaledi, *J. Chromatogr. A* 886 (2000) 245
- [81] E. Fuguet, C. Ràfols, E. Bosch, M.H. Abraham, M. Rosés, *Electrophoresis* 27 (2006) 1900
- [82] C.F. Poole, S.K. Poole, M.H. Abraham, *J. Chromatogr. A* 798 (1998) 207
- [83] J.D. Weckwerth, M.F. Vitha, P.W. Carr, *Fluid Phase Equilib.* 183-184 (2001) 143
- [84] Y. Ishihama, H. Katayama, N. Asakwa, *Anal. Biochem.* 287 (2000) 45
- [85] H. Harino, M. Tanaka, T. Araki, Y. Yasaka, A. Masuyama, Y. Nakatsuji, I. Ikeda, K. Funazo, S. Terabe, *J. Chromatogr. A* 715 (1995) 135
- [86] H. Harino, Y. Inoue, J. Yoshioka, S. Tsunoi, M. Eguchi, Y. Yasaka, K. Funazo, M. Tanaka, *J. Chromatogr. A* 755 (1996) 147

Chapter 2

Ammonium Perfluorooctanoate as a Volatile Surfactant for the Analysis of *N*-Methylcarbamates by Micellar Electrokinetic Chromatography – Electrospray Ionization – Mass Spectrometry^{1,2}

¹ G. Van Biesen, C.S. Bottaro, *Electrophoresis* 27 (2006) 4456

² Additional information can be found in Appendix 1

Abstract

Ammonium perfluorooctanoate (APFOA) was investigated as an MS-friendly surfactant for the analysis of a mixture of 10 *N*-methylcarbamates with MEKC-ESI-MS. Because of its relatively low boiling point (~ 190 °C), APFOA can be introduced into a mass spectrometer without the adverse effects of less volatile surfactants such as SDS. With a BGE consisting of 50 mM APFOA/isopropanol (IPA) 98/2 and with 30 kV applied, a very fast separation (~6 min) was possible with only one pair of analytes co-migrating. Using an experimental design with four factors (voltage, nebulizer pressure, concentration of APFOA, and concentration of IPA) we were able to resolve all analytes in just over 11 min. Sheath liquid composition and flow rate, drying gas temperature and flow rate, and fragmentor voltage were then optimized for maximum signal intensity and S/N. It was found that the faster method gave better S/N because of narrower peak widths, and detection limits in SIM mode were between 0.01 (aldicarb) and 0.08 mg/L (methomyl). Calibration curves were prepared with standards of 0.50, 1.00, and 2.00 mg/L for the analysis of samples obtained after solid phase extraction (SPE) of tap water spiked with the 10 *N*-methylcarbamates at a level of 10 µg/L. All analytes showed very good recoveries (> 86%), except for the most polar analyte aldicarb sulfone (recovery of 73%). The work presented here testifies for the use of APFOA as a surfactant in MEKC-ESI-MS.

2.1. Introduction

The hyphenation of CE and MS has been an area of active research, and several good overview articles describing interfaces and applications have been published [1-3]. While CZE-MS is now considered to be an established technique for the analysis of small charged molecules [1], analysis of neutral molecules by MEKC-MS is yet to find widespread application. The main reason is that with ESI, the most popular ionization method for CE-MS, commonly used surfactants (e.g. SDS) and buffers (e.g. tetraborate, phosphate) can cause analyte signal suppression and contamination of the mass spectrometer [1, 4-9]. For instance, Cheng et al. [6] analyzed 16 synthetic drugs, and found that with SDS concentrations higher than 20 mM the response for most analytes was less than 30% of the response when no SDS was present. Somsen et al. [7] used SDS and non-volatile buffers for the analysis of mebeverine and related compounds with MEKC-ESI-MS. Although analyte signals were significantly suppressed, they still had satisfactory detection limits of about 1 $\mu\text{g/mL}$ using extracted ion chromatograms, and below 100 ng/mL when SIM was used. However, they did notice a gradual decrease in absolute peak intensity during the course of one day (10 injections), due to fouling of the ion source. The sensitivity could be restored by cleaning the first part of the ion source (a 5-min procedure), but after a full week of intensive use, the complete ion source had to be cleaned to restore optimal MS performance.

In order to prevent these problems, the typical approach has been to avoid micelles from entering the mass spectrometer, and several techniques have been applied with varying degrees of success. In the partial filling technique [4, 9-11], the capillary is

initially filled with BGE that contains no SDS micelles. Then, BGE with micelles is injected so that the capillary contains a micelle plug on the inlet side. When the sample is injected and voltage is applied, the EOF pushes the analytes through the micelle plug, where they are retarded depending on their affinity for the micelles, and separated. When the analytes reach the SDS-free background electrolyte, they all migrate to the detector at the same velocity as the EOF. Although the EOF also causes the micelles to migrate towards the detector, they do so at a lower velocity because they are negatively charged and are attracted to the anode (at the inlet). The analysis is stopped before the micelles get a chance to reach the detector. Because of the relatively short surfactant zone and an extra band-broadening mechanism at the micelle zone – buffer interface, the resolution is lower than for normal MEKC. A further complication is that it is also possible that monomers of the surfactant reach the detector, since the micelles slowly break down during the analysis and migrate as surfactant monomers, which have a lower effective mobility than micelles (i.e. they move faster towards the detector) [9]. Molina et al. [4] found it therefore necessary to decrease the SDS concentration from 40 to 20 mM, at the expense of the resolution. Another way of preventing micelles from entering the mass spectrometer is to change their electrophoretic velocity, so that they migrate towards the anode. Yang et al. [12] used reverse migrating micelles for the analysis of triazine herbicides and barbiturates. They lowered the pH of the BGE so that the EOF was slightly lower than the electrophoretic velocity of the micelles, which now moved towards the anode. For both classes of analytes, they experienced a decrease in separation efficiency as compared to a similar MEKC-UV method, which again can be attributed to the moving SDS boundary. In addition, compounds that are strongly retained by the micelles can migrate away from

the detector and thus are not detected [4]. High molecular weight surfactants, such as the sodium salt of butyl acrylate – butyl methacrylate – methacrylic acid copolymer (MM – 40,000) have also been used in MEKC-ESI-MS [13]. These surfactants have an effective CMC of zero, and can in principle be used at very low concentrations. However, significant signal suppression was observed at concentrations as low as 0.5%, and higher concentrations than this were needed to improve the resolution of the mixtures analyzed.

Somewhat surprisingly, the use of ‘MS-friendly’ surfactants is largely unexplored. These are surfactants that are volatile enough that they can be introduced into the mass spectrometer without significantly diminishing its performance. Ishihama et al. [14] were the first to report on the use of fluorinated surfactants (PFOA and perfluorooctanesulfonic acid) in ESI-MS. Petersson et al. [5] evaluated ammonium salts of lauric acid, cholic acid and a series of perfluorated carboxylic acids (perfluorododecanoic, -nonanoic, -octanoic, -heptanoic, and -hexanoic acid) for MEKC-ESI-MS. Lauric acid formed opaque solutions directly after preparation, or after a few hours, and was not investigated any further. Likewise, most of the perfluorocompounds had solubility or purity issues, and eventually only PFOA and cholic acid were selected for further experiments. PFOA gave the best overall results, although its selectivity was quite different from that of SDS. Its CMC, as determined by surface tension measurements, was 12 mM, compared to 8 mM for SDS. Infusion experiments did not reveal any significant differences in signal intensities of analytes between the ammonium salts of acetic acid and PFOA for concentrations up to 100 mM. This was explained by the relatively low boiling point (~ 190 °C) and low surface tension (19 mN/m) of PFOA, which facilitates the electrospray process. In

comparison, SDS, for which a severe suppression of the analyte signal was observed, has a boiling point > 320 °C, and a surface tension of 34 mN/m.

Recently, Goetzinger and Cai [15] reported on the use of lauric acid and cholic acid in combination with NH₄OH or an organic base as alternative surfactant systems for SDS. In contrast to Petersson et al. [5], they did not seem to have solubility issues with lauric acid, possibly because their solutions were less concentrated (50 mM as opposed to 100 mM). Most of their article deals with CE-UV, although the authors recognize the applicability to MEKC-ESI-MS and show some preliminary results.

The alternative ionization methods atmospheric pressure chemical ionization (APCI) and atmospheric pressure photoionization (APPI) do not seem to suffer from the disadvantages encountered in ESI, but relatively little research with CE has been done so far [1, 16-17].

The results of the analysis of a mixture of 10 *N*-methylcarbamates by MEKC-ESI-MS with APFOA as surfactant are presented here. *N*-methylcarbamates are pesticides used extensively for crop protection. These were selected because our lab is generally interested in environmental contaminants, and because they have been analyzed previously by MEKC-ESI-MS (partial filling technique and reverse migrating micelles) [4] with SDS as surfactant. This allows for a comparison between different methods. First, CE-UV with SDS was used to resolve this particular mixture, which was relatively straightforward. The separation with MEKC-ESI-MS with APFOA as surfactant proved to be more complicated, and an experimental design type of approach was necessary to resolve the 10 analytes. The sheath liquid composition and various instrumental settings

were optimized to obtain maximum sensitivity. Instrumental detection limits were established in scan and SIM mode, and spiked water samples were analyzed after SPE.

2.2. Materials and Methods

2.2.1. Chemicals

PFOA (96%) was purchased from Aldrich. Stock solutions of BGE at pH 9.0 were prepared by dropwise addition of ammonium hydroxide (~10 drops, 14.8 M, ACS grade, Fisher Scientific) to a stirred solution of 1035 mg PFOA and ~22 mL of ultrapure water (18.2 M Ω .cm, Barnstead Nanopure Diamond filtration system), while continuously monitoring the pH. After dissolving, the solution was transferred to a 25 mL volumetric flask, made up to volume, and filtered through a 0.2 μ m nylon filter (National Scientific Company). The first 2-3 mL of filtered solution were discarded to condition the filter. BGE of desired concentration was prepared by diluting the BGE stock solution with ultrapure water and adjusting the pH to 9.0 with dilute ammonium hydroxide, if necessary.

Methanol (MeOH), acetonitrile (ACN), tetrahydrofuran (THF) and isopropanol (IPA) were obtained from various suppliers, and were all ACS grade. Pesticide standards were obtained from Chem Service (West Chester, PA, USA). CP-8318-2M was a mixture of aldicarb, aldicarb sulfone, propoxur, carbaryl, carbofuran, dioxacarb, 3-hydroxy carbofuran, methiocarb, methomyl, and promecarb at 1000 μ g/mL each in ACN. CP-8318S consisted of ACN or MeOH solutions of each of the above compounds, as well as oxamyl and aldicarb sulfoxide, as neat standards at 100 or 1000 μ g/mL. Samples were

prepared by transferring the appropriate amount of *N*-methylcarbamate mixture or pure standard to a CE-vial, blowing to dryness with nitrogen, and adding ultrapure water (and ~1% of ACN as EOF marker for CE-UV experiments) to obtain the desired concentration. Solutions at concentrations lower than 20 mg/L were prepared by serial dilution. Thiourea, used as an EOF marker in some of the CE-MS experiments [21], was purchased from Fisher (Certified Reagent) and was added to the samples at a final concentration of 40 mg/L.

2.2.2. Instrumentation

All experiments were performed on an Agilent ^{3D}CE system (Agilent Technologies Canada Inc., Mississauga, Ontario). For CE-UV experiments, 64.5 cm (56 cm to the detector) long capillaries with an ID of 50 μ m with an extended light path of 150 μ m (Agilent Technologies) were used. For the CE-ESI-MS experiments, the mass spectrometer (Agilent 1100 series MSD) was coupled to the CE system via an electrospray (coaxial sheath flow) interface. The nebulizer gas and drying gas were both nitrogen. The sheath liquid was delivered with an Agilent 1100 series isocratic pump in conjunction with a 1:100 splitter. Bare fused-silica capillaries (ID 50 μ m, OD 360 μ m) were purchased from MicroSolv (MicroSolv Technology Corporation, NJ, USA) and were cut to desired length. Approximately 2 mm of polyimide at the beginning and at the end of the capillaries was removed using the MicroSolv Window MakerTM. Capillaries were installed in the cassette in such a way that the DAD was bypassed. This allowed for the capillaries to be cut to a length between 60 and 67 cm, compared to the usual ~85 cm

that is needed when the DAD is also used. Minimizing capillary length leads to maximal electrical fields and thus faster separations.

The capillaries were conditioned at the beginning of each day by flushing (~ 930 mbar) with either NaOH 0.1 M (CE-UV) or ammonium hydroxide 14.8 M (MEKC-ESI-MS) for 15 minutes, pausing for 5 minutes, and then flushing with ultrapure water, followed by running buffer for 5 minutes each. Between runs, the capillaries were generally flushed with BGE for 2 minutes, and occasionally with NaOH 0.1 M (CE-UV) or ammonium hydroxide 14.8 M (MEKC-ESI-MS) for 1 minute followed by ultrapure water for 2 minutes and BGE for 4 minutes. The capillary temperature was set at 24 °C (ambient temperature). Other instrumental settings varied dependent on the experiment.

Data processing such as calculation of peak areas, peak widths, peak heights, and S/N (peak heights divided by six times the standard deviation of the baseline between 2.0 and 3.0 minutes) was performed with Chemstation software (Rev. A.08.03).

2.2.3. Solid Phase Extraction

C18-bonded SPE cartridges were obtained from Alltech (Extract-Clean Columns, High Flow C18, 500 mg, Alltech associates Inc., Deerfield, Illinois, USA). They were conditioned with 5 mL of methanol, followed by 5 mL of ultrapure water, pushed through the cartridge at a flow of ~ 2 mL/min by applying slight pressure with pressurized nitrogen. Volumes of 25 mL of tap water were spiked at a 10 µg/L level with the *N*-methylcarbamate mixture, and pushed through the cartridge at a flow of ~2 mL/min. The cartridge was then rinsed with 2 mL of ultrapure water and blown dry with nitrogen for

15 min. The analytes were eluted with 3 mL of ACN, followed by 3 mL of MeOH, and evaporated to dryness under a gentle stream of nitrogen on a waterbath at 30 – 40 °C. They were quantitatively transferred to a sample vial by redissolving in ACN, and stored at 4 °C until analysis 1 or 2 days later. Just before analysis, the samples were transferred to a CE vial, blown dry with nitrogen, and redissolved in 250 µL of ultrapure water by vortex mixing for 20 seconds.

2.3. Results and Discussion

2.3.1. MEKC-UV experiments

Mixtures of various *N*-methylcarbamates have been separated by MEKC with SDS as surfactant by several authors [4, 18-21]. Therefore, we decided to first use SDS, and compare the separation with APFOA. For this particular mixture, a BGE consisting of 40 mM SDS with 10 mM NH₄Ac at pH 9.0 provided baseline separation of all analytes in less than 9 minutes (Fig. 2.1). Peaks were identified by running individual standards under the same conditions and comparing migration times and UV spectra.

With APFOA as surfactant at a concentration of 50 mM, 2 analytes co-migrate (Fig. 2.2a). The large dip around 5.8 minutes was eliminated by dissolving the sample in BGE (Fig. 2.2b), and the application of a lower voltage increases the migration time window, although the separation is basically unaffected. In either case, the migration order is clearly different from that with SDS, indicating the different selectivity of these two surfactant systems [5]. The selectivity of analytes towards surfactants can be rationalized in terms of linear solvation energy

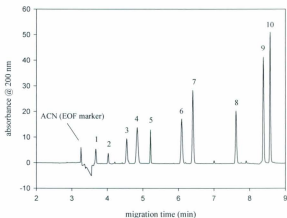


Fig. 2.1: Electropherogram of the *N*-methylcarbamate mixture (20 mg/L in water/ACN 99:1). BGE: 40 mM SDS and 10 mM NH_4Ac at pH 9.0; applied voltage: 30 kV; injection 20 mbar for 10 s; detection wavelength: 200 nm. Peaks: 1, aldicarb sulfone; 2, methomyl; 3, dioxcarb; 4, 3-hydroxy carbofuran; 5, aldicarb; 6, propoxur; 7, carbofuran; 8, carbaryl; 9, promecarb; 10, methiocarb.

relationships [22-25], and the literature indicates that perfluorinated surfactants are stronger hydrogen-bond acids, weaker hydrogen-bond bases, have a higher dipolarity, but are less polarizable than non-fluorinated surfactants.

A comparison between Figs. 2.1 and 2.2 shows that the baseline is a lot noisier with APFOA as surfactant than with SDS. This is because APFOA has a strong absorption at the detection wavelength of 200 nm (Fig. 2.3). Petersson et al. [5]

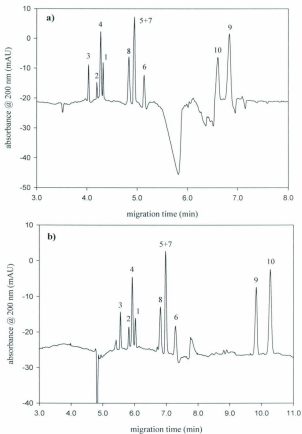


Fig. 2.2: Electropherogram of the *N*-methylcarbamate mixture at 20 mg/L. BGE: 50 mM APFOA at pH 9.0. **a)** sample in water/ACN 99/1, 30 kV applied; **b)** sample in BGE, 24 kV applied. Other conditions and peak identification: see Fig. 1.

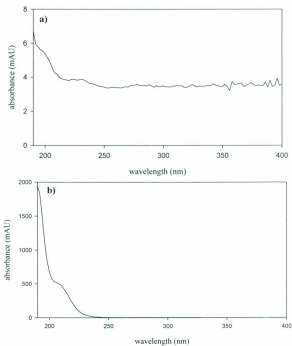


Fig. 2.3: UV spectra of **a)** 100 mM SDS and **b)** 100 mM APFOA. The spectra were measured using the DAD of the CE instrument. Note the different absorbance scales.

expected higher noise when running samples in APFOA compared to SDS, since carboxylic acids have a higher UV cut-off than sulfonic acids. However, in their experiments they did not detect a higher noise and attributed this to the lower sensitivity of their UV detector. Clearly, this was not the case here, and we found this unstable

baseline to be a disadvantage of APFOA when using an extended light path capillary and a detection wavelength lower than ~ 230 nm.

Attempts were made to resolve all 10 analytes by first increasing the APFOA concentration (up to 100 mM), and also by adding different amounts of ACN or MeOH (up to 25%) to the BGE, but we were unsuccessful. It was observed, however, that several peaks changed position when ACN or MeOH were added, but it was sometimes hard to identify peaks based solely upon the UV-spectrum. At this point, we found it more useful to switch to MEKC-ESI-MS, which was the main focus of our research, and allows for unambiguous identification of peaks.

2.3.2. MEKC-ESI-MS experiments

2.3.2.1. Optimization of the separation

For comparison with the MEKC-UV experiments, the same conditions as in Fig. 2.2b (50 mM APFOA at pH 9.0, no organic modifier, and 24 kV) were applied initially. The nebulizer flow was set at a low value of 4 L/min (see further), and the capillary was approximately the same length (~ 64 cm). Other variables can influence the sensitivity, but are not expected to influence the separation as such. Their settings were chosen based upon our own experience and the literature, and provided high enough sensitivity to perform the optimization of the resolution (Table 2.1). Total ion electropherograms (TIEs) were collected from m/z 75 – 300, and extracted ion electropherograms (EIEs) were constructed from basepeaks. The base peaks were typically protonated molecular ions, except for dioxacarb, methomyl, propoxur and aldicarb, for which the basepeaks

Table 2.1: Conditions and instrumental settings used to optimize the separation of the *N*-methylcarbamate mixture.

Sheath Liquid composition	5 mM NH ₄ Ac in H ₂ O/MeOH 50:50
Sheath Liquid flow rate	4 µL/min
Sprayer voltage	3.5 kV
Fragmentor voltage	65 V
Drying gas (N ₂) temperature	250 °C
Drying gas flow rate	10 L/min
Capillary position	+2 marks (i.e. protrudes -0.2 mm from the sprayer needle)
Injection	10 s @ 20 mbar, followed by 10 s @ 20 mbar BGE
Scan range	m/z 75-300
Collection rate	0.41 cycles/s
Extracted ions	167 (dioxacarb), 88 (methomyl), 238 (3-OH carbofuran), 223 (aldicarb sulfone), 116 (aldicarb), 202 (carbaryl), 222 (carbofuran), 168 (propoxur), 208 (promecarb), 226 (methiocarb), 77 (thiourea)

were protonated fragments. It is known that *N*-methylcarbamates easily lose methyl isocyanate [26-27], which gives a fragment with an *m/z* of $[M + H - 57]^+$, which can undergo further fragmentation.

Under these conditions, the separation is comparable to the one with MEKC-UV, with a few notable exceptions (Fig. 2.4). Peaks 1 and 4 now co-migrate, while there is considerable overlap between peaks 9 and 10. On the other hand, peaks 5 and 7 now only partially overlap. A decrease in resolution when using a coaxial sheath-flow interface can be caused by band-broadening because of diffusion at the capillary tip where the sheath liquid and the BGE are mixed [12]. Also notice that the migration times are much shorter than for CE-UV, indicating that another factor is contributing to the mobility of the analytes, presumably the nebulizer gas flow. This can also negatively impact the resolution. Even with MS detection, where overlapping peaks are often not really a problem for identification or quantification, we found it worthwhile trying to resolve all analytes, because migration time (or effective mobility) can be used as further means of

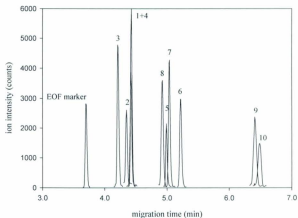


Fig. 2.4: Extracted Ion Electropherogram of the *N*-methylcarbamate mixture (20 mg/L in water). BGE: 50 mM APFOA at pH 9.0, 24 kV applied. See Table 1 for other conditions, and Fig. 1 for peak identification.

identification.

We used APFOA concentrations of 50, 75 and 100 mM, and added MeOH, ACN, THF or IPA at 1.0, 2.0, 2.5, 5.0, 10 and 20%, but were not able to achieve a complete separation. The best result was obtained with a BGE of 50 mM APFOA/IPA 98/2, with only 2 peaks co-migrating (Fig. 2.5). Given the number of variables involved in the optimization of the resolution, it was decided that a more structured approach was necessary, and an experimental design was set up in MinitabTM. Experimental designs have been extremely useful for method development and studying interaction effects in

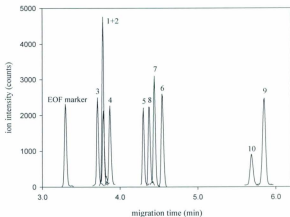


Fig. 2.5: Extracted Ion Electropherogram of the *N*-methylcarbamate mixture (20 mg/L in water). BGE: 50 mM APFOA at pH 9.0/IPA 98/2. 30 kV applied. See Table 1 for other conditions, and Fig. 1 for peak identification.

CE. Different kinds of designs are possible, such as full factorial [28-29], fractional factorial [30], central composite [29], and Box-Behnken [31]; the choice mainly depends on the number of factors of interest, the number of runs that can be performed, and how thoroughly the experimental region of interest must be covered [32]. We chose a central composite face centered design, which ensures that runs do not have to be performed at factor settings that are beyond the maximum or minimum settings chosen. Four factors that are known to significantly affect the resolution were studied at 3 levels (Table 2.2). We kept the pH at 9.0, since the APFOA system is buffered around pH 9.25 (pK_a of NH_4^+). This also ensures a relatively fast analysis since there is a strong EOF. The 10 *N*-methylcarbamates are neutral at this pH. This was confirmed experimentally by running a

Table 2.2: Factors that influence the separation, and the levels at which they were studied in the experimental design.

Factor	Levels
Separation Voltage (kV)	18 - 24 - 30
[APFOA] (mM)	55 - 70 - 85
[IPA] (%)	1.0 - 3.0 - 5.0
Nebulizer Pressure (psi)	2 - 5 - 8

sample in 10 mM APFOA (i.e. below the critical micelle concentration of ~12 mM) at pH 9.0. Under these conditions, all analytes co-migrated with the EOF-marker.

Since the preliminary experiments indicated that complete resolution was not possible with only 50 mM APFOA, the lowest APFOA concentration permitted was set slightly higher at 55 mM. The upper limit set was 85 mM, since at this concentration, the current in a 60 cm capillary is approximately 70 μ A when 30 kV is applied, which is already well above the recommended maximum of 50 μ A [33]. Joule heating at high currents can result in band-broadening [34], especially in CE-MS, where most of the capillary is outside of the CE instrument and thus not temperature controlled.

The lower limit of the voltage was set at 18 kV, to ensure reasonable migration times for even the highest APFOA concentration, while the highest limit was 30 kV (maximum setting for the instrument).

The type and concentration range of organic modifier was determined using data from the preliminary experiments. The effective mobilities of the analytes were calculated for each organic modifier (MeOH, ACN, THF, and IPA) and plotted against the concentration. In each case, it proved to be difficult to find a concentration for which

there was a clear difference in effective mobilities of all 10 analytes, but eventually IPA was selected. For the experimental design, we finally chose a minimum of 1% and a maximum of 5% IPA in the BGE.

With the Agilent system, the nebulizer flow creates a suction force at the capillary outlet and introduces a laminar flow inside the capillary, thereby increasing the apparent mobilities of analytes [28, 30, 35-36]. While this can be advantageous in speeding up the analysis, this also decreases the resolution, and for critical resolutions a low nebulizer flow might be necessary. Therefore, we chose a minimum of 2, and a maximum of 8 psi. A high nebulizer flow can also have unexpected effects. In our very first experiments with 65 cm capillaries we used a nebulizer flow of 10 psi. However, we often encountered breakdown of the current. This could eventually be traced back to air being drawn into the capillary during changing of the vials in the autosampler. Presumably, for such a short capillary, the suction with the nebulizer gas at 10 psi can be strong enough to move the whole column of fluid inside the capillary and draw in air while the vials are being changed. This problem was easily avoided by programming the nebulizer flow to 2 psi during the injection sequence, and changing it to its operating value once the run had started.

After choosing the type of experimental design, MinitabTM automatically generates the run conditions for the experiments that have to be performed (28 in this case). The responses to be optimized were the resolutions between peak pairs that were most likely to overlap (Table 2.3). We also included the migration time of the last migrating peak, since we wanted the analysis to be as fast as possible, and the current, as

it was preferred that the current was lower than 50 μ A, in order to prevent too much heat generation.

Table 2.3: Optimized responses in the experimental design. Rs1 – Rs9 are the resolutions between peak pairs.

Response		Goal	Target	Limit
Rs1	dioxacarb – aldicarb sulfone	max.	3.0	1.5
Rs2	dioxacarb - methomyl	max.	3.0	1.5
Rs3	aldicarb sulfone - methomyl	max.	3.0	1.5
Rs4	aldicarb sulfone – 3-hydroxycarbofuran	max.	3.0	1.5
Rs5	methomyl – 3-hydroxycarbofuran	max.	3.0	1.5
Rs6	aldicarb – carbaryl	max.	3.0	1.5
Rs7	carbaryl – carbofuran	max.	3.0	1.5
Rs8	carbofuran – propoxur	max.	3.0	1.5
Rs9	methiocarb - promecarb	max.	3.0	1.5
t	migration time last migrating analyte	min.	8	12
i	current	min.	30	50

The multiple responses from Table 2.3 were optimized using the Minitab™ ‘desirability’ function. The desirability of a particular response is expressed as a value between 0.0 (undesirable response) and 1.0 (highly desirable response) [32]. The optimum conditions generated by the program were: a separation voltage of 25.8 kV, a nebulizer pressure of 2.4 psi, and concentrations of APFOA and IPA of 78.7 mM and 2.9% respectively. However, the nebulizer pressure can only be changed by increments of 1, and so other conditions had to be sought that would still give a satisfactory separation. This is conveniently done with the separation dashboard (Fig. 2.6) that is automatically generated after the search for the optimum conditions, by putting in new values for a factor and see how the responses change. New optimal conditions were: a separation voltage of 23.5 kV, a nebulizer pressure of 4 psi, and concentrations of APFOA and IPA

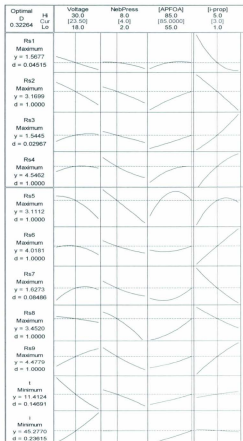


Fig. 2.6: Separation dashboard showing the influence of each of the factors (top line, with maximum, optimized, and minimum settings respectively from top to bottom) on the responses (left column, with y: predicted respons, and d: desirability). See text for further explanation.

of 85.0 mM and 3.0% respectively. These conditions were such that the 3 most critical resolutions (Rs1, Rs3, and Rs7) slightly increased compared to the previous settings, at the expense of some of the resolutions of less critical pairs. Note that the 'desirability' of some of the responses is rather low (e.g. 0.04515 and 0.02967 for RS1 and RS3 respectively) (Fig. 2.6), because they are close to their lower limit of 1.5. Nevertheless, this was deemed sufficient for this separation.

The curved lines in Fig. 2.6 show how each response depends on each factor. For instance, the current (*i*) does not depend on the nebulizer pressure, but does increase with increasing voltage and APFOA concentration, and decreases slightly with increasing IPA concentration (bottom line), as expected. The separation voltage can have both a positive (curves with positive slope) and a negative (curves with negative slope) influence on the resolution, while some curves exhibit a maximum (e.g. Rs4 and Rs7). This is in contrast with the nebulizer pressure, for which all curves have a negative slope. A lower nebulizer pressure therefore always gives a better resolution. The trade-off is that at lower values, the analysis takes longer, and therefore we preferred the somewhat higher value of 4 psi. It is clear that the nebulizer exerts a suction effect at the capillary outlet, as mentioned before, since at higher pressures, the analysis time (*t*) decreases. A higher concentration of APFOA increases the resolution for most analyte pairs (for Rs5 there is a pronounced maximum, and Rs1 shows a less pronounced maximum). Since our optimal value (85 mM), is the maximum value used in the experimental design, this might indicate that we could have used an even higher concentration. On the other hand, with an applied voltage of 23.5 kV, the current is already 45 mA, close to the limit of 50 mA, and a higher concentration of APFOA also increases the analysis time. The concentration of IPA also

has a major influence on the resolution between peak pairs, as indicated by the very steep curves in the last column. As with the separation voltage, both positive and negative slopes are possible.

The values predicted by the model were verified experimentally and proved to be in good agreement (Table 2.4 and Fig. 2.7).

Table 2.4: Comparison between predicted and experimental values for resolutions (Rs), migration time of last analyte (t), and current (i).

	Predicted	Experimental (n=3)	% Difference
Rs1	1.57	1.43	-8.7
Rs2	3.17	3.02	-4.7
Rs3	1.54	1.59	3.2
Rs4	4.55	4.42	-2.8
Rs5	3.11	3.07	-1.2
Rs6	4.02	3.66	-9.0
Rs7	1.63	1.66	1.6
Rs8	3.45	3.46	0.2
Rs9	4.48	4.49	0.2
t	11.4	11.2	-2.0
i	45	45	0.0

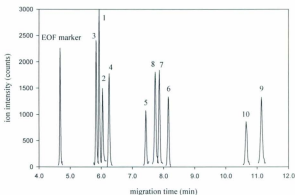


Fig. 2.7: Extracted Ion Electropherogram of the *N*-methylcarbamate mixture (20 mg/L in water). BGE: 85 mM APFOA at pH 9.0/IPA 97/3. 24.5 kV applied. See Table 1 for other conditions.

2.3.2.2. Optimization of the sensitivity

Several variables that are known to affect signal intensities and S/N were investigated independently (Table 2.5) [36]. These experiments were performed with a simpler mixture of 3 *N*-methylcarbamates (aldicarb, dioxacarb and propoxur) as model compounds each at a concentration of 50 mg/L in water, except for those to determine the influence of the fragmentor voltage, which was examined for all 10 analytes at 20 mg/L.

The sheath liquid is typically a mixture of water and an organic modifier, and for positive ionization a protic organic modifier such as MeOH or IPA is preferred since this can aid in the formation of protonated analytes [29]. Peak areas and S/N increased with increasing organic modifier content, likely due to more efficient desolvation [36], and for

Table 2.5: Conditions and instrumental settings examined to optimize the sensitivity of the method, and final conditions chosen.

	Explored settings	Optimized settings
Sheath liquid composition:		
• Organic modifier	MeOH or IPA in water (50, 70 and 90%)	IPA/water 90/10
• Conc. of NH ₄ Ac	0.0, 2.5, 5.0, 20 mM	
• Conc. of acetic acid	0, 0.1, 0.5%	
Sheath liquid flow rate	3, 4, 5, 6 μ L/min	4 μ L/min
Fragmentor voltage	45, 55, 65, 75, 85 V	55 V
Drying gas temperature	250, 300, 350 °C	250 °C
Drying gas flow rate	5, 7.5, 10 L/min	5 L/min

the same organic modifier content, IPA gave higher peak areas and S/N than MeOH. The addition of acetic acid or NH₄Ac to a sheath liquid consisting of IPA/water 90/10 gave no further improvement.

As the fragmentor voltage affects ion transmission and fragmentation, it plays an important role in S/N and sensitivity. At 75 V or higher, considerable fragmentation resulted, with base peaks for most of the analytes being protonated fragments, not protonated molecular ions, and in general, peak areas for base peaks also decreased at these high fragmentor voltages. At 45 V, the peak areas for most of the analytes were lower because of less efficient ionization. Though 65 V also provided good results, a value of 55 V was eventually chosen, because of slightly higher peak areas, and because at this voltage a molecular ion, useful for diagnostic purposes, could still be clearly distinguished for aldicarb (although it was not the base peak). Compared to Table 2.1, which lists the extracted ions for the initial conditions, there were three changes. For dioxacarb and propoxur, the protonated molecular ions (m/z respectively 224 and 210) now had the highest intensities, and for aldicarb sulfone, the most intense peak was found at m/z 240, which represents the ammonium adduct of the molecular ion.

Drying gas temperature and flow control the evaporation of the BGE. At high drying gas temperature, increased fragmentation and lower base peak intensity was observed. For instance, for propoxur, the peak area of the base peak (molecular ion) at 350 °C was only 50% of the intensity at 250 °C, and for dioxacarb and aldicarb this was ~ 70% and 80% respectively. A similar effect was observed for increasing drying gas flow rates, and the best conditions were a flow rate of 5 L/min with a temperature of 250 °C.

For comparison, 3 runs were performed under the initial and optimized conditions. Improvements in peak areas were between a factor of 1.3 (aldicarb sulfone) and 5.7 (aldicarb), while for the S/N ratio this was between 1.4 (methomyl and 3-OH carbofuran) and 4.1 (aldicarb). However, with the BGE consisting of 50 mM APFOA/IPA 98/2 with 30 kV applied (which gave the best separation before the experimental design was performed, with only 2 analytes co-migrating – Fig. 2.5), we noticed that S/N were even better (Fig. 2.8). The reason for this seemed to be the shorter run time (~ 6 min.). This gives smaller peak widths, and consequently higher peaks, because there is less longitudinal diffusion. This was demonstrated by a closer examination of analyses performed with 85 mM APFOA/IPA 97/3 and 50 mM APFOA/IPA 98/2 (both with IPA/H₂O 90/10 as sheath liquid). On average, peak widths were 2.0 times smaller for the latter, while the S/N were on average 2.1 times higher. The peak areas, however, were the same, indicating that it is indeed the longer run time that erodes S/N, and not, for instance, signal suppression because of a higher surfactant concentration.

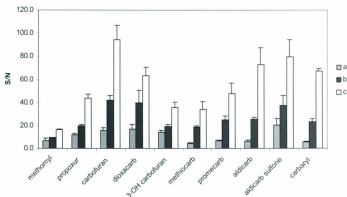


Fig. 2.8: Comparison of the S/N of the 10 *N*-methylcarbamates under different conditions.
 a) BGE 85 mM APFOA/IPA 97/3, sheath liquid 5 mM NH_4Ac in MeOH/ H_2O 50/50
 b) BGE 85 mM APFOA/IPA 97/3, sheath liquid IPA/ H_2O 90/10
 c) BGE 50 mM APFOA/IPA 98/2, sheath liquid IPA/ H_2O 90/10
 n = 3; error bars are 1 SD.

While the experimental design was extremely valuable in finding the conditions that would allow for a complete resolution of all analytes, it is not a substitute for analyst expertise. Given the shorter run time and the better S/N, we eventually preferred to use the BGE consisting of 50 mM APFOA/IPA 98/2, allowing for two peaks to co-migrate. In the next two sections, this BGE is used to establish detection limits and analyze spiked water samples.

2.3.2.3. Detection Limits

Detection limits ($S/N > 3$) were established using both extraction of ions from total ion electropherograms (m/z 75 to 300) and SIM. For samples dissolved in water, it was possible to increase the injected amount by applying a higher pressure for a longer time (15 s at 50 mbar instead of 10 s at 20 mbar) and maintaining the resolution. Quirino and Terabe [37] described this as normal stacking mode. However, high salt stacking [38] (with samples dissolved in 70 mM NH_4Ac) was not successful, and a further increase in sample loading was not possible without losing resolution. This is currently still under investigation.

The results when using scan mode (Table 2.6) are en par with Molina et al. [4], who analyzed 5 of the *N*-methylcarbamates with SDS with three different techniques: the partial filling technique, reverse migrating micelles, and reverse migrating micelles with coated capillaries (the range of detection limits for these three techniques is given in Table 2.6). They used the sum of the counts of characteristic fragments for each analyte for quantification, and also used high salt stacking, which allowed them to inject samples for 60 s at 5 kPa (50 mbar).

2.3.3. Analysis of spiked tap water

The practical applicability of the method is demonstrated with the analysis of tap water spiked with the *N*-methylcarbamate mixture at a level of 10 $\mu\text{g/L}$. The SPE provided a concentration step of 100x (25 mL \rightarrow 250 μL), and calibration curves were prepared in SIM mode with standards of 0.50, 1.00, and 2.00 mg/L. A blank and one

Table 2.6: Detection limits (mg/L) for the 10 *N*-methylcarbamates with a BGE consisting of 50 mM APFOA at pH 9.0/IPA 98/2, with 30 kV applied. Injection: 15 s at 50 mbar. Other conditions as in Table 2.5 (optimized settings).

For comparison, detection limits using SDS as surfactant (Molina et al.) are also reported. na: not analyzed

	Scan	SIM	Molina et al. [4]
methomyl	1.3	0.08	1.1 – 1.8
propoxur	0.2	0.03	0.1 – 0.2
carbofuran	0.1	0.02	0.07 – 0.1
dioxacarb	0.3	0.05	na
3-OH carbofuran	0.5	0.08	na
methiocarb	0.5	0.05	na
promecarb	0.3	0.05	na
aldicarb	0.2	0.01	0.4 – 0.5
carbaryl	0.2	0.02	0.04 – 0.1
aldicarb sulfone	0.2	0.02	na

extract were analyzed one day, and two more extracts the next day, with calibration curves prepared on both days. We found it necessary to run each standard 2 or 3 times, in order to be confident about the peak areas, and were able to obtain r^2 values between 0.993 and 0.999 on both days. Quantification in CE-MS has recently been reviewed by Ohnesorge et al. [39-40], and for best results structurally related or isotopically labelled internal standards should be used (note that their reviews did not include MEKC-ESI-MS).

The results showed excellent recoveries for the aromatic *N*-methylcarbamates, and somewhat lower, but still acceptable recoveries for the aliphatic *N*-methylcarbamates (methomyl, aldicarb, and aldicarb sulfone) (Table 2.7; Fig. 2.9). This is probably related to a weaker affinity of the latter compounds for the stationary phase. Several steps could be taken to increase the sensitivity of the analysis, but were outside the scope of our current research. For instance, we did not investigate how much sample could actually be

Table 2.7: Recovery of *N*-methylcarbamates from tap water spiked at the 10 µg/L level (n = 3).

	% Recovery	SD
methomyl	83.1	13.0
propoxur	95.2	3.2
carbofuran	95.9	4.3
dioxacarb	97.4	2.8
3-OH carbofuran	97.6	4.1
methiocarb	95.2	9.4
promecarb	93.2	6.8
aldicarb	86.3	2.3
carbaryl	99.9	4.5
aldicarb sulfone	73.1	5.3

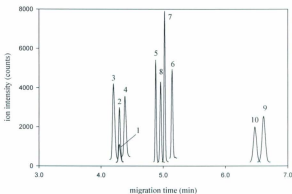


Fig. 2.9: SIM electropherogram of 25 mL of tap water spiked with 10 *N*-methylcarbamates at the 10 µg/L level after SPE and redissolving in 250 µL ultrapure water. BGE: 50 mM APFOA/IPA 98/2; injection: 15 s at 50 mbar; 30 kV applied; other conditions as in Table 5. Peak identification: see Fig. 2.1. The capillary (67 cm) was 7 cm longer than in Fig. 2.5, resulting in somewhat longer migration times than in Fig. 2.5.

loaded onto the cartridges before sample breakthrough occurs, but it is likely that higher concentration factors can be achieved, allowing for concentrations much lower than 10 $\mu\text{g/L}$ to be quantified. If necessary, samples can be reconstituted in a smaller volume of water, for example, 100 μL is enough for CE (giving an additional concentration factor of 2.5). The injection volume can also be increased, depending on how much loss in resolution is tolerated.

2.4. Concluding remarks

APFOA proved to be very successful for the analysis of a mixture of 10 *N*-methylcarbamates with MEKC-ESI-MS. Using an experimental design to optimize nebulizer pressure (4 psi), applied voltage (23.5 kV), and composition of the BGE (85 mM APFOA/IPA 97/3), it was possible to resolve all 10 analytes in just over 11 minutes. However, if two peaks are allowed to co-migrate, the analysis can be performed faster and with approximately twice as good S/N, by using lower concentrations of APFOA and IPA (50 mM APFOA/IPA 98/2), and applying a higher voltage (30 kV). Detection limits using SIM were between 0.01 and 0.08 mg/L. Analysis of the 10 *N*-methylcarbamates after SPE from tap water spiked at a 10 $\mu\text{g/L}$ level, showed very good recoveries, testifying of the fact that quantitative results are feasible.

We believe that APFOA can be an attractive alternative to SDS in MEKC-ESI-MS for a wide range of neutral (and charged) analytes, avoiding the more cumbersome techniques such as partial filling and reverse migrating micelles.

2.5. References

- [1] S.A. Shamsi, B.E. Miller, *Electrophoresis* 25 (2004) 3927
- [2] Ph. Schmitt-Kopplin, M. Frommberger, *Electrophoresis* 24 (2003) 3837
- [3] A. von Brocke, G. Nicholson, E. Bayer, *Electrophoresis* 22 (2001) 1251
- [4] M. Molina, S.K. Wiedmer, M. Jussila, M. Silva, M.-L. Riekkola, *J. Chromatogr. A* 927 (2001) 191
- [5] P. Petersson, M. Jörintén-Karlsson, M. Stålebro, *Electrophoresis* 24 (2003) 999
- [6] H.L. Cheng, M. Tseng, P. Tsai, G.R. Her, *Rapid Commun. Mass Spectrom.* 15 (2001) 1480
- [7] G.W. Somsen, R. Mol, G.J. de Jong, *J. Chromatogr. A* 1000 (2003) 953
- [8] K.L. Rundlett, D.W. Armstrong, *Anal. Chem.* 68 (1996) 3497
- [9] P.G. Muijselaar, K. Otsuka K, S. Terabe, *J. Chromatogr. A* 802 (1998) 3
- [10] J. Suomi, H. Sirén, M. Jussila, S.K. Wiemer, M.-L. Riekkola, *Anal. Bioanal. Chem.* 376 (2003) 884
- [11] K. Stubberud, A. Forsberg, K. Callmer, D. Westerlund, *Electrophoresis* 23 (2002) 572
- [12] L. Yang, K. Harrata, C.S. Lee, *Anal. Chem.* 69 (1997) 1820
- [13] H. Ozaki, S. Terabe, *J. Chromatogr. A* 794 (1998) 317
- [14] Y. Ishihama, H. Katayama, N. Asakawa, *Anal. Biochem.* 287 (2000) 45
- [15] W.K. Goetzinger, H. Cai, *J. Chromatogr. A* 1079 (2005) 372
- [16] R. Mol, G.J. de Jong, G.W. Somsen, *Anal. Chem.* 77 (2005) 5277
- [17] K. Isoo, K. Otsuka, S. Terabe, *Electrophoresis* 22 (2001) 3426
- [18] Y.S. Wu, H.K. Lee, S.F.Y. Li, *J. Microcolumn Separations* 10(1998) 239

- [19] Wu Y. S., Lee H. K., Li S. F. Y., *J. Microcolumn Separations* 10 (1998) 529
- [20] M. Molina, D. Pérez-Bendito, M. Silva, *Electrophoresis* 20 (1999) 3439
- [21] M. Rossi, D. Rotilio, *J. High Resolut. Chromatogr.* 20 (1997) 265
- [22] Z. Liu, H. Zou, M. Ye, J. Ni, Y. Zhang, *J. Chromatogr. A* 863 (1999) 69
- [23] E. Fuguet, C. Ràfols, E. Bosch, M. Rosés, M.H. Abraham, *J. Chromatogr. A* 907 (2001) 257
- [24] C.F. Poole, S.K. Poole, M.H. Abraham, *J. Chromatogr. A* 798 (1998) 207
- [25] C.F. Poole, S.K. Poole, *J. Chromatogr. A* 792 (1997) 89
- [26] C. Crescenzi, A. Di Corcia, E. Guerriero, R. Samperi, *Environ. Sci. Technol.* 31 (1997) 479
- [27] D. Baglio, D. Kotzias, B.L. Larsen, *J. Chromatogr. A* 854 (1999) 207
- [28] S.L. Nilsson, D. Bylund, M. Jörmén-Karlsson, P. Petersson, K.E. Markides, *Electrophoresis* 25 (2004) 2100
- [29] S. Rudaz, S. Cherkaoui, J.-Y. Gauthier, P. Lantéri, J.L. Veuthey, *J. Electrophoresis* 22 (2001) 3316
- [30] E. Varesio, S. Cherkaoui, J.-L. Veuthey, *J. High Resolut. Chromatogr.* 21 (1998) 653
- [31] M.I. Jimidar, T. Vennekens, W. van Ael, D. Redlich, M. De Smet, *Electrophoresis* 25 (2004) 2876
- [32] Anonymous. 2003-2005. *Response Surface Designs*. Minitab Inc.
- [33] Anonymous. Technical Note Agilent 1999. Publication # 5968-1328E.
- [34] R. Weinberger, *Practical Capillary Electrophoresis (Second Edition)*, Academic Press 2000, pp. 64-69

- [35] K. Huikko, T. Kotiaho, R. Kostianen, *Rapid Commun. Mass Spectrom.* 16 (2002) 1562
- [36] J. Zheng, M.W. Jann, Y.Y. Hon, S.A. Shamsi, *Electrophoresis* 25 (2004) 2033
- [37] J.P. Quirino, S. Terabe, *J. Chromatogr. A* 781 (1997) 119
- [38] J. Palmer, N.J. Munro, J.P. Landers, *Anal. Chem.* 71 (1999) 1679
- [39] J. Ohnesorge, C. Sanger-van de Griend, H. Watzig, *Electrophoresis* 26 (2005) 2360
- [40] J. Ohnesorge, C. Neusub, H. Watzig, *Electrophoresis* 26 (2005) 3973

Chapter 3

Linear Solvation Energy Relationships of Anionic Dimeric Surfactants in Micellar Electrokinetic Chromatography

I. Effect of the Length of a Hydrophobic Spacer^{1,2}

¹ G. Van Biesen, C.S. Bottaro, *J. Chromatogr. A* 1157 (2007) 437

² Additional information can be found in Appendices 2 and 3

Abstract

The influence of the length of a flexible hydrophobic spacer on the selectivity of anionic dimeric surfactants was investigated. Disodium 1, ω -bis (decyloxymethyl)-dioxo alkane-1, ω disulfates with a spacer containing an ethylene, butylene, hexylene, octylene, decylene or dodecylene group were synthesized, and four of these were evaluated for use in micellar electrokinetic chromatography (MEKC) via linear solvation energy relationships (LSERs). There were no significant differences in the system constants of these surfactants, indicating that their micelles all have a very similar interface with the aqueous phase, regardless of the length of the hydrophobic spacer. Compared to sodium dodecylsulfate (SDS), these dimeric surfactants are slightly more cohesive, interact better with polarizable compounds, and are somewhat better hydrogen bond acceptors and worse hydrogen bond donors, while there is no difference in dipolarity. The critical micelle concentrations (CMCs) of these surfactants were in the order of 1 mM, except for the dimeric surfactant with a spacer containing an ethylene group, which had a CMC < 0.03 mM.

Keywords: Critical micelle concentration; Dimeric surfactants; Gemini surfactants; Linear solvation energy relationships; Micellar electrokinetic chromatography; Spacer

3.1. Introduction

Separation in micellar electrokinetic chromatography (MEKC) is based upon the differential partitioning of analytes between an aqueous phase and a pseudostationary phase of micelles of an ionic surfactant at a concentration higher than its critical micelle concentration (CMC). The selectivity of the separation can be manipulated by adding organic modifiers [1] or cyclodextrins (particularly for enantiomeric separations) [2], or by using different types of surfactants or mixtures of surfactants [3-5]. Generally, the choice of surfactant seems to be the most important variable in optimizing the selectivity [6]. Of the numerous surfactants that have been evaluated for MEKC, the majority are 'conventional' amphiphiles, i.e. they consist of one long hydrophobic chain with one ionic head group; sodium dodecylsulfate (SDS) being the most widely used. At the other end of the spectrum are polymeric surfactants, which have multiple hydrophobic chains and ionic head groups. They have gained a lot of attention the past few years for a number of reasons [7-9]. They do not require self-assembly and thus can be used at low concentrations, typically $\leq 1\%$, and with relatively high concentrations of organic solvents. This is of particular importance for the analysis of very hydrophobic compounds, which are difficult to separate because of their high affinity for the pseudostationary phase, and for which the addition of an organic solvent is often necessary to decrease their partition coefficient. Polymeric surfactants also seem to be more compatible with mass spectrometric detection, presumably because of their lower surface activity [10]. However, it can be problematic to obtain monodisperse solutions, and mass-transfer kinetics may be slower than with conventional micelles, both of which can lead to lower plate counts [8].

Between these two extremes (monomeric and polymeric surfactants) are dimeric (or gemini) surfactants, which are made up of two amphiphilic moieties connected at, or close to, the head groups by a spacer [11] (Fig. 3.1). If the spacer is further away from the head groups, they are called bolaform surfactants, which do not have the features discussed below.

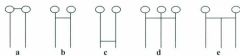


Fig. 3.1: General schematic structures of (a) a dimeric surfactant with the spacer group connecting the two head groups, (b) a dimeric surfactant with the spacer group close to the two head groups, (c) a bolaform surfactant, (d) a trimeric surfactant, and (e) a multi-arm dimeric surfactant (adapted from [13]).

There has been a considerable amount of research on dimeric surfactants in the past 20 years because of some unique properties regarding their surface activity and molecular aggregation [11-13]. With respect to their use in MEKC, the most important features are that they have CMCs typically one to two orders of magnitude lower than those of the corresponding monomeric surfactants, that they have better solubilizing properties, and that the length and the nature of the spacer can have a profound impact on micelle shape and properties. Dimeric surfactants with short spacers typically form worm-like micelles [13], as opposed to the spherical micelles of conventional surfactants. Besides simple dimeric surfactants, there are also reports on multi-armed dimeric, polyionic dimeric, and trimeric, tetrameric and oligomeric surfactants [11,13,14]. Obviously, the possibilities of combining chains and head groups are only limited by the

imagination of the synthetic chemist. It remains to be seen, however, if these non-conventional surfactants have any advantages for use in MEKC compared to the already wide array of commercially available surfactants.

There are very few reports on the use of anionic dimeric surfactants in MEKC. Harino et al. [15] synthesized three anionic dimeric surfactants, which differed in the spacer, and was able to baseline separate a mixture of eight monosubstituted naphthalenes with two of these surfactants at concentrations lower than 10 mM, while a complete separation was not possible with SDS in the concentration range of 10 – 60 mM. It was also observed that the analyte migration order in the dimeric surfactant systems was different from that in SDS. Harino et al. [16] also used two anionic dimeric surfactants with two hydrophobic chains and a dimeric surfactant with three hydrophobic chains for the separation of naphthalene and flavone derivatives. Again, a better separation and different selectivity was observed compared to SDS. More recently, Akbay et al. [17] synthesized sodium di(undecenyl) tartrate (SDUT), an anionic dimeric surfactant, and poly-SDUT, and characterized their selectivity via linear solvation energy relationships (LSERs).

For an understanding of fundamental differences in selectivity between pseudostationary phases in MEKC, LSERs are often used [1,3,6,9,18-25]. These are based upon Abraham's solvation parameter model, and solute descriptors are: McGowan's characteristic volume V (in $\text{cm}^3 \cdot \text{mol}^{-1} / 100$) (divided by 100 to scale it to the magnitude of the other descriptors), excess molar refraction E (in $\text{cm}^3 \cdot \text{mol}^{-1} / 10$) (divided by 10 as a scaling factor), dipolarity/polarizability S , hydrogen bond acidity A , and hydrogen bond basicity B . We adopted here the simplified representation of the

descriptors as proposed by Abraham [22]. The LSER are represented by the following general equation:

$$\log k = c + eE + sS + aA + bB + vV \quad (\text{Eq. 1})$$

where k is the retention factor.

The system constants c , v , e , s , a and b are calculated by multiple linear regression of typically 30 – 40 solutes with known descriptors. For the model to be chemically and statistically sound, these solutes should exhibit a wide range in the values of their descriptors, with minimal cross-correlation [21,22]. The system constants are a quantitative measure of the relative strength of these interactions in the aqueous and the micellar phase, and when positive contribute to retention of the solute in the micellar phase. Thus, v is a measure of the solute's ability to create a cavity in the aqueous phase relative to creation of a cavity in the micellar phase; e reflects the difference in capacity of the two phases to interact with solute n - and π -bonding electrons, s represents the difference in capacity of the two phases to engage in dipole-dipole and dipole-induced dipole interactions, a is a measure of the difference in hydrogen-bond accepting and b a measure of the difference in hydrogen-bond donating capabilities of the two phases. Finally, the system constant c represents information that is not explained by the model, with the phase ratio being the most significant contributor [6, 22,23]

This paper describes the synthesis of dimeric anionic surfactants (type b in Fig. 3.1), with a flexible spacer containing 2, 4, 6, 8, 10 and 12 methylene groups, and their evaluation for use in MEKC by means of LSERs. There already are systematic LSER studies of surfactants for MEKC that investigate effects of the head group [26,27], the surfactant counter-ion [19], and the length of the hydrophobic chain [20]. Dimerization should not significantly impact these effects, thus it is probably not very informative to repeat these studies on dimeric surfactants. However, the nature and the length of the spacer are two main parameters that have been shown to influence the special properties of dimeric surfactants [12,13], and with respect to their use in MEKC, a systematic investigation is warranted. For instance, while for monomeric surfactants the distribution of distances between head groups exhibits a maximum at a thermodynamic equilibrium distance of 0.7 – 0.9 nm, the distribution for dimeric surfactants is bimodal, with a second narrower maximum corresponding to the length of the spacer [12,13,28]. This length is determined by the number of atoms in the spacer, and its conformation. The spacers in these dimeric surfactants reside at or close to the interface of the micelles with the bulk aqueous phase, where a significant amount of interaction with solutes takes place [6,26,29]. Thus, it is expected that the length and the nature of the spacer can influence the selectivity of dimeric surfactants. While this report focuses on the length of a flexible hydrophobic spacer, we are currently synthesizing dimeric surfactants with hydrophilic spacers, and will report these results in due time.

3.2. Experimental

3.2.1. CE instrument and conditions

All experiments were performed on an Agilent ^{3D}CE system (Agilent Technologies Canada Inc., Mississauga), running on Chemstation software (Rev. A.08.03). Bare fused silica capillaries with an I.D. of 50 μm were purchased from MicroSolv (MicroSolv Technology Corporation, Eatontown, NJ, USA) and were cut to a length of 48 – 50 cm. The MicroSolv Window Maker was used to burn a small window 8.5 cm from the outlet and to remove approximately 2 mm of polyimide at both ends of the capillaries.

The background electrolyte (BGE) consisted of 20 mM Na_2HPO_4 and 7.5 mM dimeric surfactant, or 50 mM SDS, adjusted to $\text{pH } 7.00 \pm 0.03$ with dilute H_3PO_4 so that none of the solutes were ionized to any significant extent, and was filtered through 0.2 μm nylon filters (National Scientific Company, Rockwood, TN, USA).

The capillaries were conditioned at the beginning of each day by flushing with 0.1 M NaOH (5 min.), nanopure water (5 min.), and BGE (10 min.) respectively. Analyses were performed at 25 $^\circ\text{C}$, with 25 kV applied (ramped from 0 to 25 kV in 15 s). Samples were injected by applying 10 mbar of pressure for 5 s, followed by BGE at 10 mbar for 5 s, and the detection wavelength was 200 nm. For SDS, we used a second detection wavelength at 194 nm, since this was better for detecting the baseline disturbance from the EOF marker (methanol). Peaks were identified by comparison of their UV-spectra with entries in a spectral library. Between runs, the capillary was flushed with BGE for 3 minutes.

2.2. Solutes

Most of the test solutes (Table 3.1) were obtained from Sigma-Aldrich (Oakville, Ontario, Canada) and had a purity $\geq 98\%$, except 4-phenylphenol (97%), 1-methyl naphthalene (97%), and azobenzene (96%). The series of n-alkyl benzoates (C1 – C6, and C8) was prepared by reacting the corresponding n-alcohols (PolyScience Corporation, Evanston, IL, USA) with benzoylchloride in the presence of triethylamine. A cross-correlation matrix of the 36 solutes shows that there is no correlation between the solute descriptors (Table 3.2).

Solutions of 8-11 solutes (plus dodecanophenone as micelle marker) were prepared in methanol at concentrations between 300 and 600 mg/L. Using SDS as the micellar phase, all peaks were baseline resolved, and solutes could be distinguished based upon their UV-spectrum. Where homologous solutes such as methyl- and ethyl benzoate (which have undistinguishable UV-spectra) were added in the same solution, it was rationalized that the lower molecular weight solute would have the shorter migration time. When there was any doubt about co-migrating solutes, they were run separately. All samples were run twice, and average retention factors were calculated.

Table 3.1: Solutes and their descriptors (from [21], except for pyrimidine, pyrrole, and resorcinol [3], ethyl benzoate and 1-methyl naphthalene [26], and 2-chlorophenol [30]), and log k for selected surfactants.

	V	E	S	A	B	log k				
						SDS	IIIa	IIIb	IIIc	IIle
1 1,2,3,4-Tetrachlorobenzene	1.2060	1.180	0.92	0.00	0.00	2.00	1.62	1.66	1.68	1.70
2 1,2-Dichlorobenzene	0.9612	0.872	0.78	0.00	0.04	1.05	0.62	0.62	0.62	0.60
3 Toluene	0.8573	0.601	0.52	0.00	0.14	0.43	-0.11	-0.12	-0.13	-0.09
4 Azobenzene	1.3790	1.959	1.13	0.00	0.18	1.99	1.39	1.38	1.37	1.38
5 Naphthalene	1.0854	1.340	0.92	0.00	0.20	1.10	0.63	0.61	0.59	0.59
6 Fluorene	1.3565	1.588	1.03	0.00	0.20	1.84	1.40	1.38	1.37	1.37
7 1-Methyl naphthalene	1.2260	1.344	0.90	0.00	0.20	1.51	1.04	1.01	1.02	1.03
8 Biphenyl	1.3242	1.360	0.99	0.00	0.22	1.62	1.15	1.13	1.11	1.13
9 Nitrobenzene	0.8910	0.871	1.11	0.00	0.28	0.10	-0.54	-0.56	-0.59	-0.61
10 Anisole	0.9160	0.708	0.75	0.00	0.29	0.20	-0.42	-0.43	-0.47	-0.47
11 1-Nitronaphthalene	1.2596	1.600	1.51	0.00	0.29	1.25	0.65	0.62	0.59	0.52
12 Benzaldehyde	0.8730	0.820	1.00	0.00	0.39	0.01	-0.76	-0.80	-0.85	-0.80
13 Methyl benzoate	1.0726	0.733	0.85	0.00	0.46	0.50	-0.33	-0.36	-0.39	-0.37
14 Ethyl benzoate	1.2140	0.689	0.85	0.00	0.46	0.88	0.02	-0.02	-0.05	-0.04
15 Propyl benzoate	1.3544	0.675	0.80	0.00	0.46	1.32	0.42	0.39	0.36	0.36
16 Butyl benzoate	1.4953	0.668	0.80	0.00	0.46	1.75	0.88	0.85	0.82	0.83
17 Acetophenone	1.0139	0.818	1.01	0.00	0.48	0.20	-0.66	-0.68	-0.71	-0.68
18 Caffeine	1.3632	1.500	1.60	0.00	1.33	-0.29	-1.15	-1.22	-1.23	-1.09
19 N-Methylaniline	0.9571	0.948	0.90	0.17	0.43	0.05	-0.64	-0.68	-0.71	-0.72
20 Aniline	0.8162	0.955	0.96	0.26	0.50	-0.35	-0.94	-0.99	-1.02	-1.01
21 4-Chloroaniline	0.9390	1.060	1.13	0.30	0.35	0.27	-0.18	-0.19	-0.23	-0.29
22 2-Phenylethanol	1.0569	0.811	0.91	0.30	0.64	0.01	-0.75	-0.77	-0.80	-0.79
23 4-Phenyl-1-butanol	1.3387	0.811	0.90	0.33	0.70	0.74	-0.09	-0.11	-0.15	-0.19
24 Benzyl alcohol	0.9160	0.803	0.87	0.33	0.56	-0.27	-0.96	-0.98	-1.02	-1.01
25 2-Chlorophenol	0.8975	0.853	0.88	0.32	0.31	0.16	-0.25	-0.27	-0.32	-0.37
26 Pyrrole	0.5774	0.613	0.73	0.41	0.29	-0.84	-1.19	-1.21	-1.23	-1.24
27 4-Nitroaniline	0.9910	1.220	1.91	0.42	0.38	0.03	-0.49	-0.52	-0.56	-0.55
28 Indole	0.9460	1.200	1.12	0.44	0.31	0.26	-0.09	-0.12	-0.18	-0.27
29 Acetanilide	1.1133	0.870	1.40	0.50	0.67	-0.13	-0.79	-0.83	-0.85	-0.81
30 Benzenesulfonamide	1.0971	1.130	1.55	0.55	0.80	-0.44	-1.05	-1.10	-1.12	-1.07
31 4-Phenylphenol	1.3829	1.560	1.41	0.59	0.45	1.33	0.86	0.83	0.77	0.69
32 Phenol	0.7751	0.805	0.89	0.60	0.30	-0.32	-0.76	-0.80	-0.85	-0.87
33 2-Naphthol	1.1440	1.520	1.08	0.61	0.40	0.81	0.36	0.34	0.29	0.21
34 Methyl 3-hydroxybenzoate	1.1313	0.905	1.40	0.66	0.45	0.29	-0.43	-0.48	-0.52	-0.49
35 Propyl 4-hydroxybenzoate	1.4131	0.860	1.35	0.69	0.45	1.07	0.31	0.27	0.21	0.18
36 Resorcinol	0.8340	0.980	1.00	1.10	0.58	-0.66	-0.99	-1.01	-1.04	-1.00

Table 3.2: Cross-correlation matrix (r^2 values) of the descriptors of the 36 solutes of Table 1.

	V	E	S	A	B
V	1.000				
E	0.211	1.000			
S	0.084	0.256	1.000		
A	0.049	0.002	0.115	1.000	
B	0.032	0.003	0.179	0.080	1.000

3.2.3. Calculations

Retention factors were calculated from:

$$k = (t_m - t_0) / [t_0 (1 - t_m/t_{mc})] \quad (\text{Eq. 2})$$

with t_m the migration time of the solute, t_0 the migration time of an unretained solute (methanol), and t_{mc} the migration time of the micellar marker (dodecanophenone) [19,25].

The iterative procedure described by Bushey and Jorgenson [31], using Microsoft Excel's 'solver' tool to maximize the correlation coefficient, was used to determine the methylene selectivity (α_{C12}) from the slope (m) of a plot of $\log k$ vs. carbon number ($\alpha_{C12} = 10^m$) of a homologous series of alkyl benzoates (C_1 - C_6 or C_1 - C_6 & C_8). This slope, in fact, represents an average methylene selectivity for the entire homologous series [9].

The electrophoretic mobility μ_e ($\text{cm}^2 \text{V}^{-1} \text{s}^{-1}$) of the pseudostationary phases was calculated from:

$$\mu_e = (l/V_a) \cdot (1/t_{mc} - 1/t_0) \quad (\text{Eq. 3})$$

with l the length of the capillary to the detector, and L the total length of the capillary.

The average voltage V_a is calculated from:

$$V_a = V \cdot (1 - t_R/2t_{mc}) \quad (\text{Eq. 4})$$

where V is the end voltage (25 000 V) and t_R is the ramp time (15 s) [32].

The efficiency N was calculated as an average efficiency of the methyl- through hexyl benzoates [9].

3.3. Synthesis and Analysis of Dimeric Surfactants

Dimeric surfactants were synthesized from diols in three discrete steps (Fig. 3.2).

All reagents were purchased from Aldrich and had a purity of at least 98%.

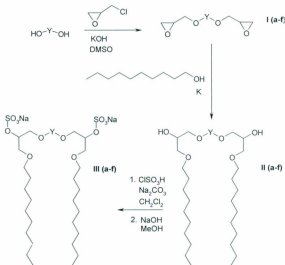


Fig. 3.2: Synthetic pathway to the dimeric surfactants used in this project. Y is an ethylene (a), butylene (b), hexylene (c), octylene (d), decylene (e), or dodecylene (f) group.

The synthesis of the diglycidyl ethers (**Ia-f**) was based upon Kida et al. [33], with some minor modifications. Briefly, 0.10 mol diol and 0.40 mol KOH were stirred in 50 mL dimethyl sulfoxide (DMSO), and 0.60 mol epichlorohydrin was added drop wise, keeping the temperature between 20 and 30 °C (35 - 40 °C for **If**). The mixture was stirred for 5 - 40 hrs, with the longer reaction times required for the higher MW diols, then filtered. The solids were washed with dichloromethane, which was combined with the filtrate. The filtrate was extracted with dichloromethane/brine. The combined organic layers were dried with anhydrous Na₂SO₄, filtered, and dichloromethane was evaporated. Distillation of the residue under reduced pressure gave products **Ia - Id** with yields of 57 - 68%. The boiling points of **Ie** and **If** were too high for distillation at 0.15 mm Hg; thus these compounds were purified, after distillation of excess epichlorohydrin, via column chromatography with hexane:ethyl acetate 60:40 (v/v) as eluent (yields: 58% and 45% respectively).

The synthesis of the long-chain diols (**IIa-f**) was according to Zhu et al. [14]. Metallic potassium (0.04 mol) was dissolved in 0.24 mol n-decanol at 60 °C under dry nitrogen, and 0.03 mol diglycidyl ether (**Ia-f**) was added drop wise. The reaction mixture was stirred for 10 - 24 hrs (3 hrs for **IIa**) at 75 °C, neutralized with 10% HCl and extracted with dichloromethane/brine. The combined organic layers were dried with Na₂SO₄, filtered and dichloromethane was evaporated. Excess n-decanol was distilled under reduced pressure. Column chromatography, typically with hexane:ethyl acetate 50:50 (v/v), gave compounds **IIa - IIf** with yields of 46 - 59%.

Finally, the synthesis of the dimeric surfactants (**IIIa-f**) was based upon Zhu et al. [34]. Chlorosulfonic acid (12 mmol) dissolved in 10 mL dichloromethane was added drop wise to a mixture of 3 mmol long-chain diol (**IIa-f**) and 12 mmol anhydrous Na_2CO_3 in 30 mL dichloromethane on an ice-bath, while the flask was flushed with dry nitrogen. After addition, stirring was continued for 3 hrs, after which the mixture was removed from the ice-bath and stirring was continued for another 30 min. The reaction mixture was then cooled again on an ice-bath, and adjusted to basic pH with methanolic NaOH. After evaporation of the solvent, the residue was dissolved in water and extracted 3x with 1-butanol, which was subsequently evaporated, to yield the crude surfactant. Column chromatography, typically with dichloromethane:methanol 85:15 (v/v), gave products **IIIa – IIIf** (disodium 1, ω -bis (decyloxymethyl)-dioxo alkane-1, ω disulfates) with yields of 45 – 65%.

Dimeric surfactants **IIIa-f** were characterized with $^1\text{H-NMR}$ (Bruker Avance 500 MHz) and ESI-MS (Agilent 1100 Series LC/MSD Trap), while for the intermediate products **Ia-f** and **IIa-f** we usually only acquired NMR spectra. CMCs were determined at 25 °C from the break point of conductance vs. molar concentration plots [13], using a YSI Model 31 conductivity bridge (Yellow Springs Instruments, Yellow Springs, OH, USA) with a 10 k Ω resistor in parallel.

3.3. Results and discussion

3.3.1. Analysis and CMCs of dimeric surfactants

The dimeric surfactants **IIIa** - **IIIc** were the first to be synthesized and initially were dissolved in CDCl_3 to obtain $^1\text{H-NMR}$ spectra. These spectra invariably showed relatively broad peaks, with poor resolution. This was attributed to averaging of the signals of surfactant molecules in the bulk solution and in the (inversed) micelles [35]. Since **III d** - **III f** did not dissolve in CDCl_3 , they were dissolved in $[\text{}^2\text{H}_6]$ DMSO ($\text{DMSO-}d_6$); this gave better resolution, and subsequently $^1\text{H-NMR}$ spectra of **IIIa** - **IIIc** were also recorded in $\text{DMSO-}d_6$ (Table 3.3). It was our experience that these surfactants are extremely hygroscopic, and the spectra in CDCl_3 showed a broad peak at δ 2.8 ppm, presumably from hydroxyl protons. It was only after storing the surfactants in a desiccator with phosphorus pentoxide under vacuum that this peak disappeared. Since the $\text{DMSO-}d_6$ itself contained some water, spectra recorded in this solvent always showed a rather large hydroxyl proton peak at δ 3.3 ppm, unfortunately slightly overlapping other diagnostic peaks. Except for a small triplet at δ 3.67 ppm in **IIIc**, also present to a much lesser extent in most of the other surfactants, the spectra did not show any peaks that could not be rationalized with the surfactant structures.

The base peak in the negative ESI-MS spectra of the dimeric surfactants corresponded to either $[\text{M} - 2\text{Na}]^{2-}$, or $[\text{M} - \text{Na}]^-$ (Table 3.3). A peak corresponding to $[\text{M} - 2\text{Na} + \text{H}]^-$ was also always present. Products **III b** and **III c** showed minor amounts of unidentified ions at a m/z of 383.1 and 236.9, respectively.

Table 3.3: Summary of NMR and MS data, and CMC of dimeric surfactants

	Formula MM	¹ H-NMR ^a (δ, ppm)	m/z (neg. ESI) ^b	CMC (mM) at 25 °C
IIIa	C ₂₃ H ₅₀ O ₁₂ S ₂ Na ₂ 694.8	0.86 (t;6H), 1.2-1.3 (m;28H), 1.46 (m;4H), 3.3-3.55 (m;16H) ^c , 4.17 (m;2H)	671.2 (100%), 324.1 (67%), 649.2 (35%)	<0.032 ^d
IIIb	C ₁₉ H ₄₀ O ₁₂ S ₂ Na ₂ 722.9	0.86 (t;6H), 1.2-1.3 (m;28H), 1.46 (m;8H), 3.3-3.5 (m;16H) ^c , 4.16 (m;2H)	699.3 (100%), 338.1 (88%), 677.2 (16%), 383.1 (7%)	0.7
IIIc	C ₁₉ H ₄₀ O ₁₂ S ₂ Na ₂ 751.0	0.86 (t;6H), 1.2-1.3 (m;32H), 1.46 (m;8H), 3.3-3.5 (m;16H) ^c , 4.15 (m;2H)	727.3 (89%), 352.1 (100%), 705.2 (13%), 236.9 (4%)	1.0
IIId	C ₁₉ H ₄₀ O ₁₂ S ₂ Na ₂ 779.0	0.85 (t;6H), 1.2-1.3 (m;36H), 1.46 (m;8H), 3.3-3.5 (m;16H) ^c , 4.14 (m;2H)	755.3 (52%), 366.2 (100%), 733.3 (14%)	1.2
IIIe	C ₁₆ H ₃₂ O ₁₂ S ₂ Na ₂ 807.1	0.86 (t;6H), 1.2-1.3 (m;40H), 1.46 (m;8H), 3.3-3.5 (m;16H) ^c , 4.14 (m;2H)	783.3 (48%), 380.2 (100%), 761.3 (11%)	0.9
IIIf	C ₁₈ H ₃₈ O ₁₂ S ₂ Na ₂ 835.1	0.85 (t;6H), 1.2-1.3 (m;44H), 1.46 (m;8H), 3.3-3.5 (m;16H) ^c , 4.14 (m;2H)	811.3 (35%), 394.2 (100%), 789.3 (8%)	0.9

a: samples in DMSO-d₆; t: triplet; m: multiplet

b: intensity as a percentage of base peak in brackets; mass to charge ratios correspond to [M - Na]⁻, [M - 2Na]²⁻, and [M - 2Na + H]⁻, respectively, other ions not identified

c: this multiplet also had a large peak from hydroxyl protons from water, invariably present in the DMSO-d₆

d: the conductance of more dilute solutions was too low to be accurately measured (see text)

The dimeric surfactant with the shortest spacer (2 methylene groups – **IIIa**) had such a low CMC that it could not reliably be determined with our equipment (Table 3.3). A series of dilutions from 1.05 mM to 0.032 mM still showed a linear relationship between conductance and concentration, so it could be concluded that the CMC was lower than 0.032 mM. Zhu et al. [34] determined the CMC of this surfactant via surface tension measurements, and found a value of 0.013 mM at 20 °C. They also synthesized compound **IIIb**, and found a value for the CMC of 0.60 mM, slightly less than our value of 0.7 mM. Their method might be inherently more accurate, because at concentrations

higher than the CMC, the surface tension is essentially constant. Therefore, the accuracy with which the intersect of both curves can be determined is mainly dependent on the accuracy of the slope of the curve before the CMC, while with conductance measurements the slopes of both curves have to be determined accurately (Fig. 3.3).

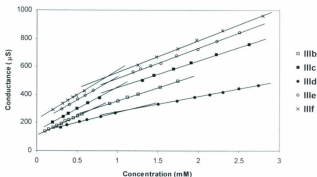


Fig. 3.3: Conductance vs. concentration plots for determination of the CMC. Note that for clarity the conductance values for IIIe, IIIe and IIIf are increased by 20%, 40% and 60%, respectively, and that due to the use of a 10 k Ω resistor, curves do not go through the origin.

The CMC increases up to 1.2 mM for surfactants with a spacer group consisting of 8 methylene groups, and then decreases again. A similar behaviour, where a maximum in a plot of CMC vs. number of methylene groups in the spacer is observed, has also been described in cationic dimeric surfactants, although with a maximum at 5-6 methylene groups [13,28]. The initial increase is thought to be caused by a conformational change of the two hydrophobic chains from *trans* for short spacers (to minimize electrostatic repulsion) to *cis* for longer spacers. With a preferential *cis* configuration, the two

hydrophobic chains may be in some contact with one another. The free energy change of transfer of a surfactant molecule from the aqueous phase to the micellized state will then be less negative, and consequently the CMC will be higher [36]. The decrease in CMC at longer spacer lengths indicates partial looping of a significant part of the spacer in the micelle hydrophobic core [28,36]. Compared to the tremendous increase (< 0.03 mM to 0.7 mM) going from 2 to 4 methylene groups, the changes in the CMC for the other dimeric surfactants seem rather trivial. These low CMCs are interesting though, since it means that these surfactants can be used at much lower concentrations than for instance SDS. This could be an advantage for applications where a low current is required to minimize Joule heating. It could also be interesting for direct coupling of MEKC with electrospray ionization - mass spectrometry, which is hampered by SDS concentrations of $20 - 50$ mM (and even lower) usually necessary for separations [10,37]. Note that for dimeric surfactant **IIIId**, the slopes of the fitted curves are much lower than for the other surfactants, and as described in the next section, this compound exhibited other unusual behaviour.

3.3.2. Linear Solvation Energy Relationships

Of the six synthesized surfactants, only four were used in the determination of LSERs. Dimeric surfactant **IIIIf** gave very cloudy solutions in 20 mM phosphate buffer, even at a lower concentration of 2.5 mM and after sonicating and filtering, and therefore was not retained for further experiments. Electropherograms with BGE containing dimeric surfactant **IIIId** showed a lot of spurious peaks, which seemed to be baseline deflections, and had longer t_{0s} compared to the other four surfactants. Aging of the

solution for 2 days seemed to diminish the problem to some extent, but it did not completely go away. As mentioned in the previous section, this compound also showed a deviant behaviour in a plot of conductance vs. molar concentration. No further experiments were performed, and we did not find a plausible explanation for this erratic behaviour.

The LSERs gave acceptable statistical results, although, as is not unusual [17,21], some solutes did not fit the calculated models very well (standardized residuals > 2). The Minitab software package used for the multiple linear regressions always identified caffeine as having a large influence on the fitted models, and this solute was excluded. Indeed, caffeine is an exceptionally strong hydrogen bond acceptor compared to the other solutes in the dataset (Table 3.1). It is very rare to see this compound, or similar strong hydrogen bond acceptors such as (hydro)cortisone or corticosterone in LSER studies of surfactants in MEKC, although Fuguet et al. [25] make a strong case for including them in an expanded dataset of over 60 solutes. The main effect of caffeine on our results is that it increased the b system constant for the dimeric surfactants (typically by $\sim 10\%$ - results not shown), making them seem to be better hydrogen bond donors. However, it did not have an effect on the system constants of SDS. After removal of caffeine and recalculation of the system constants, 1,2,3,4-tetrachlorobenzene proved to be a consistent outlier, with standardized residuals often close to 3.0, so this solute was excluded as well. It is noteworthy that this compound is the weakest hydrogen bond base in the dataset ($B = 0.00$). This omission of these compounds gave a robust fit for SDS, with system constants before and after removal of the outliers that are not significantly different (Table 3.4). For the dimeric surfactants, azobenzene was also removed because of often large standardized

Table 3.4: System constants (standard error in brackets) and regression statistics for the LSERs of SDS and the dimeric surfactants, before and after removal of outliers. Underlined values are not significantly different from zero ($p > 0.05$), n is the number of solutes.

	c	v	e	s	a	b	n	r^2	F
<i>Before removal of outliers</i>									
SDS	-1.77 (0.08)	2.97 (0.08)	0.27 (0.06)	-0.39 (0.07)	-0.22 (0.06)	-1.80 (0.07)	36	0.991	664
IIIa	-2.12 (0.13)	2.60 (0.13)	0.59 (0.09)	-0.49 (0.11)	<u>0.03</u> (0.09)	-2.14 (0.12)	36	0.977	251
IIIb	-2.13 (0.13)	2.60 (0.13)	0.60 (0.09)	-0.50 (0.12)	<u>0.03</u> (0.10)	-2.19 (0.12)	36	0.976	240
IIIc	-2.15 (0.14)	2.60 (0.14)	0.61 (0.10)	-0.52 (0.12)	<u>0.01</u> (0.10)	-2.19 (0.13)	36	0.973	217
IIId	-2.14 (0.15)	2.57 (0.15)	0.60 (0.11)	-0.51 (0.13)	<u>-0.06</u> (0.11)	-2.08 (0.13)	36	0.968	184
<i>After removal of outliers</i>									
SDS	-1.76 (0.07)	2.94 (0.07)	0.26 (0.05)	-0.40 (0.06)	-0.21 (0.05)	-1.76 (0.10)	34	0.993	798
IIIa	-2.11 (0.10)	2.61 (0.10)	0.64 (0.08)	-0.54 (0.08)	<u>0.11</u> (0.08)	-2.25 (0.14)	33	0.984	341
IIIb	-2.12 (0.10)	2.61 (0.10)	0.64 (0.09)	-0.55 (0.09)	<u>0.10</u> (0.08)	-2.28 (0.15)	33	0.984	322
IIIc	-2.13 (0.11)	2.60 (0.10)	0.65 (0.08)	-0.56 (0.09)	<u>0.08</u> (0.08)	-2.28 (0.15)	33	0.982	297
IIId	-2.10 (0.11)	2.58 (0.11)	0.60 (0.09)	-0.54 (0.10)	<u>0.04</u> (0.09)	-2.21 (0.16)	33	0.980	260

residuals. Even after the removal of azobenzene, there were still always 2 solutes with standardized residuals slightly higher than 2.0. Deleting more solutes improved the statistics, although this did not significantly change the system constants anymore (the biggest effect was seen in the value of b , which increased to -2.1 for all four surfactants) and we decided to use the remaining 33 solutes. As was the case for SDS, the system constants for the dimeric surfactants before and after the removal of outliers are not significantly different. Since the a coefficient for the dimeric surfactants was not significantly different from zero, we repeated the calculation of the system constants

without the A descriptor, but the resulting system constants did not change significantly (results not shown).

The values of the system constants for the four dimeric surfactants are remarkably similar (Table 3.4); statistically there is no difference. This is somewhat surprising, and indicates that the interface of the micelles with the aqueous phase is very similar, regardless of the length of the hydrophobic spacer. As a group, when compared with SDS, these dimeric surfactants are somewhat more cohesive (smaller v), and interact better with polarizable solutes (higher ϵ). They are also slightly better hydrogen bond acceptors (higher a , not significantly different from zero), probably attributable to the extra oxygen atoms in their structure, and somewhat worse hydrogen bond donors (smaller b) than SDS, while their capability to interact with induced dipoles and dipolar compounds is not significantly different from that of SDS. It seems that these surfactants are very similar to bile salt surfactants, specifically sodium taurocholate, with reported values for v , ϵ , s , a , and b of 2.43, 0.60, -0.34, 0, and -2.06, respectively [6].

We acknowledge that the dataset includes a significant number of solutes that have a low affinity for the dimeric surfactants (Table 3.1), and it is known that there can be a larger error associated with the determination of retention factors of solutes with very short (and very long) migration times [21]. However, retention factors were determined twice, sometimes on different days, and the average difference between both $\log k$ values for all solutes with all four dimeric surfactants was no more than 0.005. Furthermore, if the experimental error in these values were large, one would expect larger standard errors in the system constants than the ones reported in Table 3.4. They are in fact comparable with values reported in the literature [1,9,19,21].

Another convenient way of comparing the synthesized surfactants with SDS and with one another is by plotting their retention factors for the 36 solutes (Fig. 3.4).

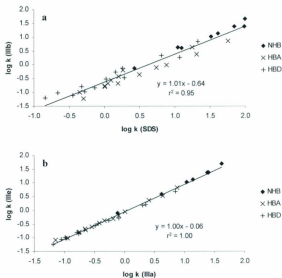


Fig. 3.4: Selectivity plots of (a) dimeric surfactant **IIIb** vs. SDS, and (b) dimeric surfactant **IIIc** vs. **IIIa**. NHB are non-hydrogen-bonding solutes (1-8 in Table 2.1), HBA are hydrogen-bond-acceptors (9-23 in Table 2.1), and HBD are hydrogen-bond-donors (24-36 in Table 2.1).

The strong correlation between log k values obtained with SDS and with surfactant **IIIb** as an example (Fig. 3.4a) shows that their selectivity is not drastically different, as was already inferred from the LSER results. On average, log k values are 0.64 units lower compared to SDS (the slope is unity), i.e. solutes in general have a higher affinity for SDS

micelles than for dimeric surfactant micelles. This is predominantly because SDS has more positive c and v values, and less negative b values. Remember that the value of c depends to a large extent on the phase ratio, and can be increased for the dimeric surfactants by using a higher concentration. We can categorize solutes as non-hydrogen-bond-donors (NHB solutes; 1-8 in Table 3.1), hydrogen-bond-acceptors (HBA solutes; 9-23 in Table 3.1), and hydrogen-bond-donors (HBD solutes; 24-36 in Table 3.1) [26], and qualitatively compare the LSER results with observed selectivity. HBA solutes plot predominantly below the fitted curve, which agrees with SDS being the stronger hydrogen-bond donating phase (less negative b value than **IIIb**). For HBD solutes we see somewhat more scatter, with a majority of solutes (8 out of 13) plotting above the fitted line. Although the dimeric surfactant is the stronger hydrogen-bond acceptor (larger a value than SDS), the difference with SDS is relatively small, and since this type of interaction is weak, its effect is easily obscured by other interactions. Finally, NHB solutes plot slightly above the fitted line, suggesting that for the dimeric surfactants, non-hydrogen-bond interactions contribute more to the retention factors than for SDS. Although these dimeric surfactants are more cohesive (smaller v value than SDS), this is apparently offset by their ability to better interact with polarizable solutes (higher e value than SDS).

As could be expected, plots of $\log k$ values of any two dimeric surfactants show excellent correlations (Fig. 3.4b). We plotted here the retention factors of the surfactants with an ethylene (**IIIa**) and a decylene spacer (**IIIe**), as the most extreme case. While the slope of the fitted curve is unity, the intercept is slightly negative (-0.06), indicating that retention factors for surfactant **IIIa** are on average somewhat higher than for surfactant

IIIe. Indeed, the general trend for the dimeric surfactants (see last four columns in Table 3.1) is a decrease in retention factor with longer spacer length, often with a minimum or a levelling off at 6 methylene groups (surfactant **IIIe**). Since there is only a modest change in the values of the retention factors, it is difficult to draw firm conclusions, but it is possible that this minimum is related to incorporation of a portion of the spacer in the micelle core for the surfactant with the longest spacer.

The methylene selectivity is proportional to the free energy of transfer of a methylene group between the aqueous and the pseudostationary phase [38], and is a measure of how well a surfactant is able to separate 2 compounds that differ by one methylene group. It is usually calculated as an average for a homologous series, often C₁-C₆ alkylphenones [9], where C₁ refers to acetophenone (we used alkyl benzoates because of their easy synthesis and in-house availability of starting products). The methylene selectivity of dimeric surfactants based upon C₁-C₆ alkyl benzoates is slightly less than for SDS (Table 3.5). However, it has to be stressed that these values are averages for the homologous series tested. When we also added octyl benzoate (C₈) to the mixture, this homologue co-migrated with hexyl benzoate in SDS, while we had baseline separation with the dimeric surfactants (Fig. 3.5), resulting in a higher methylene selectivity for the dimeric surfactants (Table 3.5). This seems to indicate that they are better than SDS at separating more hydrophobic compounds.

In MEKC, a large electrophoretic mobility of the pseudostationary phase is often preferred because it increases the migration time window and allows for a better resolution, although it also increases the analysis time. A clear trend is seen in the electrophoretic mobility of the dimeric surfactants (Table 3.5). Their mobility increases

Table 3.5: Methylene selectivity α_{CH_2} , electrophoretic mobility μ_{net} , and efficiency N (\pm standard deviation) of SDS and dimeric surfactants.

	α_{CH_2} (C_1 - C_4) (n = 4)	α_{CH_2} (C_1 - C_6 & C_8) (n = 4)	μ_{net} (10^{-4} cm ² V ⁻¹ s ⁻¹) (n = 10)	N (n = 3)
SDS	2.58 \pm 0.00	n/a	-4.32 \pm 0.01	125 000 \pm 22 000
IIIa	2.49 \pm 0.01	2.79 \pm 0.02	-4.20 \pm 0.01	71 000 \pm 33 000
IIIb	2.49 \pm 0.00	2.76 \pm 0.02	-4.23 \pm 0.02	75 000 \pm 38 000
IIIc	2.48 \pm 0.01	2.76 \pm 0.05	-4.25 \pm 0.02	74 000 \pm 42 000
IIIe	2.49 \pm 0.01	2.88 \pm 0.04	-4.29 \pm 0.02	81 000 \pm 43 000

with increasing length of the spacer, perhaps due to small differences in viscosity of the BGE, or aggregation number of the micelles. However, the absolute differences are too small to be of practical importance in MEKC method development.

Finally, the efficiency of all the dimeric surfactants is roughly the same, and less than that of SDS (Table 3.5). The standard deviation of the efficiency is higher than for SDS, indicating that the efficiency varies more with the analyte for these dimeric surfactants than it does for SDS. This can be attributed to more severe peak broadening for some of the analytes [9]. This is also evident from the electropherograms in Fig. 3.5, where there is much more variation in peak widths for dimeric surfactant **IIIb** (Fig. 3.5b) than for SDS (Fig. 3.5a).

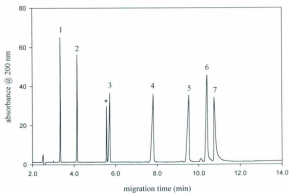
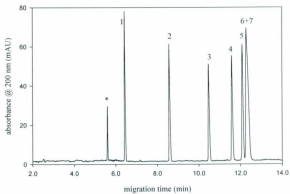


Fig. 3.5: Separation of a homologous series of alkyl benzoates with (a) 50 mM SDS and (b) 7.5 mM dimeric surfactant **IIIa**, both in 20 mM Na_2HPO_4 at pH 7.0. See experimental section for further details. Numbered peaks are methyl (1) through hexyl (6), and octyl (7) benzoate. * impurity.

3.4. Conclusion

This was the first systematic study on the influence of the spacer on the selectivity of anionic dimeric surfactants in MEKC. We demonstrated via LSERs that the disodium 1, ω -bis(decyloxymethyl)-dioxo alkane-1, ω disulfates with spacers containing 2, 4, 6 or 10 methylene groups, essentially have the same selectivity. This means that the cohesiveness of the micelles and their interface with the aqueous bulk phase is very similar, regardless of the length of the hydrophobic spacer. While these dimeric surfactants do not have a drastically different selectivity compared to other more common surfactants, they do seem to be better at separating more hydrophobic solutes than SDS. They can also be used at much lower concentrations than SDS, because of their lower CMCs. This could be an advantage for applications where a low current is required to minimize Joule heating, or for direct coupling of MEKC with mass spectrometry.

3.5. Acknowledgements

The financial support of the Canadian Foundation for Innovation and the Newfoundland and Labrador Industrial Research and Innovation Fund in the purchase of the Agilent ^{3D}CE system is gratefully acknowledged.

3.6. References

- [1] Z. Liu, H. Zou, M. Ye, J. Ni, Y. Zhang, *J. Chromatogr. A* 863 (1999) 69
- [2] J. Hernández-Borges, M.A. Rodríguez-Delgado, F.J. García-Montelongo, A. Cifuentes, *Electrophoresis* 26 (2005) 3799
- [3] E. Fuguet, C. Ràfols, E. Bosch, M. Rosés, M.H. Abraham, *J. Chromatogr. A* 907 (2001) 257
- [4] M. Aguilar, A. Farran, C. Serra, M.J. Sepaniak, K.W. Whitaker, *J. Chromatogr. A* 778 (1997) 201
- [5] J.G. Bumgarner, M.G. Khaledi, *J. Chromatogr. A* 738 (1996) 275
- [6] C.F. Poole, S.K. Poole, *J. Chromatogr. A* 792 (1997) 89
- [7] S.A. Shamsi, C.P. Palmer, I.M. Warner, *Anal. Chem.* 73 (2001) 140A
- [8] C.P. Palmer, *Electrophoresis* 23 (2002) 3993
- [9] D.S. Peterson, C.P. Palmer, *Electrophoresis* 22 (2001) 1314
- [10] K.L. Rundlett, D.W. Armstrong, *Anal. Chem.* 68 (1996) 3493
- [11] I. Ikeda, in R. Zana, J. Zia (Editors), *Gemini Surfactants – Synthesis, Interfacial and Solution-Phase Behavior, and Applications* (Surfactant Science Series Vol. 117), Marcel Dekker, New York, Basel, 2004, pp. 9-35
- [12] R. Zana, *J. Colloid Interface Sci.* 248 (2002), 203
- [13] R. Zana, *Adv. Colloid Interface Sci.* 97 (2002) 205
- [14] Y. Zhu, A. Masuyama, Y. Kirito, M. Okahara, M.J. Rosen, *J. Am. Oil Chem. Soc.* 69 (1992) 626
- [15] H. Harino, M. Tanaka, T. Araki, Y. Yasaka, A. Masuyama, Y. Nakatsuji, I. Ikeda, K. Funazo, S. Terabe, *J. Chromatogr. A* 715 (1995) 135

- [16] H. Harino, Y. Inoue, J. Yoshioka, S. Tsunoi, M. Eguchi, Y. Yasaka, K. Funazo, M. Tanaka, *J. Chromatogr. A* 755 (1996) 147
- [17] C. Akbay, R.A. Agbaria, I.M. Warner, *Electrophoresis* 26 (2005) 426
- [18] C.F. Poole, S.K. Poole, *J. Chromatogr. A* 965 (2002) 263
- [19] M.D. Trone, J.P. Mack, H.P. Goodell, M.G. Khaledi, *J. Chromatogr. A* 888 (2000) 229
- [20] M.D. Trone, M.G. Khaledi, *J. Micro. Sep.* 12 (2000) 433
- [21] C.F. Poole, S.K. Poole, M.H. Abraham, *J. Chromatogr. A* 798 (1998) 207
- [22] C.F. Poole, *The Essence of Chromatography*, Elsevier, Amsterdam, 2003, pp. 13-19
- [23] E. Fuguet, C. Ràfols, E. Bosch, M.H. Abraham, M. Rosés, *Electrophoresis* 27 (2006) 1900
- [24] M. Vitha, P.W. Carr, *J. Chromatogr. A* 1126 (2006) 143
- [25] E. Fuguet, C. Ràfols, E. Bosch, M.H. Abraham, M. Rosés, *J. Chromatogr. A* 942 (2002) 237
- [26] M.D. Trone, M.G. Khaledi, *Anal. Chem.* 71 (1999) 1270
- [27] M.D. Trone, M.G. Khaledi, *Electrophoresis* 21 (2000) 2390
- [28] S. De, V.K. Aswal, P.S. Goyal, S. Bhattacharya, *J. Phys. Chem.* 100 (1996) 11664
- [29] M. Aamodt, M. Landgren, B. Jönsson, *J. Phys. Chem.* 96 (1992) 945
- [30] M.H. Abraham, *Chem. Soc. Rev.* 22 (1993) 73
- [31] M.M. Bushey, J.W. Jorgenson, *Anal. Chem.* 61 (1989) 491
- [32] Anonymous, *Agilent ChemStation for CE systems*, Edition 06/03, Agilent Technologies 2003, Waldbronn, Germany, order No. G2172-90007

- [33] T. Kida, M. Yokota, A. Masuyama, Y. Nakatsuji, M. Okahara. *Synthesis* (1993) 487
- [34] Y-P. Zhu, A. Masuyama, M. Okahara, *J. Am. Oil Chem. Soc.* 67 (1990) 459
- [35] R. Oda, I. Huc, D. Danino, Y. Talmon, *Langmuir* 16 (2000) 9759
- [36] R. Zana, M. Benraou, R. Rueff, *Langmuir* 7 (1991) 1072
- [37] G.W. Somsen, R. Mol, G.J. de Jong, *J. Chromatogr. A* 1000 (2003) 953
- [38] K.R. Nielsen, J.P. Foley, *J. Microcol. Sep.* 6 (1994) 139

Chapter 4

Linear Solvation Energy Relationships of Anionic Dimeric Surfactants in Micellar Electrokinetic Chromatography II. Effect of the Length of a Hydrophilic Spacer^{1,2}

¹ G. Van Biesen, C.S. Bottaro, *J. Chromatogr. A* 1180 (2008) 171

² Additional info can be found in Appendices 4-7

Abstract

Anionic dimeric surfactants with hydrophilic spacers containing two to six oxygen atoms were synthesized and applied as pseudostationary phases in micellar electrokinetic chromatography. Their selectivity was determined via linear solvation energy relationships. There were no differences in cohesiveness, polarizability or dipolarity with increasing spacer length, but there was a clear trend in increasing hydrogen bond accepting ability, and a concomitant decrease in hydrogen bond donating ability. The different selectivity of these dimeric surfactants compared to sodium dodecylsulfate can be useful for optimizing separations of mixtures of solutes for which these types of interactions are important. Their critical micelle concentrations were in the range of 0.2 - 0.3 mM, except for the surfactant with the shortest spacer (<0.03 mM), and are much lower than those of conventional surfactants used in micellar electrokinetic chromatography.

Keywords: Critical micelle concentration; Dimeric surfactants; Gemini surfactants; Linear solvation energy relationships; Micellar electrokinetic chromatography; Spacer

4.1. Introduction

Since its inception by Terabe in 1984 [1], micellar electrokinetic chromatography (MEKC) has become a popular technique for the separation of both charged and uncharged analytes, as demonstrated by an ever growing number of publications and by regular reviews on recent advances in the field [2-4]. While sodium dodecylsulfate (SDS) is the pseudo-stationary phase (PSP) of choice for the majority of applications, other commercially available anionic surfactants such as various bile salts [5,6], and cationic surfactants such as cetyltrimethylammonium bromide and tetradecyltrimethylammonium bromide [7,8] have also found application. The type of PSP can have a significant effect on the selectivity of a specific separation, and in the last couple of years considerable effort has been invested in synthesizing and evaluating novel PSPs for MEKC. Polymeric surfactants in particular have been an active area of research [9], mainly because their zero critical micelle concentration (CMC) does not require any self-assembly of micelles in solution, and because of the variety of chemical structures available. Other PSPs include zwitterions [10], non-ionic PSPs charged in situ [11] or used for the analysis of anionic solutes [12], and mixed micelles of either two ionic surfactants [13] or a non-ionic and an ionic surfactant [14]. Recently, ionic liquids have caught the attention of separation scientists, and they have been found useful as PSP modifiers for polymeric PSPs [15] and for SDS [16]. Ionic liquid type cationic surfactants also gave very satisfactory separations and it is expected that their structure can be tailored to provide desired selectivity [17].

The selectivity differences between PSPs are best understood using linear solvation energy relationship (LSERs) [18-21], in a form suitable for MEKC represented by the following equation:

$$\log k = c + eE + sS + aA + bB + vV \quad (\text{Eq. 4.1})$$

where the solute descriptors are the excess molar refraction E (related to the polarizability of the solute – mainly from the presence of n-bonding and π -bonding electrons), the dipolarity S (the ability to engage in dipole-dipole or induced dipole-dipole interactions, with some contribution from polarizability), the hydrogen bond donating ability A , the hydrogen bond accepting ability B , and McGowan's characteristic volume V . The $\log k$ values of a set of typically 30 – 40 solutes can be related to their descriptors using multiple linear regression to obtain the system constants. The c system constant depends in part on the phase ratio and takes into account effects not incorporated in the descriptors, while the other system constants (e , s , a , b and v) describe the ability of the PSP, relative to the aqueous phase, to engage in the aforementioned types of interactions.

Anionic dimeric (or gemini) surfactants have not been thoroughly evaluated for use in MEKC, despite some potentially attractive features. They have CMCs typically one to two orders of magnitude lower than those of the corresponding monomeric surfactants, they seem to have better solubilizing properties, and the micelle shape and properties depend to some extent on the length of the spacer [22]. It is expected that the length and the nature of the spacer could be used to manipulate the selectivity of these dimeric

surfactants. There is a lot of experimental evidence that both polar and non-polar solutes interact with the so-called palisade layer of the micelles, which is the region of the micelles at the interface with the aqueous phase, and which contains significant amounts of water [19,23-25]. The spacer in dimeric surfactants is situated at the edge of the palisade layer close to the aqueous phase. Depending on the presence of specific functional groups in the spacer, we can expect its interaction with water and with different types of solutes to be either enhanced or reduced. We showed in a previous report [26] that there are no differences in selectivity between dimeric surfactants with hydrophobic spacers differing only in the number of methylene groups. As a group, compared to SDS, they are slightly more cohesive, interact somewhat better with polarizable solutes, are better hydrogen bond acceptors and worse hydrogen bond donors, while there is no significant difference in dipolarity. The better hydrogen bond accepting ability is likely due to the presence of the two oxygen atoms in the spacer. Generally, anionic PSPs are weak hydrogen bond acceptors (negative or small positive a system constants) compared to the bulk aqueous phase [27] so there could be some interest in anionic PSPs that are better hydrogen bond acceptors. We now report on the synthesis and selectivity of dimeric surfactants with hydrophilic spacers containing two to six oxygen atoms, introduced as ethoxy groups. We expect these surfactants to be increasingly better hydrogen bond acceptors and worse hydrogen bond donors. It is not possible, however, to make any quantitative predictions; e.g. by how much the a system constant will increase, or the b system constant will decrease.

4.2. Experimental

4.2.1. Capillary electrophoresis instrument and conditions

All experiments were performed on an Agilent ^{3D}CE system (Agilent Technologies Canada, Mississauga), running on Chemstation software (Rev. A.08.03). Bare fused silica capillaries with an I.D. of 50 μm were purchased from MicroSolv (MicroSolv Technology Corporation, Eatontown, NJ, USA) and were cut to a length of 48 – 50 cm. The MicroSolv Window Maker was used to burn a small window 8.5 cm from the outlet and to remove approximately 2 mm of polyimide at both ends of the capillaries.

The background electrolyte (BGE) consisted of 20 mM Na_2HPO_4 and 20 mM dimeric surfactant, or 50 mM SDS (except where noted), adjusted to $\text{pH } 7.00 \pm 0.03$ with dilute H_3PO_4 so that none of the solutes were ionized to any significant extent. All solutions were filtered through 0.2 μm nylon filters (National Scientific Company, Rockwood, TN, USA). The capillaries were conditioned at the beginning of each day by flushing with 0.1 M NaOH (5 min.), nanopure water (5 min.), and BGE (10 min.) respectively. Analyses were performed at 25 $^\circ\text{C}$, with 25 kV applied (ramped from 0 to 25 kV in 15 s). Samples were injected by applying 10 mbar of pressure for 5 s, followed by BGE at 10 mbar for 5 s, and the detection wavelength was 200 nm. For SDS, we used a second detection wavelength at 194 nm, since this was better for detecting the baseline disturbance from the electroosmotic flow (EOF) marker (methanol). Peaks were identified by comparison of their UV-spectra with entries in a spectral library. Between runs, the capillary was flushed with BGE for 3 minutes.

4.2.2. Solutes

Most of the test solutes (Table 4.1) were obtained from Sigma-Aldrich (Oakville, Canada) and had a purity $\geq 98\%$, except 4-phenylphenol (97%) and 1-methylnaphthalene (97%). The series of n-alkyl benzoates ($C_1 - C_6$, and C_8) was prepared by reacting the corresponding n-alcohols (PolyScience Corporation, Evanston, IL, USA) with benzoylchloride in the presence of triethylamine. A cross-correlation matrix of the 41 solutes shows that there is no correlation between the solute descriptors (Table 4.2).

Solutions of 4 or 5 solutes (plus dodecanophenone as micelle marker) were prepared in methanol at concentrations between 300 and 600 mg/L. No co-migration of solutes was observed with any of the PSPs, and solutes could be identified based upon their UV-spectrum. Where homologous solutes such as methyl- and ethyl benzoate (which have undistinguishable UV-spectra) were added in the same solution, it was rationalized that the lower molecular weight solute would have the shorter migration time. All samples were run three to four times, and average retention factors were calculated (Table 1).

4.2.3. Calculations

Retention factors were calculated from:

$$k = (t_m - t_0) / [t_0 (1 - t_m/t_{mc})] \quad (\text{Eq.4.2})$$

with t_m the migration time of the solute, t_0 the migration time of an unretained solute (methanol), and t_{mc} the migration time of the micellar marker (dodecanophenone) [20].

The iterative procedure described by Bushey and Jorgenson [29], using Microsoft Excel's 'solver' tool to maximize the correlation coefficient, was used to determine the

Table 4.1: Solutes and their descriptors (from [15], except for pyrrole and resorcinol [16], ethyl benzoate and 1-methyl naphthalene [18], and 2-chlorophenol [23]), and log k

	<i>V</i>	<i>E</i>	<i>S</i>	<i>A</i>	<i>B</i>	log k					
						SDS	IIa	IIIb	IIIc	IIId	IIIf
1 1,2-Dichlorobenzene	0.9612	0.872	0.78	0.00	0.04	1.06	1.07	1.13	1.17	1.20	1.24
2 Chlorobenzene	0.8388	0.718	0.65	0.00	0.07	0.55	0.51	0.56	0.58	0.61	0.64
3 Bromobenzene	0.8914	0.882	0.73	0.00	0.09	0.70	0.66	0.71	0.75	0.78	0.80
4 Toluene	0.8573	0.601	0.52	0.00	0.14	0.44	0.33	0.36	0.38	0.39	0.42
5 Naphthalene	1.0854	1.340	0.92	0.00	0.20	1.12	1.07	1.10	1.15	1.17	1.20
6 Fluorene	1.3565	1.588	1.03	0.00	0.20	1.88	1.84	1.89	1.92	1.94	1.97
7 1-Methylnaphthalene	1.2260	1.344	0.90	0.00	0.20	1.52	1.48	1.53	1.56	1.58	1.61
8 Biphenyl	1.3242	1.360	0.99	0.00	0.22	1.63	1.58	1.63	1.66	1.69	1.72
9 Nitrobenzene	0.8910	0.871	1.11	0.00	0.28	0.11	-0.11	-0.08	-0.04	-0.01	0.02
10 Anisole	0.9160	0.708	0.75	0.00	0.29	0.22	0.00	0.04	0.05	0.07	0.10
11 1-Nitronaphthalene	1.2596	1.600	1.51	0.00	0.29	1.26	1.08	1.14	1.19	1.23	1.27
12 Benzaldehyde	0.8730	0.820	1.00	0.00	0.39	0.02	-0.36	-0.35	-0.35	-0.34	-0.32
13 Methyl benzoate	1.0726	0.733	0.85	0.00	0.46	0.52	0.10	0.09	0.09	0.11	0.13
14 Ethyl benzoate	1.2140	0.689	0.85	0.00	0.46	0.90	0.44	0.44	0.44	0.45	0.48
15 Propyl benzoate	1.3544	0.675	0.80	0.00	0.46	1.33	0.85	0.85	0.86	0.87	0.89
16 Butyl benzoate	1.4953	0.668	0.80	0.00	0.46	1.77	1.30	1.30	1.31	1.31	1.34
17 Acetophenone	1.0139	0.818	1.01	0.00	0.48	0.21	-0.24	-0.25	-0.25	-0.25	-0.23
18 Valerophenone	1.4370	0.795	0.95	0.00	0.50	1.30	0.83	0.83	0.84	0.85	0.86
19 Phenyl acetate	1.0730	0.661	1.13	0.00	0.54	0.18	-0.28	-0.27	-0.30	-0.28	-0.27
20 N-Methylaniline	0.9571	0.948	0.90	0.17	0.43	0.06	-0.22	-0.18	-0.16	-0.14	-0.12
21 Aniline	0.8162	0.955	0.96	0.26	0.50	-0.34	-0.54	-0.51	-0.50	-0.49	-0.47
22 4-Chloroaniline	0.9390	1.060	1.13	0.30	0.35	0.28	0.25	0.33	0.37	0.41	0.44
23 2-Phenylethanol	1.0569	0.811	0.91	0.30	0.64	0.02	-0.33	-0.32	-0.33	-0.33	-0.32
24 4-Phenyl-1-butanol	1.3387	0.811	0.90	0.33	0.70	0.75	0.33	0.33	0.34	0.35	0.37
25 Benzyl alcohol	0.9160	0.803	0.87	0.33	0.56	-0.26	-0.56	-0.55	-0.55	-0.55	-0.53
26 Geraniol	1.4903	0.513	0.63	0.39	0.66	1.26	0.77	0.78	0.76	0.77	0.79
27 Acetanilide	1.1133	0.870	1.40	0.50	0.67	-0.12	-0.40	-0.38	-0.37	-0.35	-0.33
28 Benzenesulfonamide	1.0971	1.130	1.55	0.55	0.80	-0.43	-0.68	-0.67	-0.66	-0.65	-0.64
29 2-Chlorophenol	0.8975	0.853	0.88	0.32	0.31	0.17	0.17	0.25	0.31	0.38	0.42
30 Pyrrole	0.5774	0.613	0.73	0.41	0.29	-0.81	-0.80	-0.74	-0.72	-0.68	-0.65
31 4-Nitroaniline	0.9910	1.220	1.91	0.42	0.38	0.01	-0.07	0.01	0.07	0.14	0.18
32 Indole	0.9460	1.200	1.12	0.44	0.31	0.27	0.35	0.45	0.51	0.58	0.62
33 4-Phenylphenol	1.3829	1.560	1.41	0.59	0.45	1.35	1.29	1.38	1.43	1.51	1.55
34 Phenol	0.7751	0.805	0.89	0.60	0.30	-0.30	-0.39	-0.32	-0.29	-0.24	-0.20
35 2-Naphthol	1.1440	1.520	1.08	0.61	0.40	0.83	0.80	0.88	0.94	1.01	1.05
36 Methyl 3-hydroxybenzoate	1.1313	0.905	1.40	0.66	0.45	0.29	-0.03	0.00	0.03	0.07	0.10
37 4-Chlorophenol	0.8975	0.915	1.08	0.67	0.20	0.36	0.40	0.50	0.55	0.62	0.67
38 Propyl 4-hydroxybenzoate	1.4131	0.860	1.35	0.69	0.45	1.09	0.74	0.77	0.81	0.87	0.91
39 Catechol	0.8338	0.970	1.10	0.88	0.47	-0.46	-0.51	-0.45	-0.43	-0.39	-0.35
40 Resorcinol	0.8338	0.980	1.00	1.10	0.58	-0.65	-0.63	-0.57	-0.53	-0.47	-0.43
41 Hydroquinone	0.8338	1.000	1.00	1.16	0.60	-0.87	-0.86	-0.80	-0.80	-0.75	-0.72

Table 4.2: Cross-correlation matrix (r^2 values) of the descriptors of the 41 solutes of Table 4.1

	<i>V</i>	<i>E</i>	<i>S</i>	<i>A</i>	<i>B</i>
<i>V</i>	1.00				
<i>E</i>	0.05	1.00			
<i>S</i>	0.03	0.29	1.00		
<i>A</i>	0.05	0.01	0.13	1.00	
<i>B</i>	0.07	0.04	0.09	0.18	1.00

methylene selectivity (α_{C12}) from the slope (*m*) of a plot of log *k* vs. carbon number ($\alpha_{C12} = 10^m$) of a homologous series of alkyl benzoates (C₁-C₆ or C₁-C₆ & C₈). This slope represents an average methylene selectivity for the entire homologous series [30].

The electrophoretic mobility μ_e (cm² V⁻¹ s⁻¹) of the pseudostationary phases was calculated from:

$$\mu_e = (lL/V_a) \cdot (1/t_{mc} - 1/t_0) \quad (\text{Eq. 4.3})$$

with *l* the length of the capillary to the detector, and *L* the total length of the capillary.

The average voltage V_a is calculated from:

$$V_a = V \cdot (1 + t_R/2t_{mc}) \quad (\text{Eq. 4.4})$$

where *V* is the end voltage (25 000 V) and *t_R* is the ramp time (15 s) [31].

4.2.4. Synthesis and analysis of dimeric surfactants

Dimeric surfactants with a hydrophilic spacer were synthesized from oligoethylene glycols in three steps (Fig. 4.1). All reagents were purchased from Aldrich

and had a purity of at least 97%. Note that compounds **Ia**, **IIa** and **IIIa** in this article and in our previous report [26] are identical.

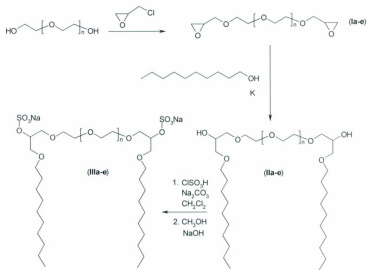


Fig. 4.1: Synthetic pathway to the dimeric surfactants for this project; $n = 0$ (**Ia-IIIa**), $n = 1$ (**Ib-IIIb**), $n = 2$ (**Ic-IIIc**), $n = 3$ (**Id-IIId**), $n = 4$ (**Ie-IIIE**)

The synthesis of the diglycidyl ethers (**Ia-e**) was based upon Gu et al. [32]. Oligoethylene glycol (0.10 mol) was added drop wise into a mixture of epichlorohydrin (0.60 mol), sodium hydroxide pellets (0.60 mol), water (2.4 mL), and tetrabutylammonium bisulphate (TBAB) (0.002 mol) with rapid stirring at a temperature

of 40-45 °C. The reaction mixture was stirred for a total of 45 min at 40-45 °C, and was then filtered. The solid material was washed with dichloromethane; dichloromethane and excess epichlorohydrin were evaporated under reduced pressure. The pure oligoethylene diglycidyl ethers (**Ia-e**) were obtained after silica column chromatography, typically with dichloromethane:methanol 97:3 (v/v), with yields of 50 – 83%.

The synthesis of the long-chain diols (**IIa-e**) has been reported in detail elsewhere [26]; however, reaction times have been reduced to 2 – 2.5 hrs, and column chromatography was typically performed with hexane:ethyl acetate 40:60 (v/v), giving compounds **IIa-e** with yields of 40 – 64%. The synthesis of the dimeric surfactants is also described elsewhere [26]. We have found it convenient to follow the progress of the reaction with negative ESI-MS, and if after 1 hr of reaction time monosulfated product **IIa-e** was still present, extra chlorosulfonic acid was added. Yields were 61-71%.

All products were characterized with ¹H-NMR (Bruker Avance 500 MHz). Intermediate products **Ia-e** and **IIa-e** were dissolved in chloroform-*d* (CDCl₃). Dimeric surfactants **IIIa-e** were dissolved in [²H₆] dimethyl sulfoxide (DMSO-*d*₆), after storing in a desiccator under vacuum over night, because the ¹H-NMR spectra showed better resolution than in CDCl₃ [26]. Dimeric surfactants **IIIa-e** were also characterized by negative electrospray ionization mass spectrometry (ESI-MS), using an Agilent 1100 Series LC/MSD Trap. Samples were dissolved in methanol at a concentration of approximately 300 mg/L, and run with methanol:water 50:50 (v/v) as eluent. For the determination of the CMC, the probe of a Hach Model CO150 Conductivity Meter with automatic temperature compensation (Hach Company, Loveland, CO, USA) was placed in an accurately measured volume of nanopure water at room temperature. Small volumes

of an accurately prepared solution of dimeric surfactant (-0.002 M) were added with a pipettor, while the solution was stirred. The solution was allowed to equilibrate for approximately one minute between each addition before the conductance was recorded. CMCs were determined from the break point of conductance at 25 °C vs. molar concentration plots [22].

4.3. Results and discussion

4.3.1. Analysis and CMCs of dimeric surfactants

$^1\text{H-NMR}$ spectra and negative ESI-MS spectra were in accordance with the expected structures (Table 4.3). Mass spectra typically showed peaks corresponding to $[\text{M} - \text{Na}]^-$, $[\text{M} - 2\text{Na}]^{2-}$, and $[\text{M} - 2\text{Na} + \text{H}]^-$; **IIIc** and **III d** had minor amounts (3 and 6% respectively) of unidentified ions.

Table 4.3: $^1\text{H-NMR}$ and ESI-MS data, and CMCs of dimeric surfactants

	Formula MM	$^1\text{H-NMR}^a$ (δ , ppm)	m/z (neg. ESI) ^b	CMC (mM) at 25 °C
IIIa	$\text{C}_{20}\text{H}_{36}\text{O}_{12}\text{S}_2\text{Na}_2$ 694.8	0.86 (t;6H), 1.24 (m;28H), 1.46 (m;4H), 3.35 (m;4H) ^c , 3.45-3.55 (m;12H) 4.17 (m;2H)	671.2 (100%), 324.1 (67%), 649.2 (35%)	<0.03
IIIb	$\text{C}_{30}\text{H}_{56}\text{O}_{13}\text{S}_2\text{Na}_2$ 738.9	0.85 (t;6H), 1.25 (m;28H), 1.46 (m;4H), 3.35 (m;4H) ^c , 3.45-3.55 (m;16H), 4.17 (m;2H)	715.4 (73%), 346.2 (100%), 693.3 (31%)	0.28
IIIc	$\text{C}_{22}\text{H}_{38}\text{O}_{14}\text{S}_2\text{Na}_2$ 783.0	0.86 (t;6H), 1.25 (m;28H), 1.46 (m;4H), 3.35 (m;4H) ^c , 3.45-3.55 (m;20H), 4.17 (m;2H)	759.4 (60%), 368.2 (100%), 737.4 (31%), 451.3 (3%)	0.20
III d	$\text{C}_{34}\text{H}_{66}\text{O}_{15}\text{S}_2\text{Na}_2$ 827.0	0.85 (t;6H), 1.25 (m;28H), 1.46 (m;4H), 3.35 (m;4H) ^c , 3.45-3.55 (m;24H), 4.16 (m;2H)	803.4 (48%), 390.3 (100%), 781.4 (19%), 543.2 (6%)	0.33
IIIe	$\text{C}_{34}\text{H}_{72}\text{O}_{16}\text{S}_2\text{Na}_2$ 871.1	0.85 (t;6H), 1.24 (m;28H), 1.46 (m;4H), 3.35 (m;4H) ^c , 3.45-3.55 (m;28H), 4.17 (m;2H)	847.5 (33%), 412.3 (100%), 825.5 (17%)	0.30

^a Samples in DMSO- d_6 ; t: triplet; m: multiplet

^b Intensity as a percentage of base peak in parentheses; mass to charge ratios correspond to $[\text{M} - \text{Na}]^-$, $[\text{M} - 2\text{Na}]^{2-}$, and $[\text{M} - 2\text{Na} + \text{H}]^-$, respectively, other ions not identified

^c This multiplet also had a large peak from hydroxyl protons from water, invariably present in the DMSO- d_6 .

There was no clear trend in the CMCs of the dimeric surfactants related to number of ethoxy groups in the spacer (Table 4.3). The CMCs of surfactants **IIIa** and **IIIe**, determined via surface tension measurements, are available from the literature [33]. The CMC of **IIIa** was too low to be verified via conductivity measurements [26]. The value we obtained for the CMC of **IIIe** (0.20 mM) was considerably higher than the reported value of 0.032 mM, but was independently confirmed via pyrene fluorescence quenching by Dr. R. Zana, who estimated the CMC at 0.15 - 0.30 mM. The CMC of **IIIe** was also confirmed with the same method. There is evidence that some dimeric surfactants can form small, non-globular aggregates below the CMC. These are of sufficient size to keep the surface tension constant after an initial drop, and differences between CMC values obtained via the surface tension method on the one hand, and conductivity and fluorescence quenching on the other hand, have been reported [34]. In these cases, the 'conventional' CMC is obtained by the latter techniques.

4.3.2. Linear Solvation Energy Relationships

LSERs of SDS and the five dimeric surfactants were determined using all 41 solutes (Table 4.4). The statistics can be considered good, with minimum F-values and r^2 -values of 308 and 0.978, respectively, and standard errors of fit ≤ 0.12 . Calculated $\log k$ values agreed well with experimental $\log k$ values for all LSERs, with standardized residuals (experimental $\log k$ minus calculated $\log k$ divided by an estimate of the standard deviation of the residual) rarely higher than 2 (the highest value was 2.1). Therefore, there were no solutes that had to be excluded from the data set due to a poor

fit. As discussed below, the results obtained also make sense from a chemical point of view, further underscoring the validity of the LSERs.

Table 4.4: System constants (standard error in brackets) and regression statistics for the LSERs of SDS and dimeric surfactants, using the 41 solutes from Table 1. Underlined value is not statistically different from zero ($p > 0.05$); SE is standard error of the fit.

	c	v	e	s	a	b	r^2	F	SE
SDS	-1.73 (0.07)	2.94 (0.06)	0.27 (0.06)	-0.39 (0.06)	-0.20 (0.04)	-1.86 (0.09)	0.992	827	0.07
IIIa	-1.69 (0.09)	2.67 (0.08)	0.60 (0.08)	-0.50 (0.08)	<u>0.02</u> (0.06)	-2.41 (0.12)	0.984	428	0.10
IIIb	-1.64 (0.09)	2.65 (0.09)	0.64 (0.08)	-0.49 (0.08)	0.13 (0.07)	-2.52 (0.13)	0.982	377	0.10
IIIc	-1.64 (0.10)	2.66 (0.09)	0.66 (0.09)	-0.47 (0.09)	0.16 (0.07)	-2.62 (0.14)	0.980	345	0.11
IIId	-1.62 (0.10)	2.66 (0.10)	0.66 (0.09)	-0.44 (0.09)	0.21 (0.07)	-2.71 (0.14)	0.979	319	0.11
IIIe	-1.60 (0.11)	2.68 (0.10)	0.66 (0.09)	-0.43 (0.09)	0.24 (0.07)	-2.77 (0.15)	0.978	308	0.12

We previously determined the system constants for SDS and **IIIa** using 34 and 33 solutes, respectively [26], and those values agree very well with those of the expanded data set that we report here. The biggest (but statistically insignificant) change is for the b system constant, which is now somewhat more negative for both SDS and **IIIa**. Note that the more positive value of c for **IIIa** reported here is due to use of a higher concentration (20 mM as opposed to 7.5 mM). This is also the reason that the log k values of **IIIa** (Table 1) are offset by a value of approximately 0.43 compared to the ones reported previously [26]. The rationale for increasing the surfactant concentrations was that we had quite a number of solutes with short migration times. There is a relatively large error associated with the determination of the retention factors of solutes with short (and long)

migration times [20], and increasing the surfactant concentration is one way to increase the migration times.

The dimeric surfactants with hydrophilic spacers all have the same cohesiveness (same value of v), which is somewhat lower than that for SDS. The polarizability (e system constant) is also the same for all dimeric surfactants, and higher than for SDS. There is a modest trend towards increasing ability to engage in dipole- (induced) dipole interactions (s system constant) with increasing number of ethoxy groups in the spacer, although statistically there are no differences between any of the surfactants in Table 4.4. As we expected, the hydrogen bond accepting ability (a system constant) gradually increases as the number of ethoxy groups in the spacer increases. The increase, however, is not dramatic: 0.03 – 0.06 units per ethoxy group. It is also evident that the hydrogen bond donating ability (b system constant) decreases with increasing number of ethoxy groups in the spacer. Since the PSPs do not have any hydrogen atoms that can engage in this type of interaction, their hydrogen bond donating ability is attributed to bound water molecules [19,27]. With increasing number of ethoxy groups in the spacers, the PSPs become better hydrogen bond acceptors because there are more sites with which hydrogen bond donating solutes can interact. Water molecules will also interact more strongly with the PSPs, and will consequently be less able to share their protons with solutes that are hydrogen bond acceptors. The decrease in the b system constant (0.06 – 0.11 units per ethoxy group) is roughly double the increase of the a system constant, although the standard errors are twice as high as well. Note that simply increasing the length of the spacer by itself does not necessarily change the selectivity, as we have shown earlier [26]. Rather, the change in selectivity is clearly attributed to the presence of

the ethoxy groups. It is also interesting to see that cohesiveness, polarizability and dipolarity are essentially the same as for dimeric surfactants with hydrophobic spacers [26].

The selectivities of these dimeric PSPs with hydrophilic spacers can be compared with the selectivities of the 55 PSPs compiled by Fuguet et al. [18], based upon normalized system constants. They are perhaps most similar to AGESS (13% C₁₂) (an allyl glycidyl ether sulfonate siloxane with pendant C₁₂ chains). A good match with a monomeric surfactant is harder to find, but mixtures of 50 mM SDS and 20-35 mM Brij 35 (polyoxyethylene (23) laurylether) provide a close match [18,35] (these were not included in the 55 PSPs, but appear in a separate table in [18]). The trend with increasing concentration of Brij 35 is similar to increasing the length of the spacer of dimeric PSPs with ethoxy groups: an increase in *a* and decrease in *b* values, while the other system constants change little. All these observations are consistent with the interphase model of retention, whereby polar solutes interact predominantly with the hydrated headgroup region of micelles [35,36]. An advantage of using the dimeric PSPs instead of SDS/Brij 35 mixtures would be that Brij 35 can adsorb to the capillary wall, requiring lengthy cleaning cycles between injections [35]. Note that with mixtures of sodium N-lauroyl-N-methyltaurate (LMT) and Brij 35, the effect of increasing concentration of Brij 35 is much less [18,36]. This may be due to the fact that LMT already is a considerably better hydrogen bond acceptor and worse hydrogen bond donor than SDS.

We can roughly categorize the 41 solutes of Table 4.1 in three groups, based upon their hydrogen bonding abilities [23]. Since all the solutes (except for geraniol) have at least one aromatic ring for easy UV detection, they are inherently weak hydrogen bond

acceptors, i.e. their B values are not zero. However, solutes with a B value ≤ 0.22 (solute 1-8 in Table 4.1) can be considered as non-hydrogen-bond solutes (NHB solutes) for the purposes of this classification. Hydrogen-bond-acceptors (HBA solutes) have B values > 0.22 and their B values are also higher than their A values (solute 9-28 in Table 4.1). Finally, hydrogen-bond-donors (HBD solutes) have A values higher than their B values (solute 29-41 in Table 4.1). A plot of the retention factors of the 41 solutes of Table 1 for SDS vs. those for **IIIe** (Fig. 4.2a) shows the effect of the different selectivities of these PSPs on different types of solutes. It has to be stressed that the retention of a solute by a particular PSP is always the result of multiple interactions working simultaneously. Furthermore, not all solutes fit neatly into one of the above categories. For instance, some solutes have almost equally good hydrogen bond donating and accepting abilities (e.g. 2-chlorophenol and 4-chloroaniline). Nevertheless, the selectivity of the PSPs can be rationalized mainly through hydrogen bond interactions (Fig. 4.2a) [23]. HBA solutes plot predominantly (18 out of 20) below the fitted curve, which means that they have a stronger interaction with SDS. This is consistent with SDS being a better hydrogen bond donor (more positive b system constant) than **IIIe**. Conversely, HBD solutes plot mainly (11 out of 13) above the fitted curve because **IIIe** is the better hydrogen bond acceptor (higher a value). The stronger interaction of NHB solutes with **IIIe** (they all plot above the fitted curve) is mainly a consequence of the higher e system constant of this PSP compared to that of SDS, since the s system constants are not that different. The differences between the dimeric PSPs are much less, as can be seen from a plot of retention factors of PSP **IIIa** (shortest spacer) vs. **IIIe** (longest spacer) (Fig. 4.2b). However, the small differences in hydrogen bond accepting and donating abilities

between these PSPs are still reflected in the graph: all HBD solutes plot above the fitted line (**IIIe** is the better hydrogen bond acceptor), while the vast majority of HBA solutes plot below the fitted line (**IIIa** is the better hydrogen bond donor). Since there are no significant differences between the other system constants, NHB solutes plot on the fitted line.

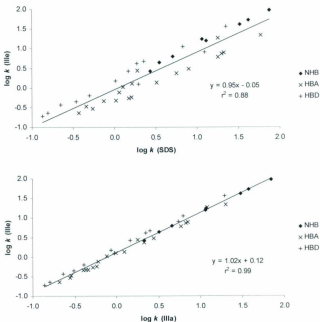


Fig. 4.2: Selectivity plot of dimeric surfactant (a) **IIIe** vs. SDS and (b) **IIIe** vs **IIIa**. NHB are non-hydrogen-bonding solutes (1-8 in Table 1), HBA are hydrogen-bond-acceptors (9-28 in Table 1), and HBD are hydrogen-bond-donors (29-41 in Table 4.1).

An example of how the differences in selectivity between SDS and the dimeric PSPs can affect the migration order of specific solutes is shown in Fig. 4.3. Since the dimeric PSPs have two long chains per molecule, we think it is appropriate to compare a BGE with 40 mM SDS with a BGE with 20 mM dimeric PSP. The reversal in migration order for benzyl alcohol and phenol with SDS and with PSP **IIIa** (Fig. 4.3a and b) can be rationalized by their different abilities to engage in hydrogen bonding, since the other system descriptors are almost the same. Benzyl alcohol is a better hydrogen bond acceptor than phenol (larger B value), and since the b system constant of PSP **IIIa** is large and negative, the bB term for benzyl alcohol will also be large and more negative than that for phenol, favouring distribution to the aqueous phase. Since the b system constant of SDS is smaller than that of PSP **IIIa**, the differences in retention between benzyl alcohol and phenol will be less with SDS as the PSP. The small values of the aA terms for both solutes in both PSPs are almost inconsequential. A similar rationale explains the reversal in migration order for toluene and methyl benzoate, but for geraniol and 1-nitronaphthalene, differences in the E and S descriptors also contribute significantly to the different migration behaviours with SDS and with PSP **IIIa**. The most significant effect of increasing spacer length (Fig. 4.3b-d) seems to be an increase in the resolution between benzyl alcohol and phenol. This is due to an increase in the retention factor of phenol, while the retention factor of benzyl alcohol hardly changes at all (Table 4.1). This illustrates that for certain solutes even relatively small changes in system constants of PSPs can be exploited to fine-tune their separation.

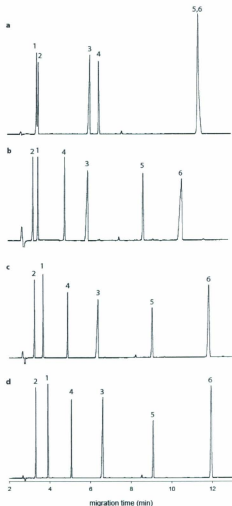


Fig. 4.3: Electropherograms of a mixture of phenol (1), benzyl alcohol (2), toluene (3), methyl benzoate (4), geraniol (5) and 1-nitronaphthalene (6) with (a) 40 mM SDS and 20 mM dimeric surfactant, (b) IIIa, (c) IIIc and (d) IIIe, all in 20 mM phosphate buffer at pH 7.0. See text for further details.

The methylene selectivity, a measure for how well a PSP can resolve solutes that differ by one methylene group, was independent of spacer length (Table 4.5), and virtually the same as for SDS. There was also no obvious trend for the electrophoretic mobility (Table 4.5), which was generally slightly less than for SDS.

Table 4.5: Methylene selectivity and electrophoretic mobility (\pm standard deviation) of SDS and dimeric surfactants

	α_{CH_2} ($n = 3$)	μ_{mc} (10^{-4} cm ² ·V ⁻¹ ·s ⁻¹) ($n = 30$)
SDS	2.56 \pm 0.00	-4.32 \pm 0.02
IIIa	2.55 \pm 0.00	-4.22 \pm 0.02
IIIb	2.54 \pm 0.00	-4.29 \pm 0.02
IIIc	2.55 \pm 0.01	-4.29 \pm 0.03
IIId	2.52 \pm 0.01	-4.20 \pm 0.02
IIIe	2.53 \pm 0.00	-4.15 \pm 0.01

4.4. Conclusions

This report shows that incorporating functional groups into the spacer can change the selectivity of dimeric surfactants. Specifically, LSERs indicate that the presence of up to six oxygen atoms in the spacer steadily increases the hydrogen bond accepting ability (a system constant) and decreases the hydrogen bond donating ability (b system constant). These effects, although relatively modest, can be useful in optimizing separations, and are similar to the ones observed for mixtures of SDS and Brij 35. They are consistent with the interphase model of retention. Interestingly, the LSER results so far indicate that the cohesiveness, polarizability and dipolarity of dimeric surfactants are essentially the same, regardless of the length and the nature (hydrophobic or hydrophilic) of the spacer.

4.5. Acknowledgements

We sincerely thank Dr. R. Zana at the Institut Charles Sadron (France) for his help in the confirmation of the CMCs of two of the dimeric surfactants.

The financial support of the Canadian Foundation for Innovation and the Newfoundland and Labrador Industrial Research and Innovation Fund in the purchase of the Agilent ³⁰CE system, and the Natural Sciences and Engineering Research Council of Canada, are gratefully acknowledged.

4.6. References

- [1] S. Terabe, K. Otsuka, K. Ichikawa, A. Tsuchiya, T. Ando, *Anal. Chem.* 56 (1984) 111
- [2] M. Molina, M. Silva, *Electrophoresis* 23 (2002) 3907
- [3] M. Silva, *Electrophoresis* 28 (2007) 174
- [4] T.J. Pappas, M. Gayton-Ely, L.A. Holland, *Electrophoresis* 26 (2005) 719
- [5] J. Olivares, M.J. Conner, C.A. Vass, W.E. Kurtin, M.M. Bushey, *Electrophoresis* 26 (2005) 920
- [6] J.M. Bermúdez-Saldaña, M.A. García, M.J. Medina-Hernández, M.L. Marina, *J. Chromatogr. A* 1052 (2004) 171
- [7] J.-B. Kim, J.P. Quirino, K. Otsuka, S. Terabe, *J. Chromatogr. A* 916 (2001) 123
- [8] H.-J. Shen, C.-H. Lin, *Electrophoresis* 27 (2006) 1255
- [9] C.P. Palmer, J.P. McCarney, *J. Chromatogr. A* 1044 (2004) 159
- [10] M.R. Hadley, M.W. Harrison, A.J. Hutt, *Electrophoresis* 24 (2003) 2508
- [11] J.T. Smith, W. Nashabeh, Z. El Rassi, *Anal. Chem.* 66 (1994) 1119

- [12] M. Molina, M. Silva, *Electrophoresis* 22 (2001) 1175
- [13] E. Fuguet, C. Ráfols, E. Bosch, M. Rosés, M.H. Abraham, *J. Chromatogr. A* 907 (2001) 257
- [14] E. Orejuela, M. Silva, *Electrophoresis* 26 (2005) 2991
- [15] S.M. Mwangela, A. Numan, N.L. Gill, R.A. Agbaria, I.M. Warner, *Anal. Chem.* 75 (2003) 6089
- [16] K. Tian, S. Qi, Y. Cheng, X. Chen, Z. Hu, *J. Chromatogr. A* 1078 (2005) 181
- [17] V.P. Schnee, G.A. Baker, E. Rauk, C.P. Palmer, *Electrophoresis* 27 (2006) 4141
- [18] E. Fuguet, C. Ráfols, E. Bosch, M.H. Abraham, M. Rosés, *Electrophoresis* 27 (2006) 1900
- [19] M. Vitha, P.W. Carr, *J. Chromatogr. A* 1126 (2006) 143
- [20] C.F. Poole, S.K. Poole, M.H. Abraham, *J. Chromatogr. A* 798 (1998) 207
- [21] E. Fuguet, C. Ráfols, E. Bosch, M.H. Abraham, M. Rosés, *J. Chromatogr. A* 942 (2002) 237
- [22] R. Zana, *Adv. Colloid Interface Sci.* 97 (2002) 205
- [23] M.D. Trone, M.G. Khaledi, *Anal. Chem.* 71 (1999) 1270
- [24] M. Aamodt, M. Landgren, B. Jönsson, *J. Phys. Chem.* 96 (1992) 945
- [25] C.F. Poole, S.K. Poole, *J. Chromatogr. A* 792 (1997) 89
- [26] G. Van Biesen, C.S. Bottaro, *J. Chromatogr. A* 1157 (2007) 437
- [27] S.T. Burns, A.A. Agbodjan, M.G. Khaledi, *J. Chromatogr. A* 973 (2002) 167
- [28] M.H. Abraham, *Chem. Soc. Rev.* 22 (1993) 73
- [29] M.M. Bushey, J.W. Jorgenson, *Anal. Chem.* 61 (1989) 491
- [30] D.S. Peterson, C.P. Palmer, *Electrophoresis* 22 (2001) 1314

- [31] Anonymous, Agilent ChemStation for CE systems, Edition 06/03, Agilent Technologies 2003, Waldbronn, Germany, order No. G2172-90007
- [32] X.-P. Gu, I. Ikeda, M. Okahara, *Synthesis* 1985 (1985) 649
- [33] Y.-P. Zhu, A. Masuyama, M. Okahara, *J. Am. Oil Chem. Soc.* 67 (1990) 459
- [34] A. Pinazo, X. Wen, L. Pérez, M.-R. Infante, E.I. Franses, *Langmuir* 15 (1999) 3134
- [35] S.K. Poole, C.F. Poole, *J. High Resolut. Chromatogr.* 20 (1997) 174
- [36] S.K. Poole, C.F. Poole, *Anal. Commun.* 34 (1997) 57

Chapter 5

Linear Solvation Energy Relationships of Anionic Dimeric Surfactants in Micellar Electrokinetic Chromatography

III. Effect of Fluorination^{1,2}

¹ A version of this chapter (excluding Section 5.7) has been submitted to *J. Chromatogr. A*

² Additional information can be found in Appendices 8-10

Abstract

The range of selectivities of pseudostationary phases (PSPs) available for micellar electrokinetic chromatography (MEKC) is limited, and there continues to be interest in the synthesis and evaluation of novel PSPs. With the unique selectivity of lithium perfluorooctanesulfonate (LPFOS) in mind, we synthesized anionic dimeric surfactants with fluorinated spacers of various lengths. Their selectivity was analyzed via linear solvation energy relationships (LSERs) and is not very different from that of their non-fluorinated analogues, although they are somewhat less polarizable and they are worse hydrogen bond acceptors. Fluorination does not have as dramatic an effect on the selectivity as in LPFOS. This is explained in terms of the inferred poor hydration of the fluorinated spacer, and of the position of the fluorine substituents. They are too far away from the surfactant head groups to fully exert the strong inductive effect required to significantly influence the head group chemistry.

Keywords: Critical micelle concentration; Dimeric surfactants; Fluorination; Gemini surfactants; Linear solvation energy relationships; Micellar electrokinetic chromatography; Spacer

5.1. Introduction

We continue our investigation of the influence of the spacer on the selectivity of anionic dimeric surfactants in micellar electrokinetic chromatography (MEKC) [1,2] by examining the effect of fluorination. The physical properties of organic compounds can be affected dramatically when hydrogen atoms are substituted for fluorine, mainly because of fluorine's high electronegativity and small size (low polarizability). For instance, as a result of weaker intermolecular forces, saturated perfluorinated compounds exhibit boiling points and surface tensions much lower than the analogous hydrocarbons [3]. Likewise, surfactants with fluorocarbon chains exhibit unique properties compared to those of hydrocarbon surfactants. They often have a tendency to produce rod-like micelles instead of spherical micelles, attributed to both the conformation (twisted helical structure [4]) and stiffness of the perfluorocarbon chain [3,5]. Since the perfluorocarbon chain is both hydrophobic and lipophobic, fluorinated amphiphiles also exhibit limited miscibility with hydrocarbon amphiphiles or organic solvents [6]. In general, their critical micelle concentrations (CMCs) are approximately equal to those of the hydrocarbon analogues with 50% longer chains [3].

There are a wide variety of pseudostationary phases (PSPs) available for MEKC, and linear solvation energy relationships (LSERs) are often used to study their selectivities [7]. The application of LSERs and their chemical interpretation has been described in detail elsewhere in some excellent articles [8,9]. Briefly, multiple linear regression is used to fit the $\log k$ values of a set of 30-40 or more solutes to equation 1:

$$\log k = c + eE + sS + aA + bB + vV \quad (1)$$

where E , S , A , B and V are the known solute descriptors (polarizability, dipolarity, hydrogen bond donating ability, hydrogen bond accepting ability, and cohesiveness, respectively), and c , e , s , a , b , and v are the system constants to be determined. Fuguet et al [7] compiled a list of system constants of 55 single and mixed monomeric and polymeric PSPs. Their analysis indicates that the behaviour of the lone fluorinated PSP in their set, lithium perfluorooctanesulfonate (LPFOS - the lithium salt is used because of its better water solubility than the sodium salt), stands out. The unique properties of this fluorinated PSP are also evident in other reports [8-12]. LPFOS is slightly less polarizable than the aqueous phase; it is one of only a few PSPs with a small negative e system constant. It is a much better hydrogen bond donor than any other PSP studied to date (small negative b system constant), only slightly worse than water, and is also a very poor hydrogen bond acceptor (largest negative a system constant of all PSPs). LPFOS is also one of the most dipolar PSPs (positive to small negative s system constant), while it forms very cohesive micelles (one of the smallest v system constants). It should be noted that there is quite some variation in the system constants determined for LPFOS by different authors [7,9,11,12]. This is in contrast to the system constants for other PSPs, which usually fall within a relatively narrow range. The reason for this is not entirely clear, but might be the result of differences in the sets of solutes used to determine the LSERs, although differences in the purity of LPFOS cannot be excluded [12]. Regardless of the variation among sources of the system constants, the above description of the selectivity of LPFOS is believed to be accurate and seems to be generally accepted.

Most attention in the EKC literature with regards to fluorinated PSPs has focused on LPFOS, but other fluorinated PSPs may also be of interest. For instance, ammonium

perfluorooctanoate is a PSP with a relatively low boiling point. This can be useful in MEKC – electrospray ionization – mass spectrometry (MEKC-ESI-MS) [13,14], where traditional PSPs are notorious for causing signal suppression [15,16]. It is thought that ammonium perfluorooctanoate has a high enough surface activity to promote the formation of small droplets, and is volatile enough not to concentrate in the shrinking droplets [13]. Therefore, there is much less interference with the transfer of cationic analytes from the droplets to the gas phase due to Coulombic attractions, than with non-volatile PSPs. The unique selectivity imparted by fluorination seems to be lost for cationic polymeric PSPs with pendant perfluorinated groups, which have a similar selectivity as their hydrocarbon analogues, although they are slightly more cohesive and are better hydrogen bond donors [17].

The monomeric fluorinated PSPs investigated so far have long fluorinated chains, which, according to the interphase model [18], form the hydrophobic core of the micelles in an aqueous solution (the first few carbon atoms of the chain, next to the head group, probably are within the interphase). We were interested in determining the effect of the presence of fluorine in the spacer of anionic dimeric surfactants, since the spacer is situated in the interphase, where extensive interaction with solutes takes place [18]. We synthesized anionic dimeric surfactants with 4, 8, and 12 fluorine atoms in the spacer (Fig. 5.1: **Ia-c**), and also an anionic dimeric surfactant with a hydrocarbon spacer but with fluorinated long chains (Fig. 5.1: **II**). However, the latter had a relatively high absorption in the UV region, because of the thioether functionalities, and was not deemed suitable for MEKC with UV detection, and only the selectivities of **Ia-c** were determined via LSERS.

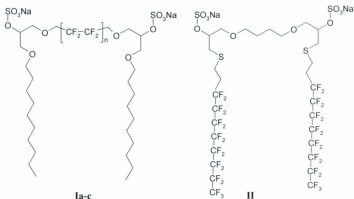


Fig. S.1: Structures of dimeric surfactants with fluorinated spacers and fluorinated chains; $n = 1$ (Ia), 2 (Ib), 3 (Ic).

5.2. Experimental

5.2.1. Capillary electrophoresis instrument and conditions

All experiments were performed on an Agilent ^{3D}CE system (Agilent Technologies Canada Inc., Mississauga) with Chemstation software (Rev. A.08.03). Bare fused silica capillaries with an I.D. of 50 μm were purchased from MicroSolv (MicroSolv Technology Corporation, Eatontown, NJ, USA) and were cut to lengths of 48 – 50 cm. New capillaries were used for each PSP, and they were conditioned by flushing with 0.1 M NaOH (5 min.), nanopure water (5 min.), and BGE (10 min.) respectively. The background electrolyte (BGE) consisted of 20 mM Na_2HPO_4 and 20 mM dimeric surfactant, adjusted to $\text{pH } 7.00 \pm 0.03$ with dilute H_3PO_4 . The PSPs were dissolved by

stirring, followed by sonication for 15 minutes, and were filtered through 0.2 μm nylon filters (National Scientific Company, Rockwood, TN, USA).

Analyses were performed at 25 $^{\circ}\text{C}$, with 25 kV applied (ramped from 0 to 25 kV in 15 s). Samples were injected by applying 10 mbar of pressure for 5 s, followed by BGE at 10 mbar for 5 s, and the detection wavelength was 200 nm. Between runs, the capillary was flushed with BGE for 3 minutes.

5.2.2. Solutes

Most of the test solutes [2] were obtained from Sigma-Aldrich (Oakville, Canada) and had a purity $\geq 98\%$, except 4-phenylphenol (97%) and 1-methylnaphthalene (97%). The series of n-alkyl benzoates ($\text{C}_1 - \text{C}_6$), used to determine the methylene selectivity, was prepared by reacting the corresponding n-alcohols (PolyScience Corporation, Evanston, IL, USA) with benzoylchloride in the presence of triethylamine. The cross-correlation matrix of the 41 solutes shows no correlation between the solute descriptors [2].

Solutions of 4 or 5 solutes (plus dodecanophenone as micelle marker) were prepared in methanol at concentrations between 300 and 600 mg/L, and solutes were identified by comparison of their UV-spectra with entries in a spectral library. All samples were run three to four times, and average retention factors were calculated.

5.2.3. Calculations

Retention factors were calculated from:

$$k = (t_m - t_0) / [t_0 (1 - t_m/t_{mc})] \quad (2)$$

with t_m the migration time of the solute, t_0 the migration time of an unretained solute (methanol), and t_{mc} the migration time of the micelle marker (dodecanophenone) [19].

The iterative procedure described by Bushey and Jorgenson [20], using Microsoft Excel's 'solver' tool to maximize the correlation coefficient, was used to determine the methylene selectivity ($\alpha_{C_{12}}$) from the slope (m) of a plot of $\log k$ vs. carbon number ($\alpha_{C_{12}} = 10^m$) of a homologous series of alkyl benzoates (C_1 - C_6).

The electrophoretic mobility μ_e ($\text{cm}^2 \text{V}^{-1} \text{s}^{-1}$) of the pseudostationary phases was calculated from:

$$\mu_e = (l/V_a)(1/t_{mc} - 1/t_0) \quad (3)$$

with l the length of the capillary to the detector, and l the total length of the capillary.

The average voltage V_a is calculated from:

$$V_a = V(1 - t_R/2t_{mc}) \quad (4)$$

where V is the end voltage (25 000 V) and t_R is the ramp time (15 s) [21].

5.2.4. Synthesis and analysis of fluorinated dimeric surfactants

The fluorinated compounds 2,2,3,3-tetrafluoro-1,4-butanediol; 2,2,3,3,4,4,5,5-octafluoro-1,6-hexanediol and 2,2,3,3,4,4,5,5,6,6,7,7-dodecafluoro-1,8-octanediol (all 98%) were purchased from Oakwood Products Inc. (West Columbia, SC, USA). Other

reagents were purchased from Aldrich and had a purity of at least 97%, except for 3-chloroperbenzoic acid ($\leq 77\%$).

The synthesis of the dimeric surfactants with fluorinated spacers proceeded in four steps. The direct reaction between fluorinated diols and epichlorohydrin, as described previously for non-fluorinated diols [1,2], did not give the desired diglycidylethers. Instead, we followed a procedure described by Montefusco et al. [22] whereby the diallylethers are formed first (yields: 83-95%), which are then oxidized with 3-chloroperbenzoic acid to the diglycidylethers (yields: 70-79%). The latter reaction was performed at room temperature and required 48-72 hours of reaction time. It should be pointed out that after completion of the experimental work, a procedure was found that can produce these fluorinated diglycidylethers in one step, starting with the fluorinated diols and epichlorohydrin [23]. The synthesis of the long-chain diols (yields: 40-54%) and finally the dimeric surfactants with fluorinated spacers (Fig. 5.1) (yields: 60-67%) proceeded as described previously [1,2].

The dimeric surfactants were characterized by $^1\text{H-NMR}$ (Bruker Avance 500 MHz), $^{19}\text{F-NMR}$ (Bruker Avance II 600 MHz) and negative ESI-MS (Agilent 1100 Series LC/MSD Trap), and their CMCs were determined with a Hach Model CO150 Conductivity Meter, as described previously [2].

5.3. Results and discussion

5.3.1. Analysis and CMCs of dimeric surfactants

¹H-NMR spectra and negative ESI-MS spectra were in accordance with the expected structures (Table 5.1). The ¹⁹F-NMR spectra that were also acquired confirmed the proposed structures (results not shown). Mass spectra typically showed peaks corresponding to [MM-Na]⁻, [(MM-2Na)/2]²⁻, and [MM-2Na+H]⁻; the spectra of **Ib** and **Ic** showed minor amounts of decylsulfate (Table 5.1).

The CMC values are well below 1 mM and show a decrease with increasing number of F atoms in the spacer. Since these types of surfactants have not been reported in the literature so far, there are no literature values with which to compare them.

Table 5.1: ¹H-NMR and ESI-MS data, and CMCs of dimeric surfactants with fluorinated spacers.

	Formula MM	¹ H-NMR ^a (δ, ppm)	m/z (neg. ESI) ^b	CMC (mM) at 25 °C
Ia	C ₁₆ H ₅₀ O ₁₂ S ₂ F ₄ Na ₂ 794.9	0.85 (t;6H), 1.24 (m;28H), 1.46 (m;4H), 3.35 (m;4H) ^c , 3.46 (m;4H) 3.66 (m;4H), 3.95 (t, 4H), 4.19 (m;2H)	771.4 (100%), 374.2 (77%), 749.4 (55%)	0.57
Ib	C ₁₂ H ₃₀ O ₁₂ S ₂ F ₄ Na ₂ 894.9	0.85 (t;6H), 1.24 (m;28H), 1.46 (m;4H), 3.35 (m;4H) ^c , 3.45 (m;4H) 3.66 (m;4H), 4.09 (t, 4H), 4.19 (m;2H)	871.4 (79%), 424.1 (24%), 849.4 (100%), 237.0 (3.8%)	0.32
Ic	C ₁₄ H ₃₆ O ₁₂ S ₂ F ₁₂ Na ₂ 994.9	0.85 (t;6H), 1.25 (m;28H), 1.46 (m;4H), 3.35 (m;4H) ^c , 3.45 (m;4H) 3.71 (m;4H), 4.20 (m, 6H)	971.3 (35%), 474.2 (100%), 949.3 (23%), 237.0 (4.4%)	0.17

^a Samples in DMSO-*d*₆; t: triplet; m: multiplet

^b Intensity as a percentage of base peak in parentheses; mass to charge ratios correspond to [M - Na]⁻, [M - 2Na]²⁻, and [M - 2Na + H]⁻, respectively; ions with m/z 237 in the spectra of **Ib** and **Ic** correspond to decylsulfate.

^c This multiplet also had a large peak from hydroxyl protons from water, invariably present in the DMSO-*d*₆.

5.3.2. Linear Solvation Energy Relationships

We start our examination of the LSERs by considering the statistics. Four solutes had to be excluded from the original data set of 41 because their predicted values deviated considerably from the experimental values (standardized residuals > 2.0), and the statistics were very poor (e.g. F-values ~ 33, r^2 values ~ 0.83). For acetanilide and pyrrole the experimental values were much lower, and for geraniol and indole the experimental values were higher than predicted. It is unclear why these solutes are outliers; their descriptors are not unusual, and they do not seem to be related in any way. LSERs were recalculated with the remaining 37 solutes, with markedly improved statistics (Table 5.2), although there were always two solutes with standardized residuals slightly higher than 2.0.

Table 5.2: System constants (standard error in brackets) and regression statistics for the LSERs of SDS, LPFOS, and dimeric surfactants. Underlined values are not significantly different from zero; ^a standard error of the fit.

	<i>c</i>	<i>v</i>	<i>e</i>	<i>s</i>	<i>a</i>	<i>b</i>	<i>n</i>	r^2	F	SE ^a
1a	-1.61 (0.10)	2.60 (0.10)	0.48 (0.09)	-0.46 (0.09)	-0.16 (0.07)	-2.23 (0.15)	37	0.981	312	0.11
1b	-1.65 (0.10)	2.64 (0.10)	0.43 (0.09)	-0.48 (0.09)	-0.23 (0.07)	-2.18 (0.14)	37	0.982	335	0.11
1c	-1.63 (0.10)	2.66 (0.10)	0.40 (0.09)	-0.49 (0.09)	-0.26 (0.07)	-2.19 (0.15)	37	0.981	327	0.11
IIIa [2]	-1.69 (0.09)	2.67 (0.08)	0.60 (0.08)	-0.50 (0.08)	0.07 (0.06)	-2.41 (0.12)	41	0.984	322	0.10
SDS [2]	-1.73 (0.07)	2.94 (0.06)	0.27 (0.06)	-0.39 (0.06)	-0.20 (0.04)	-1.86 (0.09)	41	0.992	827	0.07
LPFOS [12]	-1.41 (0.09)	1.97 (0.10)	<u>-0.11</u> (0.13)	-0.24 (0.10)	-0.88 (0.08)	-0.46 (0.11)	62	0.941	180	0.19

Predicted log *k* values of the 37 solutes are plotted against experimental values in Fig. 5.2, with a distinction made between non-hydrogen bond solutes (NHB), hydrogen bond acceptors (HBA), and hydrogen bond donors (HBD) [2]. There does not seem to be any

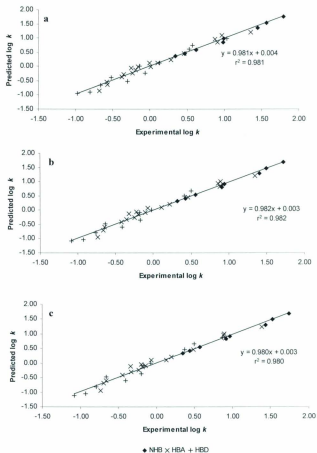


Fig. S.2: Plots of predicted vs. experimental $\log k$ values for (a) Ia, (b) Ib and (c) Ic

serious bias for a particular solute class; i.e. the solutes of each class are almost equally spread out above and below the fitted curves, indicating the general nature of the equations. We examined the robustness of the LSER analysis of **Ia-c** with a bootstrapping procedure [8]. The data set of the 37 solutes was sampled at random (with replacement) 37 times. The LSER for the new data set, in which some solutes will be left out while others will be represented multiple times, was then calculated. This was repeated for a total of 30 times, and the average system constants and their standard deviations were calculated (Table 5.3). There is a very good agreement between the averaged system constants and those of the original analysis (Table 5.2), and the standard deviations are very reasonable as well. This indicates that there are no solutes in the data set that disproportionately influence the system constants, and increases confidence in the reported results.

Table 5.3: Average system constants ($n=30$; standard deviation in brackets) of the three dimeric surfactants with fluorinated spacers using a bootstrapping procedure on a data set of 37 solutes (see text for explanation).

	<i>c</i>	<i>v</i>	<i>e</i>	<i>s</i>	<i>a</i>	<i>b</i>
Ia	-1.64 (0.12)	2.63 (0.13)	0.48 (0.11)	-0.46 (0.12)	-0.14 (0.07)	-2.24 (0.16)
Ib	-1.66 (0.13)	2.66 (0.14)	0.44 (0.10)	-0.51 (0.13)	-0.21 (0.09)	-2.16 (0.13)
Ic	-1.63 (0.12)	2.65 (0.10)	0.42 (0.09)	-0.51 (0.13)	-0.28 (0.08)	-2.16 (0.14)

Do the results also make sense from a chemical point of view? We included in Table 5.2 the system constants of SDS, LPFOS, and PSP **IIIa** from reference [2] for comparison. The latter is representative of dimeric surfactants with aliphatic spacers. As

usual, we are not concerned with the c system constant, which depends to a large extent on the phase ratio of the system [8,19].

The cohesiveness (v system constant) is the same for surfactants **Ia-c**, and is similar to that of **IIIa**. It is also the same as for dimeric surfactants with hydrophilic spacers [2]. We can draw the general conclusion that the cohesiveness of this type of dimeric surfactants does not in any way depend on the length or the nature of the spacer. Notice that LPFOS is much more cohesive than any other PSP in Table 5.2. Although perfluorinated chains exhibit little intermolecular interaction and could be expected to have a low cohesiveness, they are also lipophobic, and dispersion forces between the hydrocarbon moieties of solutes and perfluorinated chains are much weaker than those between the hydrocarbon moieties of solutes and hydrogenated chains [11,24]. It is reiterated here that the vF interaction has a significant contribution from polarizability as well [8].

The polarizability (e system constant) is slightly less for surfactants **Ia-c** than for **IIIa**, but is higher than for SDS. This indicates that at least some of the polarizability of dimeric surfactants comes from the spacer. The decrease in polarizability with fluorination can then be explained by two effects. On the one hand, the polarizability of C-F bonds is less than that of C-H bonds (see introduction). On the other hand, the strongly electronegative fluorine atoms withdraw the lone electron pairs of oxygen on the neighbouring carbon atoms, making them less able to interact via this type of interaction. The polarizability of **Ia-c** is still considerably higher than for LPFOS, where fluorine atoms directly impact the head group.

The dipolarity s shows the least variation of all system constants in Table 5.2. It is essentially the same for dimeric surfactants with hydrophobic and fluorinated spacers, is comparable to that of SDS, and only slightly less than for LPFOS. Although C-F bonds are highly polarized [3], the individual dipoles cancel one another.

The hydrogen bond accepting ability (a system constant) of surfactants **Ia-c** is considerably less than that of the non-fluorinated analogue **IIIa**. This could be expected, since the strongly electronegative fluorine atoms withdraw the lone electron pairs of oxygen on the neighbouring carbon atoms. We previously attributed the stronger hydrogen bond accepting abilities of dimeric surfactants with hydrophobic spacers relative to SDS to the presence of the extra oxygen atoms in the spacer [1]. The results reported here seem to confirm this, since by 'deactivating' these oxygen atoms, the hydrogen bond accepting abilities of surfactants **Ia-c** fall to approximately the same level as for SDS. The literature does not address the reason for the anomalously low a system constant of LPFOS, but this could be related to the decrease in the dissociation constant (pK_a) of the sulfonate head group by the strongly electron-withdrawing fluorine [3]. This would be consistent with the observation of Trone and Khaledi [19] that as the pK_a of the head group decreases, the a system constant becomes more negative.

Finally, the hydrogen bond donating ability (b system constant) is the same for **Ia-c**, and somewhat better than for **IIIa**, but is much lower than for LPFOS. The relatively strong hydrogen bond donating ability of LPFOS is usually attributed to the inductive effect of fluorine on water molecules in contact with the sulfonate head group [11,18]. The fluorine atoms in the spacers of **Ia-c** are too far away from the head groups to affect

them inductively, and due to the lack of any strong interactions between water molecules and the fluorinated spacer, it is not expected that the spacer itself be strongly hydrated.

A plot of the retention factors of the 37 solutes of **1a** vs. SDS (Fig. 5.3) shows that these PSPs do not have very different selectivity ($r^2 = 0.965$). The plot also shows the curve drawn for only the NHB solutes. This is better for comparing selectivity differences based upon differences in hydrogen bonding, which usually explains most of the selectivity differences between PSPs [19]. All HBA solutes plot well below this curve; i.e. they have a stronger interaction with SDS. This is expected, since SDS is a much better hydrogen bond donor than **1a**. Despite the fact that the hydrogen bond accepting ability of both PSPs are pretty much the same, all HBD solutes also plot below this curve. The reason for this is that HBD solutes also have considerable HBA character (Table 1 in [2]), and the large negative bb term strongly decreases the retention by **1a**.

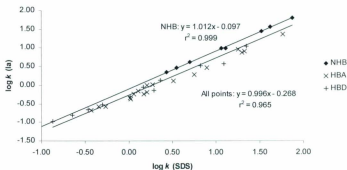


Fig. 5.3: Selectivity plot of dimeric surfactant **1a** vs. SDS. NHB, HBA and HBD are non-hydrogen bond solutes, hydrogen bond acceptors and hydrogen bond donors, respectively.

Similar plots of retention factors of SDS vs. **Ib** and SDS vs. **Ic** have r^2 values of 0.971 and 0.968 respectively, while plots of the retention factors of **Ia** vs. **Ib**, **Ia** vs. **Ic** and **Ib** vs. **Ic** all have r^2 values > 0.99 .

For completeness, and to be consistent with our previous publications on dimeric surfactants [1,2], we also report the electrophoretic mobilities and methylene selectivities of **Ia-c** (Table 3). With the exception of the electrophoretic mobility of **Ia**, which is somewhat higher (in absolute value), these values are comparable to those for SDS.

Table 5.4: Methylene selectivity and electrophoretic mobility (\pm standard deviation) of SDS and PSPs **Ia-c**

	α_{CH_2} (n = 3)	μ_{iso} (10^{-4} cm ² V ⁻¹ s ⁻¹) (n = 30)
SDS [1]	2.56 \pm 0.00	-4.32 \pm 0.02
Ia	2.58 \pm 0.01	-4.50 \pm 0.03
Ib	2.59 \pm 0.01	-4.33 \pm 0.03
Ic	2.59 \pm 0.02	-4.30 \pm 0.02

5.4. Conclusions

Anionic dimeric surfactants with fluorinated spacers show limited selectivity differences with their non-fluorinated counterparts. Modest effects on polarizability and hydrogen bonding abilities can be rationalized from the low polarizability of the C-F bonds, and from inductive effects of fluorine on nearby oxygen atoms in the spacer. It has been suggested [12,19] that it is mainly water residing in the interphase region that determines hydrogen bonding and polarity. Thus, the amount of water and the strength of the forces that hold water molecules in the interphase should have a strong influence on the selectivity. We surmise here that the fluorocarbon chain is poorly hydrated, and in that

respect constitutes a too 'hostile' environment for most types of molecules to interact with. LPFOS occupies a truly unique position in the spectre of selectivities of PSPs for two reasons. First, the fluorine substitution is in the chain that constitutes the hydrophobic core of the micelle, and thus directly affects its cohesiveness. Second, the fluorine substitution starts at the carbon atom that holds the head group, where it exerts a strong inductive effect, and thus affects the hydration of the head group. Strategies for modifying the selectivity of PSPs using fluorine substitution should be aimed towards positioning fluorine directly onto carbon atoms that carry functional groups, where full advantage can be taken of its strong inductive effects.

5.5. Acknowledgements

The financial support of the Canadian Foundation for Innovation and the Newfoundland and Labrador Industrial Research and Innovation Fund in the purchase of the Agilent ³⁰CE system, and the Natural Sciences and Engineering Research Council of Canada, are gratefully acknowledged.

5.6. References

- [1] G. Van Biesen, C.S. Bottaro, *J. Chromatogr. A* 1157 (2007) 437
- [2] G. Van Biesen, C.S. Bottaro, *J. Chromatogr. A* 1180 (2008) 171
- [3] B.E. Smart, in: R.E. Banks, B.E. Smart, J.C. Tatlow (Eds.), *Organofluorine Chemistry: Principles and Commercial Applications. Topics in Applied Chemistry*. Plenum Press, New York, 1994, p. 57-88
- [4] X. Zhang, M.M. Lerner, *Phys. Chem. Chem. Phys.* 1 (1999) 5065

- [5] S.J. Burkitt, R.H. Ottewill, J.B. Hayter, B.T. Ingram, *Colloid Polym. Sci.* 265 (1987) 619
- [6] R. Oda, I. Huc, D. Danino, Y. Talmon, *Langmuir* 16 (2000) 9759
- [7] E. Fuguet, C. Ràfols, E. Bosch, M.H. Abraham, M. Rosés, *Electrophoresis* 27 (2006) 1900
- [8] M. Vitha, P.W. Carr, *J. Chromatogr. A* 1126 (2006) 143
- [9] C.F. Poole, S.K. Poole, M.H. Abraham, *J. Chromatogr. A* 798 (1998) 207
- [10] S.K. Poole, C.F. Poole, *Analyst* 122 (1997) 267
- [11] E. Fuguet, C. Ràfols, E. Bosch, M. Rosés, M.H. Abraham, *J. Chromatogr. A* 907 (2001) 257
- [12] E. Fuguet, C. Ràfols, E. Bosch, M.H. Abraham, M. Rosés, *J. Chromatogr. A* 942 (2002) 237
- [13] P. Petersson, M. Jömtén-Karlsson, M. Stålebro, *Electrophoresis* 24 (2003) 999
- [14] G. Van Biesen, C.S. Bottaro, *Electrophoresis* 27 (2006) 4456
- [15] G.W. Somsen, R.M. Mol, G.J. de Jong, *J. Chromatogr. A* 1000 (2003) 953
- [16] K.L. Rundlett, D.W. Armstrong, *Anal. Chem.* 68 (1996) 3493
- [17] E. Rauk, A. Kotzev, A. Laschewsky, C.P. Palmer, *J. Chromatogr. A* 1106 (2006) 29
- [18] C.F. Poole, S.K. Poole, *J. Chromatogr. A* 792 (1997) 89
- [19] M.D. Trone, M.G. Khaledi, *Anal. Chem.* 71 (1999) 1270
- [20] M.M. Bushey, J.W. Jorgenson, *Anal. Chem.* 61 (1989) 491
- [21] Anonymous, Agilent ChemStation for CE systems, Edition 06/03, Agilent Technologies 2003, Waldbronn, Germany, order No. G2172-90007

- [22] F. Montefusco, R. Bongiovanni, M. Sangermano, A. Priola, A. Harden, N. Rehnberg, *Polymer* 45 (2004) 4663
- [23] C.B. Serrurier, A. Cambon, *J. Fluorine Chem* 87 (1998) 37
- [24] S. Yang, M.G. Khaledi, *Anal. Chem.* 67 (1995) 499

5.7. Addendum:

5.7.1. Synthesis of a dimeric surfactant with fluorinated chains

Dimeric surfactant **II** (Fig. 5.1) was briefly mentioned in Section 5.1, and some additional details on its synthesis are provided below.

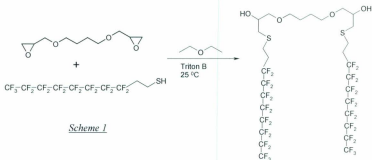
The original idea to synthesize a dimeric surfactant with fluorinated chains was to stick to the original general structure of **Ia-c**, but without fluorination in the spacer; i.e. with the oxoether functionalities. This required preparing the diglycidylether of 1,4-butanediol (as described in Section 3.2.4), and reacting this with the anion of 1H,1H,2H,2H-perfluorodecanol. In order to make this anion, metallic potassium has to be dissolved in 1H,1H,2H,2H-perfluorodecanol, and two problems were encountered here. First of all, 1H,1H,2H,2H-perfluorodecanol is a lot more expensive than decanol, which was usually used both as reagent and as solvent in this step. Second, when this reaction was attempted on a small scale (5 g 1H,1H,2H,2H- perfluorodecanol, 0.35 g K), the reaction mixture turned brown-black and eventually combusted. Understandably, a second attempt to synthesize this compound was not undertaken.

Since thiols are much better nucleophiles than alcohols, 1H,1H,2H,2H-perfluorodecanethiol was reacted with 1,4-butanediol diglycidylether, to give the long chain diol with thioether functionalities (Fig. 5.4 – Scheme 1), via a slightly modified literature procedure [1]. Briefly, 1.03 g (5 mmol) diglycidylether of 1,4-butanediol was dissolved in 10 mL diethylether in a 50 mL round bottom flask, and 5.3 g (11 mmol) 1H,1H,2H,2H- perfluorodecanethiol was added. The mixture was put on an ice-bath and was stirred with a magnetic stirrer. Ten drops of Triton B (a 40% solution of benzyl trimethylammoniumhydroxide in methanol) were added, the ice-bath was removed after a

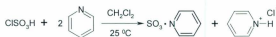
few minutes and the reaction mixture was allowed to warm up to room temperature. After stirring for 24 hours, brine was added and the reaction mixture was transferred to a separatory funnel, the product was extracted into the diethylether layer, which was separated, dried on sodium sulphate, and evaporated. The crude product (~6.1 g) was purified via column chromatography (eluent: $\text{CH}_2\text{Cl}_2:\text{CH}_3\text{OH}$ 97:3) and two fractions were obtained: 3.4 g pure long chain diol, and 2.4 g slightly less pure product (one extra spot seen on TLC). The overall yield was estimated to be more than 90%.

The synthesis of the surfactant from the long chain diol entails sulfation of the hydroxyl groups, and was initially attempted as described earlier (Section 3.2.4). However, negative ESI-MS of the reaction mixture showed few signs of the expected peaks at m/z 1343.7 (MM-Na), 1321.7 (MM-2Na+H) and 660.4 (MM-2Na / 2). Apparently, the reaction conditions were too harsh, and the product probably reacted predominantly via the thioether functionalities. We then tried a gentler approach using a sulfur trioxide-pyridine complex [2], prepared by mixing 0.98 mL (12 mmol) pyridine with 25 mL CH_2Cl_2 on an ice-bath, and drop wise adding 0.40 mL (6 mmol) ClSO_3H dissolved in 5 mL CH_2Cl_2 (Fig. 5.4 – Scheme 2). After stirring for 15 minutes, the long chain diol of Scheme 1, dissolved in 10 mL CH_2Cl_2 , was added drop wise to the sulfur trioxide-pyridine complex (Fig. 5.4 – Scheme 3). The ice-bath was removed after the addition, and the progress of the reaction was followed by negative ESI-MS by removing a sample from the reaction mixture and diluting approximately 1000 fold in methanol. While after 1 hr, a large amount of monosulfated product is present (Fig. 5.5a – peak at m/z 1241), the reaction is near completion after 5 hrs (Fig. 5.5b). The reaction mixture was stirred for a total of 8 hrs, and adjusted to pH ~ 10 with an approximately 5% NaOH

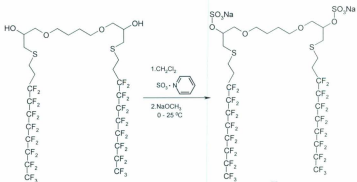
solution in methanol. It was not possible to extract the surfactant with 1-butanol, as was done with other dimeric surfactants (Section 3.2.4), because its solubility in 1-butanol was too low. Therefore, the reaction mixture was filtered, the precipitate was redissolved in 50 mL hot methanol, and filtered again. The filtrate was blown down with nitrogen to ~20 mL, and put on an ice-bath. The precipitated product was filtered, kept aside, and the solvent was evaporated under a stream of N₂ until more product precipitated. This precipitate was filtered again, and was combined with the other precipitate to a total of 0.75 g fluorinated dimeric surfactant **II** (yield ~ 38%). Negative ESI-MS showed only peaks at expected m/z ratios (see above), and no trace of monosulfated diol (Fig. 5.6). The ¹H-NMR spectrum (Fig. 5.7) also confirms the proposed structure. By comparison with its non-fluorinated analogue **IIIb** of Chapter 2 (Fig. A1.15), the signal of the H_c protons (2H) at δ 4.2 ppm can be observed. The H_i and H_l protons (both 4H) also appear in the same position for both compounds (δ ~3.35 and ~1.5 ppm, respectively), but for **IIIb** these signal integrate to eight protons because of the contribution of protons with similar shifts in the long chains. H_f and H_g both appear as doublets of doublets at δ 3.45 – 3.60 ppm (2 x 2H), at roughly the same position as for **IIIb**. Since H_c and H_d now have a neighbouring sulfur atom, instead of an oxygen atom as in **IIIb**, their signals do not coincide with those of H_f and H_g anymore, but are somewhat shifted upfield to δ 2.7 – 2.9 ppm. One of these doublets of doublets now coincides with H_b protons (4H), so that the signal at δ 2.7 ppm is from six protons. The signal of the H_a protons (4H) probably overlaps with the DMSO peak at δ ~ 2.5 ppm, since this peak is much broader at the base than usual.



Scheme 1



Scheme 2



Scheme 3

Fig. 5.4: Reactions for the synthesis of dimeric surfactant II.

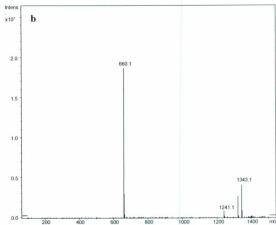
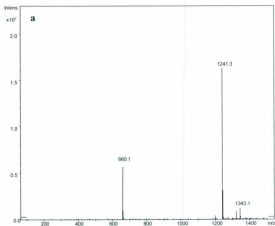


Fig. 5.5: Neg. ESI-MS of reaction mixture after (a) 1 hr and (b) 5 hrs.

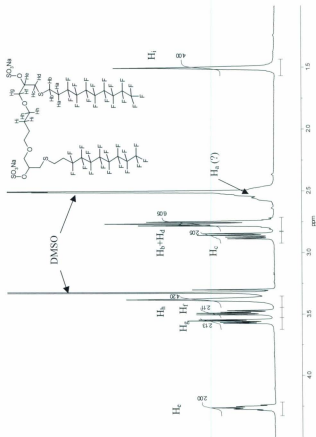


Fig. 5.6: $^1\text{H-NMR}$ spectrum of dimeric surfactant II.

5.7.2. Application of dimeric surfactant **II** in MEKC

It proved to be difficult to dissolve **II** in the 20 mM Na_2HPO_4 buffer that was normally used for the MEKC analysis (several hours of stirring followed by 30 minutes of sonication), and the resulting solution was very viscous and difficult to filter through a 0.2 μm filter. The filtered solution also did not seem to be completely clear. It may be that the lithium salt has better solubility, as is the case for perfluorooctanesulfonate. The CMC of this dimeric surfactant was less than 0.03 mM (Appendix 8).

When applied to MEKC, solutions of **II** in 20 mM Na_2HPO_4 buffer gave extremely noisy electropherograms, even at concentrations as low as 2 mM (Fig. 5.7), and were clearly unsuitable. It was unfortunately not possible to determine the exact cause of this anomalous behaviour.

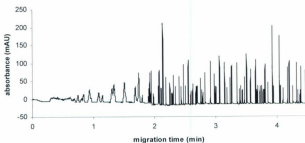


Fig. 5.7: Electropherogram with 2 mM **II** in 20 mM Na_2HPO_4 at pH 7 as BGE

In any event, the presence of the thioether functions also causes an increase in the UV absorbance. This can be seen from the UV spectra of the non-fluorinated analogue of **II** (G49 - prepared using the same reaction scheme as for **II**), and its non-fluorinated

analogue with the oxoether functions G12 (**IIIb** from Chapter 3) (Fig.5.8). G49 clearly has a much higher absorption in the UV region than G12, and is therefore far from ideal for MEKC with UV detection (Fig. 5.9), because of an unstable baseline, much like APFOA in Chapter 2 (Fig. 2.2 and 2.3).

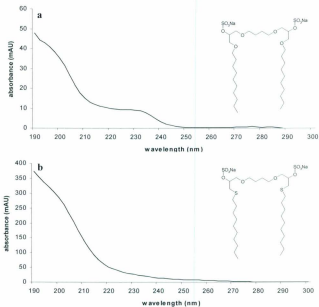


Fig. 5.8: UV spectra of (a) 20 mM G12 (**IIIb** from Chapter 3) and (b) 20 mM G49. Reference is 20 mM Na_2HPO_4 . Notice the different absorbance scales.

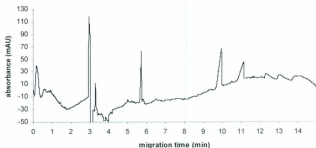


Fig. 5.9. Electropherogram of mixture 1 (see Appendix 7 – Fig. A7.1) with 20 mM G49 in 20 mM Na_2HPO_4 at pH 7 as BGE.

5.7.3. References

- [1] N.G. Jaoued, A. Hedhli, *J. Dispersion Sci. Technol.* 24 (2003) 749
- [2] E.E. Gilbert, *Chem. Rev.* 62 (1962) 549

Chapter 6

Conclusions¹

¹ Additional information can be found in Appendix 11

Micellar electrokinetic chromatography is a powerful and established technique for the analysis of neutral and charged solutes, and is now routinely applied for the analysis of pharmaceuticals, natural products, environmental contaminants, and a host of other analytes [1]. Yet, further developments are constantly needed in order to meet ever increasing demands on resolution, detection limits, quantification and identification. From this point of view, the potential of MEKC-MS has not been fully met, largely because of the poor compatibility of traditional PSPs with ESI-MS. While several avenues for circumventing this problem are being explored by different groups (Section 1.4.4), the simplest solution would be to have an 'MS-friendly' PSP. APFOA seems to meet this criterion, as first recognized by Ishihama et al. [2]. While Petersson et al. [3] performed a more in-depth study on a number of pharmaceutical compounds, prior to our study there were no real applications described in the literature for APFOA in MEKC-ESI-MS. The summary table in the Guideline for Canadian Drinking Water Quality [4] mentions the maximum allowable concentrations of three *N*-methylcarbamates: aldicarb (0.009 mg/L), carbaryl (0.09 mg/L) and carbofuran (0.09 mg/L). These concentrations are well within reach of the described method¹, and it should also be noted that the detection limits can be improved by loading more sample onto the SPE cartridges (it is very likely that much more than 25 mL of sample can be applied without break-through), and by using stacking or sweeping procedures. The main problem encountered was quantitation of the signals. While short term reproducibility (< 1 hr) was reasonable (e.g. satisfactory correlation coefficients were obtained for the calibration curves), on a longer period of time more

¹ The detection limits reported in Table 2.6 are the actual concentrations in the CE vials. For detection limits in drinking water, the concentration factor of the SPE procedure (100x) also has to be taken into account.

variation in signal intensities was observed. Problems with CE-ESI-MS quantitation are well-known and have only recently been addressed in some detail for CZE-ESI-MS [5,6], and not yet for MEKC-ESI-MS. In general, in order to achieve reproducible results with ESI, the ionization conditions need to be constant, and a stable spray current needs to be maintained. Use of an internal standard, ideally a deuterated internal standard, is highly recommended [6]. These issues were not addressed during the short timeframe working on this project.

Poole and Poole [7] identify four key parameters for successful separations in MEKC: differences in solute distribution constants (selectivity), favourable kinetics (efficiency), an adequate migration window (peak capacity), and a reasonable total analysis time. Selectivity is mainly determined by the nature of the surfactant, and the presence of organic solvent modifiers. Generally, the effects of the latter are small. Likewise, selectivity differences between different types of surfactants are relatively small as well, reflecting the rather uniform character of common surfactants in MEKC: they all have one hydrophilic head group and one hydrophobic tail. From this point of view, dimeric surfactants, with their two amphiphilic chains connected by a spacer, are somewhat unusual. One of their most interesting aspects is that modifications to the spacer can be made without interfering too much with the micelle forming properties of the molecule. Thus, as we saw in previous chapters, increasing the length of the spacer, incorporating hydrophilic groups, or substituting hydrogen atoms for fluorine atoms, can all be done while still preserving the essence of these molecules that makes them so useful in MEKC: their ability to form micelles. When it comes to selectivity in MEKC,

these modifications, for the types of dimeric surfactants discussed in this work, have modest, but often measurable, effects. According to the interphase model of retention [1], selectivity is mainly shaped by differences in solvation properties between the interphase and the bulk solution, i.e. by the amount and the strength of the forces holding water molecules in the interphase. The results of the work presented in the previous chapters are in accordance with this model. It could be argued to some extent that *qualitatively*, some of the results were predictable, and this is correct. For instance, it was predicted that incorporating hydrophilic groups into the spacer would increase the hydrogen bond accepting ability. However, our current knowledge does not allow for any *quantitative* predictions. This, in addition to the fact that the selectivity of dimeric surfactants had never been evaluated via LSERs, made this an intellectually fulfilling endeavour.

The final word on the usefulness and applicability of dimeric surfactants in MEKC has not been said, and there remain many avenues for further research. First of all, other functional groups (ester, amide, amine etc.)¹ could be incorporated in or on the spacer as well. As alluded to in the conclusion of Chapter 5, advantage could be taken of the strong inductive effect of fluorine, by positioning fluorine atoms as close as possible to functional groups that are strongly hydrated (this pertains to monomeric surfactants as well), thus influencing the amount of water bound to the micelles and consequently the selectivity.

The main concern of Chapters 3-5 was the selectivity of the dimeric surfactants. However, from the point of view of a successful analysis, the efficiency and peak

¹ Some of these functionalities may not be compatible with all the reactions of the pathway leading to the dimeric surfactants as described in this work. However, alternative reaction schemes are available [8].

capacity are also important, and these have not been studied in detail. We did address the efficiency of dimeric surfactants with hydrophobic spacers in Chapter 3, but feel that the particular set of solutes used was not adequate. There is so much variation between the efficiencies of solutes with short and long migration times that an average efficiency invariably leads to large standard deviations, and this makes comparisons with other PSPs not very useful.

Further research is also needed into how much advantage can be taken of the low CMCs of these surfactants (typically <1 mM). If applicable at very low concentrations, for instance <10 mM, would they be compatible with MS detection?

Another interesting project would be to synthesize dimeric surfactants that have spacers with asymmetric carbon atoms. These could be used for the separation of enantiomers [9]. There are currently very few PSPs that have an asymmetric carbon atom built into their structure; notable exceptions are the various bile salts [10], and amino acid-derived surfactants [11]. A project like this would probably require cooperation with organic labs experienced in the synthesis of enantiomers, since enantiomerically pure starting products (i.e. diols) are hard to come by and expensive to purchase.

Finally, on several occasions, the selectivity of the dimeric surfactants synthesized and evaluated during the course of this work was compared to the selectivity of SDS and other PSPs. This was mainly done by comparing the values of the system constants with those of the 55 PSPs (monomeric and polymeric) collected by Fuguet et al. [12]. These authors also performed a principal components analysis (PCA), which is a powerful tool to visualize similarities and differences between the entries in a data set [13-15]. In

essence, PCA is a data reduction technique used to identify a small number of variables that account for most of the variation in a data set. These variables are the principal components (PCs), and they are linear combinations of the original variables (the system constants in this particular case), with their importance indicated by the loadings. We thought it would be instructive to repeat their analysis, including the dimeric surfactants from Chapters 3-5 in order to get an idea of where these surfactants would fit in. However, we were not able to reproduce their analysis and graphs with our software (Minitab™ – Fuguet et al. used Matlab). Consulting with Dr. P.D. Wentzell (Dalhousie University), the probable reason was that Fuguet et al. did not perform mean-centering of the data (i.e. they did not subtract the mean of each column from every column entry). This is automatically done by Minitab, and to our knowledge it is not possible to disable this function. Mean-centering is also a very common practice in PCA [13-15]. We then proceeded with reanalyzing their data set of 55 PSPs, supplemented by our own data for dimeric surfactants, with the Minitab PCA function. Fuguet et al. [12] performed the PCA with and without coefficient normalization. The former evaluates the chemistry, while the latter evaluates the selectivity of the PSPs. For instance, if two PSPs have different values for their system constants, they obviously interact differently with solutes, but if these system constants are proportional, the PSPs have the same selectivity. Coefficient normalization here entails dividing each system constant by a factor $(e^2 + s^2 + a^2 + b^2 + v^2)^{1/2}$, and was performed on all data shown hereafter (see also Appendix 9). Since the variables are measured on the same scale, the covariance matrix rather than the correlation matrix is used for the PCA, although when the analysis was repeated using the correlation matrix, the conclusions from that analysis were exactly the same.

The results of the PCA analysis (Table 6.1) indicate that most of the variation (74.2%) in the data set is accounted for by two PCs. Therefore, most of the variation in the data set can be seen from a plot of PC2 vs. PC1 (Scores plot - Fig. 6.1). Each number in the plot indicates a PSP (Appendix 11 – Table A11.2), with the dimeric surfactants in bold.

Table 6.1: Principal Component Analysis of 55 PSPs and 11 dimeric surfactants

Eigenanalysis of the Covariance Matrix

Eigenvalue	0.018461	0.006506	0.004912	0.003305	0.000455
Proportion	0.549	0.193	0.146	0.098	0.014
Cumulative	0.549	0.742	0.888	0.986	1.000

Variable	PC1	PC2	PC3	PC4	PC5
e	0.257	-0.323	0.826	0.375	-0.084
s	-0.190	-0.857	-0.378	0.255	0.146
a	0.593	-0.347	0.012	-0.726	0.030
b	-0.602	-0.079	0.403	-0.424	0.538
v	-0.430	-0.183	0.113	-0.296	-0.825

loadings

It is immediately noticed that the dimeric surfactants do not have unusual selectivity, as for instance LPFOS (18 in Fig. 6.1), which plots far away from all the other PSPs. The dimeric surfactants with hydrophobic spacers (56-59) all plot close together, as could be expected since their system constants are statistically indistinguishable. For the dimeric surfactants with hydrophilic spacers (60-63), there is a trend away from the center with increasing spacer length, towards the cationic surfactants (25-28). These are also known to be good hydrogen bond acceptors, and poor hydrogen donors. Dimeric surfactants with fluorinated spacers (64-66) move in the opposite direction.

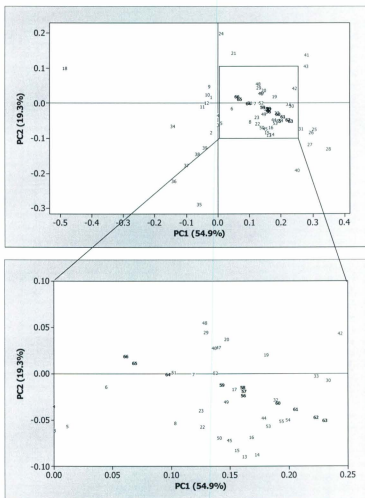


Fig. 6.1: Scores plots of PC2 vs. PC1. The lower plot is an enlargement of the section indicated by the square in the top plot. Dimeric surfactants are in bold – see Appendix A11.

The loading plot (Fig. 6.2) provides the projection of the loadings of the PCs. The correlation of the system constants is described by the cosine of the angle between the vectors in the plot; the smaller the angle, the higher the correlation [13]. Thus, b and v are relatively strongly correlated, as are e and a . The system constant s , on the other hand, is almost orthogonal to the other system constants, and is therefore poorly correlated to the other system constants. Notice also that a and b have a strong negative correlation (they are almost 180° apart), which could be expected, since a good hydrogen bond donor necessarily is a bad hydrogen acceptor. The size of the loadings is a measure of the importance of the system constants for a particular PC. For instance, for PC1, a and b have the largest absolute values and are much more important as distinguishing characteristics than s . This agrees well with the general impression that hydrogen bond

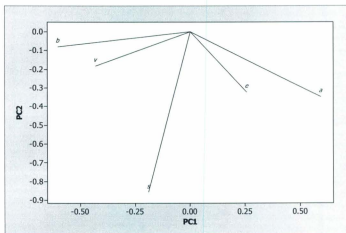


Fig. 6.2: PC1 and PC2 loading plot.

interactions are very important descriptors of selectivity (even though the α system constant is usually small). For PC2 on the other hand, s has the largest absolute value, and is here the dominant factor in the discrimination between the PSPs (see also Table 6.1).

References

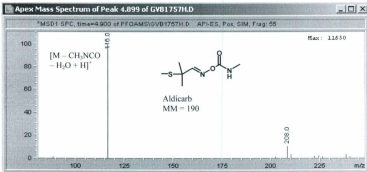
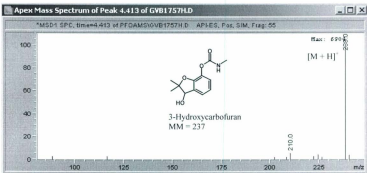
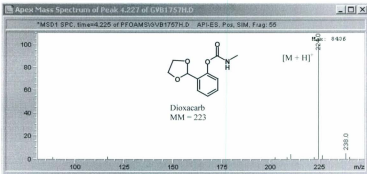
- [1] T.J. Pappas, M. Gayton-Ely, L.A. Holland, *Electrophoresis* 26 (2005) 719
- [2] Y. Ishihama, H. Katayama, N. Asakawa, *Anal. Biochem.* 287 (2000) 45
- [3] P. Petersson, M. Jörintén-Karlsson, M. Stålebro, *Electrophoresis* 24 (2003) 999
- [4] Guidelines for Canadian Drinking Water Quality – accessed Jan. 02 (2008).
http://www.hc-sc.gc.ca/ewh-semt/pubs/water-eau/doc_sup/appui/sum_guide-res_recom/chemical-chimiques_e.html#4
- [5] J. Ohnesorge, C. Sängler-van de Griend, H. Wätzig, *Electrophoresis* 26 (2005) 2360
- [6] J. Ohnesorge, C. Neusüß, H. Wätzig, *Electrophoresis* 26 (2005) 3973
- [7] S.K. Poole, C.F. Poole, *Anal. Commun.* 34 (1997) 57
- [8] R. Zana, J. Zia (Eds.), *Gemini surfactants – Synthesis, interfacial and solution-phase behaviour, and applications*. Surfactant Science Series vol. 117, Marcel Dekker, Basel, New York, 2004
- [9] R.O. Cole, M.J. Sepaniak, W.L. Hinze, J. Gorse, K. Oldiges, *J. Chromatogr. A* 557 (1991) 113
- [10] S.A.A. Rizvi, J. Zheng, R.P. Apkarian, S.N. Dublin, S.A. Shamsi, *Anal.Chem.* 79 (2007) 879
- [11] T.J. Ward, D.-M. Hamburg, *Anal.Chem.* 76 (2004) 4635

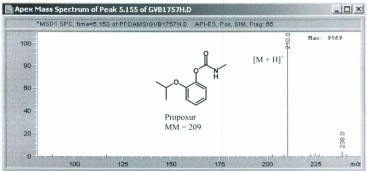
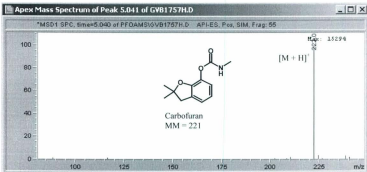
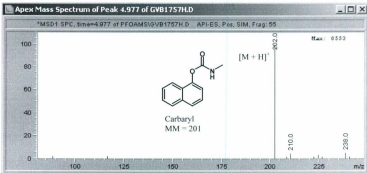
- [12] E. Fuguet, C. Ràfols, E. Bosch, M.H. Abraham, M. Rosés, *Electrophoresis* 27 (2006) 1900
- [13] M. Otto, *Chemometrics – Statistics and computer applications in analytical chemistry*, Wiley-VCH Verlag GmbH, 1999
- [14] S.J. Pachuta, *Appl. Surf. Sci.* 231-232 (2004) 217
- [15] M. Statheropoulos, A. Pappa, P. Karamertzanis, H.L.C. Meuzelaar, *Anal. Chim. Acta* 401 (1999) 35

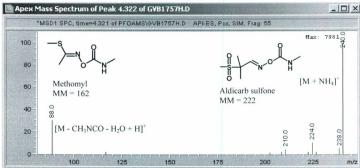
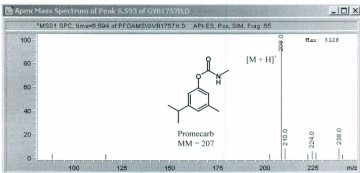
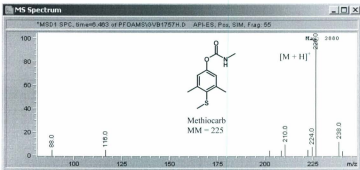
Appendices

Appendix I

ESI-MS and structures of *N*-methylcarbamates







Appendix 2

¹H-NMR spectra of dimeric surfactants and intermediate products of Chapter 3

Fig. A2.1-5: Diglycidylethers

Fig. A2.6-13: Long Chain Diols

Fig. A2.14-21: Dimeric Surfactants

Guide to interpretation of NMR spectra

All compounds are assigned the same identification number as in Chapter 3. This is followed by a unique identification number in brackets that was used in the lab books.

Where peaks are assigned to hydrogen atoms, only the hydrogen atoms on one half of the molecule are labelled, since all synthesized compounds have a plane of symmetry.

Diglycidylethers (Ia-f)

Peak assignment for **Ia** (Fig A2.1) is according to Mouzin et. al¹. Due to the presence of hydrogen H_c on the asymmetric carbon atom, H_a and H_b have different chemical shifts, and both show up as a doublet of doublets. The same rationale explains the different shifts of H_d and H_e.

Increasing the length of the spacer by one ethylene unit (**Ib** – Fig. A2.2) gives an additional signal (multiplet – 4H) at δ 1.67 ppm, from the hydrogens on the two carbon atoms in the middle of the spacer. This signal is slightly shifted downfield due to the deshielding effect of the oxygen atoms on the α carbon atoms. Further increasing the length of the spacer by one ethylene unit (**Ic** - Fig. A2.3) gives an additional signal (multiplet – 4H) at δ 1.35 ppm, again from the hydrogens on the carbon atoms in the middle. These protons are now beyond the influence of the oxygen atoms, and further extending the spacer (**Id-f** – Figs. A2.4-5) generates no new signals, but increases the intensity of this signal (8H, 12H, 16H). Notice that some of the integrated signals are smaller than expected, especially from the hydrogens with a shift of \sim 3.15 ppm.

¹ G. Mouzin, H. Cousse, J.-P. Rieu, A. Duflos, *Synthesis* (1983) 117

Long-chain diols (IIa-f)

Although many different magnetically non-equivalent nuclei are present in the structure of **IIa** (Fig. A2.6), these cannot all be easily discerned from the spectrum of **IIa**. The methyl (H_a - 0.85 ppm) and methylene (H_b - 1.20 - 1.35 ppm) protons of the aliphatic chain show up at shifts that could reasonably be expected for these types of protons¹. H_c protons (δ 1.60 ppm) are slightly shifted downfield compared to H_b protons because they start 'feeling' the effect of the oxygen atoms. The hydroxyl protons H_d at δ 2.55 ppm for **IIb** are unambiguously identified, because they disappear by the addition of D_2O (Fig. A2.8), and they occur at similar shifts for the other diols. The hydrogen atoms on the asymmetric carbon atom (H_i) have the largest shift (δ 3.95) because of the presence of an oxygen atom on the asymmetric carbon atom and on the two α carbon atoms. The signal of the H_j atoms (δ 3.65 ppm), which is shifted by both oxygen atoms of the spacer, can also be identified, because it disappears for diols with a longer spacer. All other signals fall between 3.35 - 3.60 ppm.

Increasing the length of the spacer with one ethylene unit (**IIb** - Fig. A2.7) removes the signal at 3.65 ppm, as noted above. An extra signal is seen at δ 1.70 ppm from the four hydrogen atoms on the two carbon atoms in the centre of the spacer (the peak at δ 1.70 in Fig. A2.6 is from an impurity). Apparently, the influence of the oxygen atom on the β carbon atom is sufficient to shift the signal just slightly more downfield than for H_c atoms. This signal, however, disappears again as the spacer is further extended by an ethylene group (Fig. A2.10), and shows up at the same chemical shift as for H_c atoms

¹ J.B. Lambert, H.F. Shurvell, D.A. Lightner, R.G. Cooks, *Organic Structural Spectroscopy*, Prentice-Hall, New Jersey, 1998

(this signal now integrates to eight protons). The four hydrogen atoms on the carbon atoms that are now in the middle of the spacer have virtually the same shift as the H_b hydrogens, but can still be discerned as a shoulder on this peak, which now integrates to 32 protons. Any additional ethylene groups increase the area of the latter peak by four protons (Fig. A2.11-13).

Dimeric Surfactants (IIa-f)

The ¹H-NMR spectra of the dimeric surfactants differ in three respects from the spectra of the long chain diols. For an easy comparison, it is best to use the same solvent, but usually the spectra of the diols were obtained in CDCl₃. However, for reasons explained in Chapter 3, the spectra of the surfactants were obtained in DMSO-*d*₆. Therefore, one of the diols (**IIb**) was prepared in DMSO-*d*₆ as well (Fig. A2.9), and this spectrum is compared to that of the corresponding dimeric surfactant **IIb** (Fig. A2.15). A 'blank' spectrum of DMSO-*d*₆ is also recorded (Fig. A2.16), showing residual ¹H DMSO protons at δ 2.50 ppm, a large peak at δ 3.33 ppm from water protons (DMSO is hygroscopic), and a few smaller unidentified peaks.

The first obvious difference is that the hydroxyl protons in the spectra of the dimeric surfactants are not there anymore. This is actually best seen from Fig. A2.7 and A2.17, where both compounds are dissolved in CDCl₃, and the hydroxyl protons (δ ~ 2.5 ppm) are well separated from other protons. Secondly (and now comparing Figs. A2.9 and A2.15), the protons on the asymmetric carbon atom (at δ ~ 3.7 ppm for the diols) are shifted more downfield for the dimeric surfactants (δ ~ 4.2 ppm), since a sulfate group is

more deshielding than a hydroxyl group. The third difference is the small shift in the signals of the protons on the carbon atoms next to the asymmetric carbon atom, again due to the presence of the strongly deshielding sulfate group. Where for the diols all the hydrogens on carbon atoms next to an oxygen atom have approximately the same chemical shift (δ 3.25 - 3.40 ppm), there is a small but distinct shift further downfield to δ 3.45 ppm for eight hydrogen atoms, so that there are now two sets of signals. As mentioned above, there is a large peak due to water in the DMSO- d_6 at δ 3.33 ppm. This peak is included in the integration in Fig. A2.9, but not in Fig.A2.15, where it was easier to distinguish it from the other peaks.

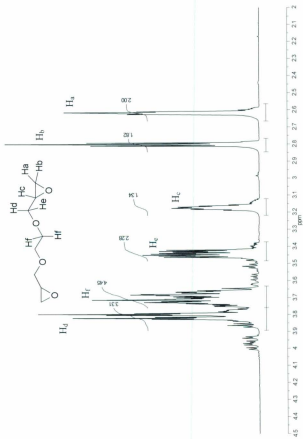


Fig. A2.1: $^1\text{H-NMR}$ spectrum of **1a** (G05) in CDCl_3 .

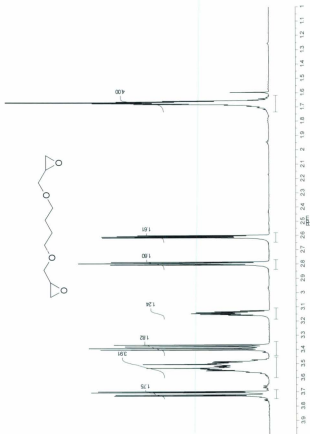


Fig. A2.2: ¹H-NMR spectrum of 1b (G02) in CDCl₃.

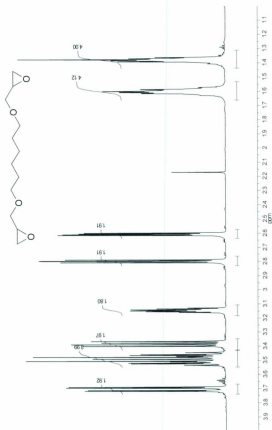


Fig. A2.3: $^1\text{H-NMR}$ spectrum of **1c** (G04) in CDCl_3 .

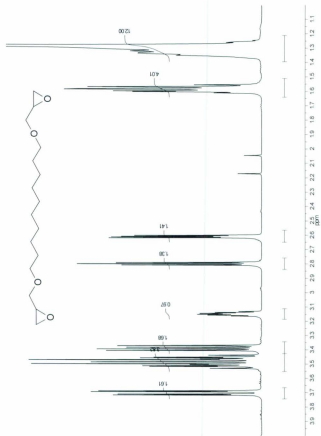


Fig. A2.4. ¹H-NMR spectrum of 1e (G10) in CDCl₃.

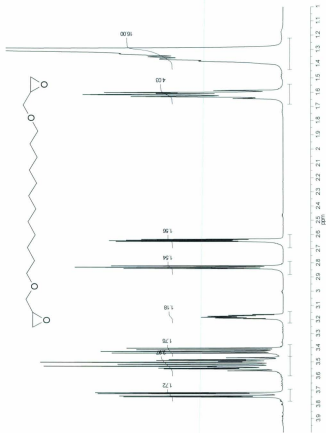


Fig. A2.5: $^1\text{H-NMR}$ spectrum of **1e** (**G20**) in CDCl_3 .

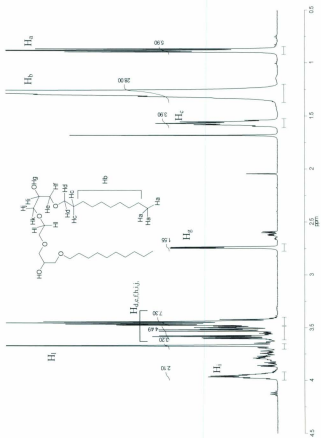


Fig. A2.6: ¹H-NMR spectrum of IIa (G17) in CDCl₃.

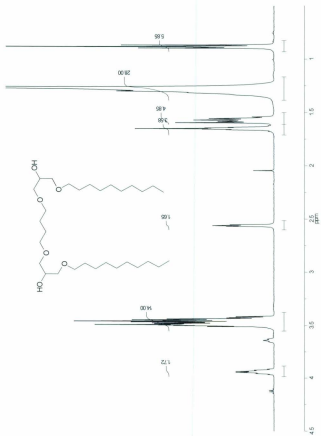


Fig. A2.7: ¹H-NMR spectrum of 11b (G11) in CDCl₃.

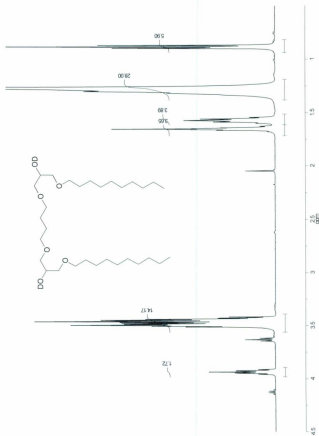


Fig. A2.8: ¹H-NMR of IIIb (G11) in CDCl₃, after addition of D₂O. Compare to Fig. A2.7.

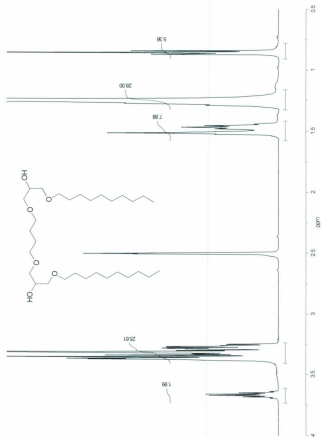


Fig. A2.9: $^1\text{H-NMR}$ of IB (G11) in DMSO-d_6 .

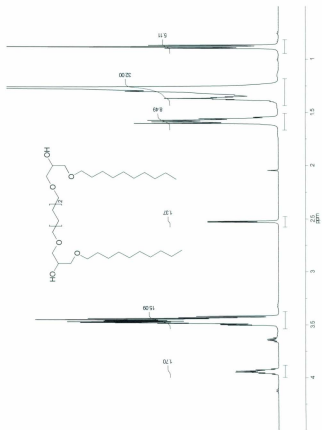


Fig. A2.10: $^1\text{H-NMR}$ spectrum of **11c** (G13) in CDCl_3 .

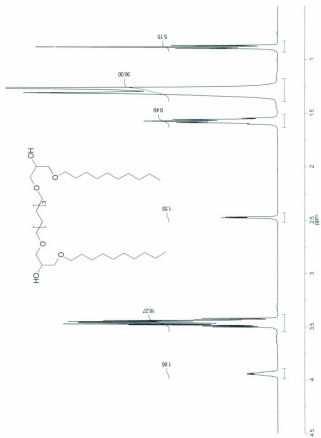


Fig. A2.11: ¹H-NMR spectrum of 11d (G21) in CDCl₃.

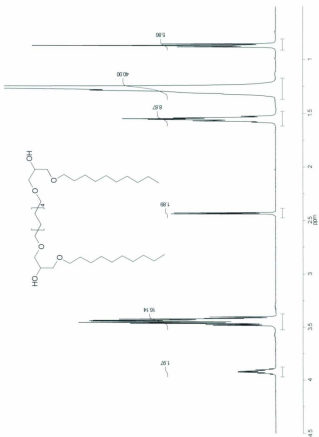


Fig. A2.12: $^1\text{H-NMR}$ spectrum of 11c (G14) in CDCl_3 .

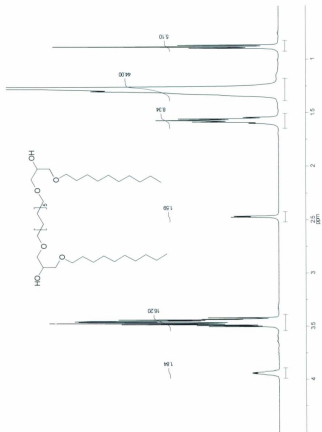


Fig. A2.13: $^1\text{H-NMR}$ spectrum of III (G22) in CDCl_3 .

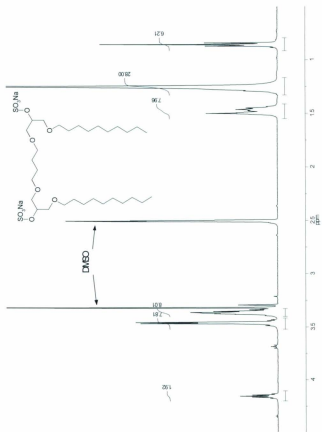


Fig. A2.15: $^1\text{H-NMR}$ spectrum of IIIb (G12) in $\text{DMSO-}d_6$.

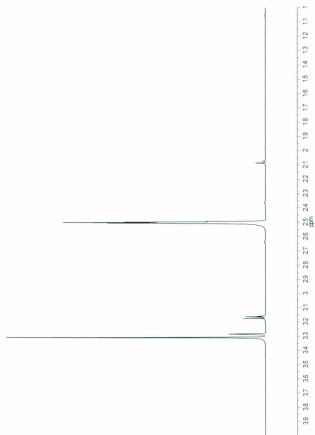


Fig. A2.16: $^1\text{H-NMR}$ spectrum of $\text{DMSO-}d_6$.

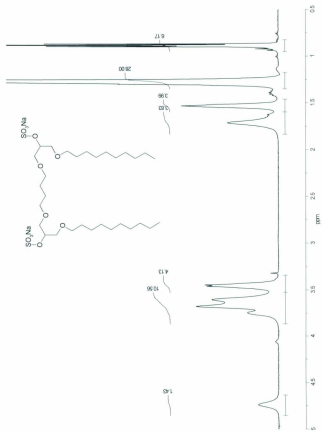


Fig. A2.17: ¹H-NMR spectrum of IIIb (G12) in CDCl₃.

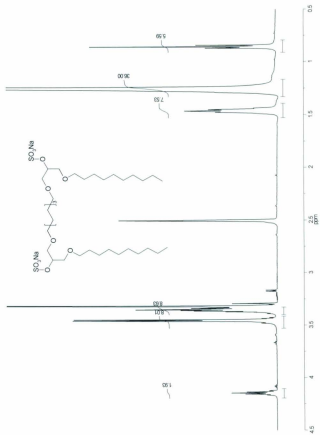


Fig. A2.19: $^1\text{H-NMR}$ spectrum of IIIId (G23) in $\text{DMSO-}d_6$.

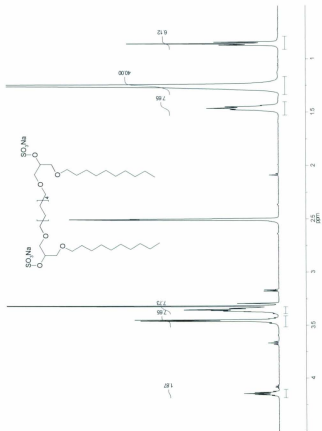


Fig. A2.20: $^1\text{H-NMR}$ spectrum of IIIc (G16) in $\text{DMSO-}d_6$.

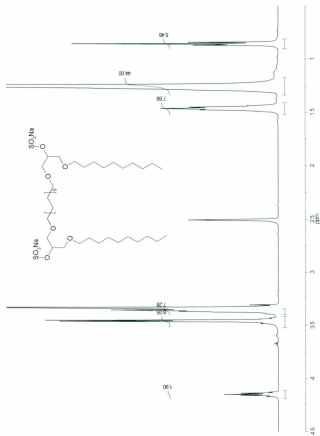


Fig. A.2.21: $^1\text{H-NMR}$ spectrum of HHT (G24) in $\text{DMSO-}d_6$.

Appendix 3

ESI-MS of dimeric surfactants of Chapter 3

Acquisition Parameters:

Mass Range Mode:	Std/Normal
Ion Polarity:	Negative
Ion Source Type:	ESI
Dry Temp (Set):	350 °C
Nebulizer (Set):	60.00 psi
Dry Gas (Set):	11.00 L/min
Trap Drive:	71.5
Octopole RF Amplitude:	200.0 Vpp
Capillary Exit:	-136.0 V
Skimmer:	-40.0 V
Oct 1 DC	-12.00 V
Oct 2 DC	-1.74 V
Scan Begin:	100 m/z
Scan End:	1000 m/z
Averages:	7 Spectra
Max. Accu Time:	200000 μ s
ICC Target:	10000
Charge Control:	On

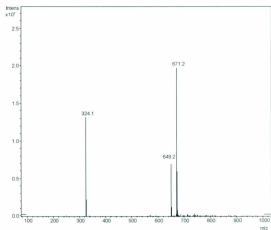


Fig. A3.1: Neg. ESI-MS of dimeric surfactant IIIa (Chapter 3)

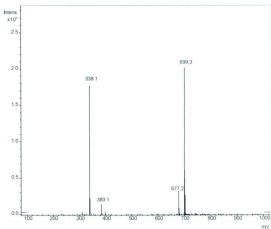


Fig. A3.2: Neg. ESI-MS of dimeric surfactant IIIb (Chapter 3)

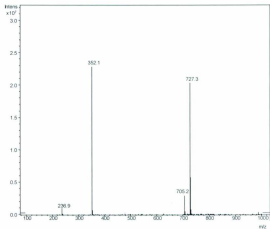


Fig. A3.3: Neg. ESI-MS of dimeric surfactant IIIc (Chapter 3)

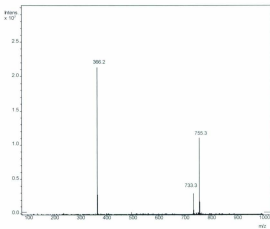


Fig. A3.4: Neg. ESI-MS of dimeric surfactant IIIId (Chapter 3)

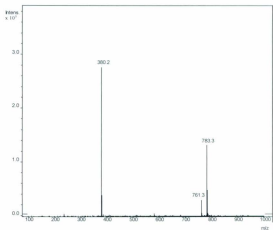


Fig. A3.5: Neg. ESI-MS of dimeric surfactant IIIe (Chapter 3)

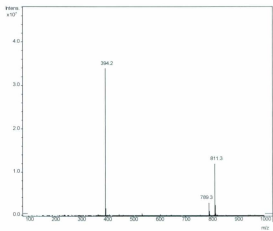


Fig. A3.6: Neg. ESI-MS of dimeric surfactant IIIf (Chapter 3)

Appendix 4

¹H-NMR spectra of dimeric surfactants and intermediate products of Chapter 4

Fig. A4.1-4: Diglycidylethers

Fig. A4.5-12: Long Chain Diols

Fig. A4.13-16: Dimeric Surfactants

Guide to interpretation of NMR spectra

All compounds are assigned the same identification number as in Chapter 4. This is followed by a unique identification number in brackets that was used in the lab books.

Compounds **Ia**, **IIa**, and **IIIa** of this chapter are identical to compounds **Ia**, **IIa**, and **IIIa** of Chapter 3, and the reader is referred to Appendix 2 for the $^1\text{H-NMR}$ spectra.

Diglycidylethers (Ib-e)

The spectra all show six multiplets at the same shifts as for compound **Ia** of Chapter 3 (Fig. A2.1), and the assignment of hydrogen atoms to these multiplets is as explained before (Appendix 2). As the number of ethoxy groups increases, the signal at δ 3.65 – 3.75 ppm increases with four units, from four (**Ia** - Fig. A2.1), eight (**Ib** - Fig. A4.1), twelve (**Ic** - Fig. A4.2), sixteen (**Id** - Fig. A4.3) to twenty (**Ie** - Fig. A4.4).

Long chain diols (IIb-e)

A comparison between the spectra of diol **IIb** (Fig. A4.5) and **IIa** (Fig. A2.6) shows that with one exception, all the peaks occur at the same chemical shift. The multiplet at δ 3.65 ppm now integrates to 8 protons for **IIb**, as expected. Extending the spacer with additional ethoxy units further increases the area of this peak by four protons at a time (Fig. A4.7, A4.9 and A4.11). The one exception mentioned above is the position of the hydroxyl protons. These are barely visible at 3.55 ppm in **IIb**, but are unambiguously identified by the addition of D_2O (Fig. A4.6). For longer hydrophilic spacers, this signal shifts further upfield (Fig. A4.7-12).

Dimeric Surfactants (IIIb-e)

We will not go through the exercise of comparing the surfactants with the diols again, as was done for the surfactants with the hydrophobic spacers. We simply note that the spectra are in agreement with our expectations: for every additional ethoxy group, the area of the peak at $\delta = 3.55$ ppm increases with four units.

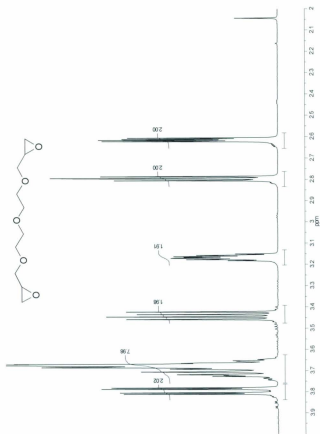


Fig. A4.1: ¹H-NMR of 1b (G25) in CDCl₃.

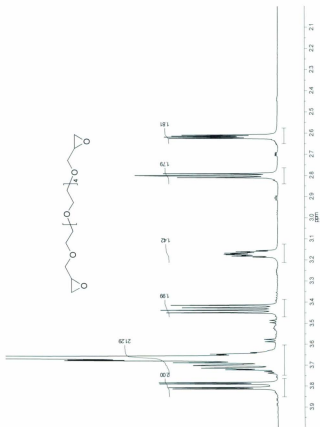


Fig. A4-4: $^1\text{H-NMR}$ of Ic (G34) in CDCl_3 .

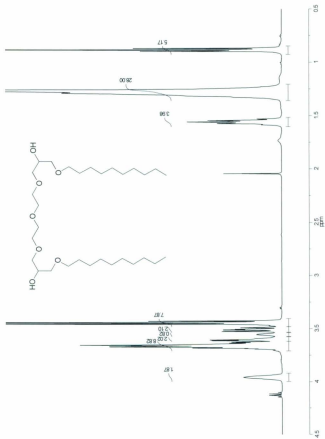


Fig. A4.5: ¹H-NMR of 11b (G28) in CDCl₃.

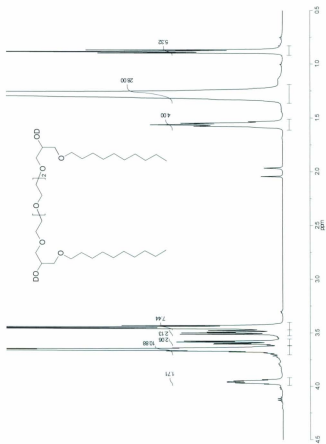


Fig. A.4.8: $^1\text{H-NMR}$ of **16c** in CDCl_3 after the addition of D_2O .

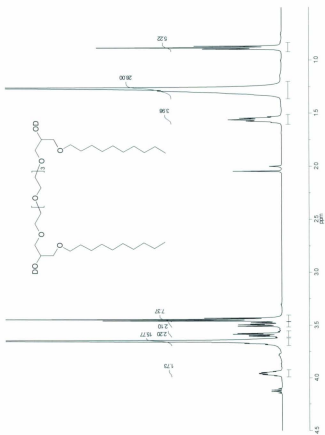


Fig. A-4.10: ¹H-NMR of 11d (G30) in CDCl₃ after the addition of D₂O.

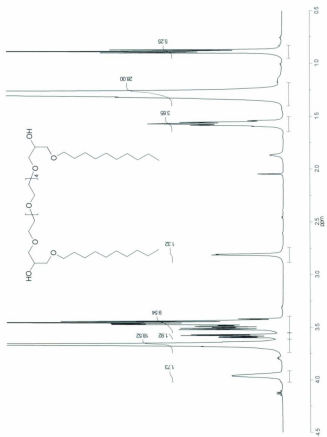


Fig. A4.11: $^1\text{H-NMR}$ of He (G35) in CDCl_3 .

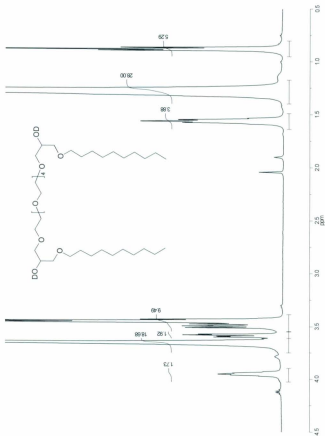


Fig. A4.12: $^1\text{H-NMR}$ of IIIc in CDCl_3 after the addition of D_2O .

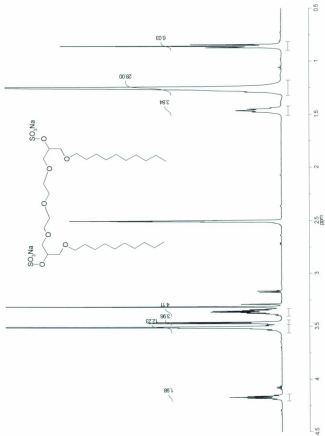


Fig. A4.13: $^1\text{H-NMR}$ of 1,3-bis(10-dodecyl-3-sulfonatopropoxy)propane in $\text{DMSO-}d_6$.

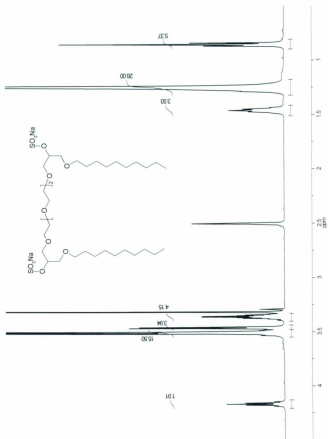


Fig. A4.14. $^1\text{H-NMR}$ of HHe (G32) in $\text{DMSO-}d_6$.

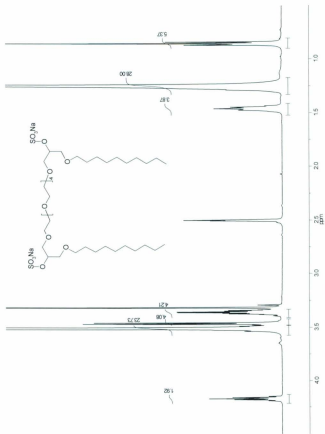


Fig. A4.16: ¹H-NMR of IIIc (G36) in DMSO-*d*₆.

Appendix 5

ESI-MS of dimeric surfactants of Chapter 4

Acquisition Parameters:

Mass Range Mode:	Std/Normal
Ion Polarity:	Negative
Ion Source Type:	ESI
Dry Temp (Set):	350 °C
Nebulizer (Set):	60.00 psi
Dry Gas (Set):	11.00 L/min
Trap Drive:	71.5
Octopole RF Amplitude:	200.0 Vpp
Capillary Exit:	-136.0 V
Skimmer:	-40.0 V
Oct 1 DC	-12.00 V
Oct 2 DC	-1.74 V
Scan Begin:	100 m/z
Scan End:	1000 m/z
Averages:	7 Spectra
Max. Accu Time:	200000 µs
ICC Target:	10000
Charge Control:	On

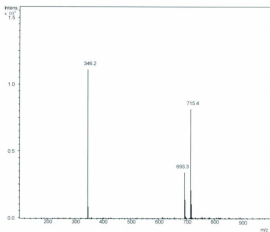


Fig. A5.1: Neg. ESI-MS of dimeric surfactant IIIb (Chapter 4)

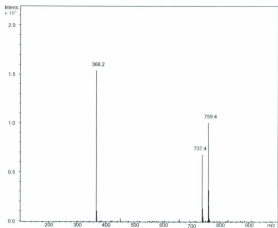


Fig. A5.2: Neg. ESI-MS of dimeric surfactant IIIc (Chapter 4)

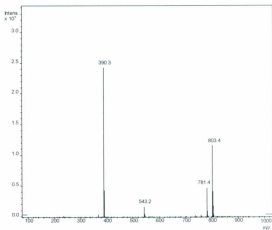


Fig. A5.3: Neg. ESI-MS of dimeric surfactant IIIc (Chapter 4)

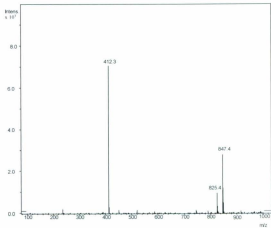


Fig. A5.4: Neg. ESI-MS of dimeric surfactant IIIe (Chapter 4)

Appendix 6

CMC determinations of dimeric surfactants of Chapter 4

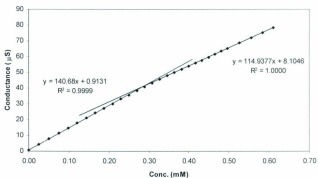


Fig. A6.1: Conductance vs. concentration plot for the determination of the CMC of dimeric surfactant **IIIb** (CMC = 0.28 mM)

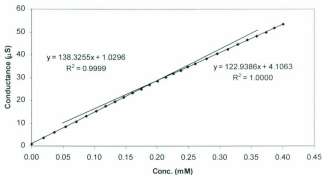


Fig. A6.2: Conductance vs. concentration plot for the determination of the CMC of dimeric surfactant **IIIe** (CMC = 0.20 mM)

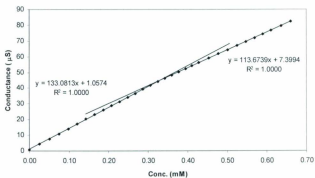


Fig. A6.3: Conductance vs. concentration plot for the determination of the CMC of dimeric surfactant **IIIc** (CMC = 0.33 mM)

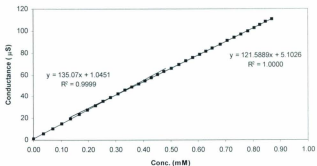


Fig. A6.4: Conductance vs. concentration plot for the determination of the CMC of dimeric surfactant **IIIe** (CMC = 0.30 mM)

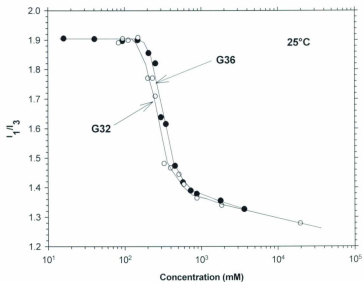


Fig. A6.5: Determination of the CMC of IIIc (G32) and IIIe (G36) via pyrene fluorescence. Courtesy of Dr. R. Zana.

Appendix 7

Electropherograms of LSER mixtures

Figures A7.1-10 are examples of electropherograms used to calculate the retention factors of solutes for the determination of the I,SERs of dimeric surfactant **IIIb** (G31) of Chapter 4. Notice that the EOF peak is often hardly noticeable, but simultaneously monitoring the signal at 195 nm (not shown) gives a more distinct signal.

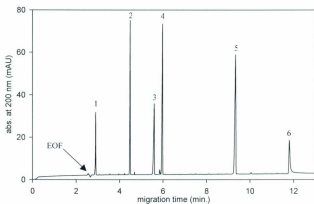


Fig. A7.1: Electropherogram of mixture 1. 1: pyrrole; 2: methyl benzoate; 3: toluene; 4: ethyl benzoate; 5: naphthalene; 6: dodecanophenone

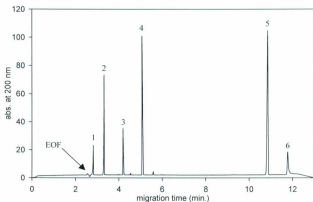


Fig. A7.2: Electropherogram of mixture 2. 1: caffeine; 2: acetanilide; 3: 4-nitroaniline; 4: 2-chlorophenol; 5: biphenyl; 6: dodecanophenone

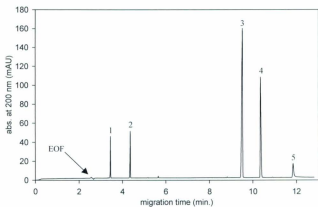


Fig. A7.3: Electropherogram of mixture 3. 1: phenol; 2: anisole; 3: dichlorobenzene; 4: 2-phenylphenol; 5: dodecanophenone

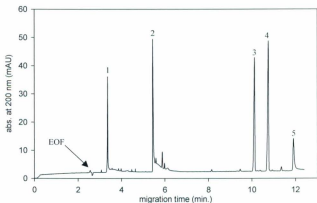


Fig. A7.4: Electropherogram of mixture 4. 1: benzaldehyde; 2: 4-chloroaniline; 3: butyl benzoate; 4: methyl naphthalene; 5: dodecanophenone

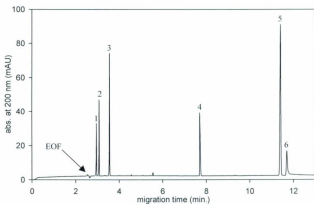


Fig. A7.5: Electropherogram of mixture 5. 1: benzenesulfonamide; 2: benzylalcohol; 3: acetophenone; 4: propyl 4-hydroxybenzoate; 5: tetrachlorobenzene; 6: dodecanophenone

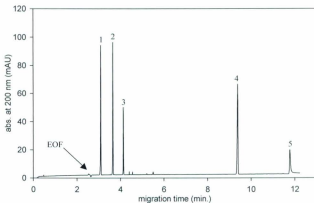


Fig. A7.6: Electropherogram of mixture 6. 1: aniline; 2: N-methylaniline; 3: methyl 3-hydroxybenzoate; 4: 1-nitronaphthalene; 5: dodecanophenone

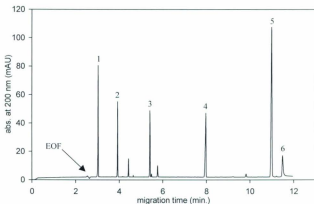


Fig. A7.7: Electropherogram of mixture 7. 1: resorcinol; 2: 4-nitrobenzene; 3: 4-phenyl-1-butanol; 4: propyl benzoate; 5: fluorene; 6: dodecanophenone

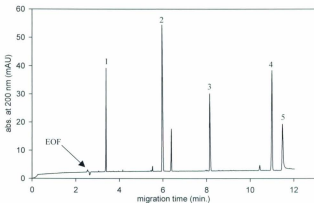


Fig. A7.8: Electropherogram of mixture 8. 1: 2-phenyl-1-ethanol; 2: indole; 3: 2-naphthol; 4: azobenzene; 5: dodecanophenone

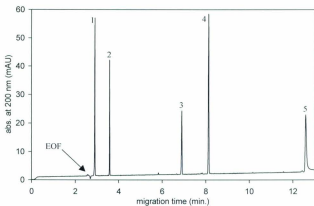


Fig. A7.9: Electropherogram of mixture 9. 1: hydroquinone; 2: phenylacetate; 3: chlorobenzene; 4: geraniol; 5: dodecanophenone

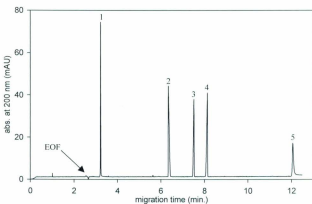


Fig. A7.10: Electropherogram of mixture 10. 1: catechol; 2: 4-chlorophenol; 3: bromobenzene; 4: valerophenone; 5: dodecanophenone

Appendix 8

¹H-NMR spectra of dimeric surfactants and intermediate products of Chapter 5

Fig. A8.1-3: Diallylethers

Fig. A8.4-6: Diglycidylethers

Fig. A8.7-10: Long Chain Diols

Fig. A8.11-13: Dimeric Surfactants

Guide to interpretation of NMR spectra

The dimeric surfactants with fluorinated spacers are assigned the same identification number as in Chapter 5. This is followed by a unique identification number in brackets that was used in the lab books. The intermediate products only have the latter number.

Diallylethers (G44, G39, and G42)

The spectra of the three diallylethers look exactly the same, as expected, since the compounds only differ in the number of fluorine atoms inserted in the middle of the spacer. The assignment is according to Montefusco et al.¹ H_a and H_b (4 H) appear as a doublet of doublets at δ 5.25 – 5.35 ppm. H_c (2 H) is the multiplet at δ 5.8 ppm, while the doublet at δ 4.2 ppm corresponds to the H_d protons (4 H), and H_e protons are the triplet at δ 3.9 ppm.

Diglycidylethers (G37, G40, G43)

We start by comparing the spectrum of G37 (Fig. A8.4) with that of its non-fluorinated analogue (Fig. A2.2). The peaks attributed to the ring protons (Fig. A2.1) are found at the same chemical shifts (δ 2.63, 2.82 and 3.17 ppm) for both compounds. The protons on the carbon attached to the oxirane ring have shifts of 3.38 and 3.78 ppm for the non-fluorinated analogue, and these signals are shifted more downfield for G37 (δ 3.53 and 3.94 ppm). This may already be an effect of the strongly electron-withdrawing (i.e. deshielding) fluorine atoms. The protons next to the fluorine and oxygen atoms are

¹ F. Montefusco, R. Bongiovanni, M. Sangermano, A. Priola, A. Harden, N. Rehnberg, *Polymer* 45 (2004) 4663

deshielded the most, with $\delta \sim 4.0$, and are further downfield than for the non-fluorinated compound (δ 3.5 – 3.6). Obviously, the signal at δ 1.67 ppm for the non-fluorinated analogue (from the protons in the middle of the spacer) is absent from that of G37 since these are now replaced by fluorine atoms. This, however, cannot be seen from Fig. A8.4 since the spectrum is cut off at 2.0 ppm.

Increasing the length of the spacer by insertion of C_2F_4 units has only one minor effect on the NMR spectra (Fig. A8.5 and A8.6): there is somewhat less overlap between the signals at δ 3.94 and 4.0 ppm. Apparently, increasing the number of fluorine atoms does shift the signal of the nearby protons slightly further downfield.

Long chain diols (G45, G50, G52)

We follow the same procedure as for the diglycidylethers and compare G45 (Fig. A8.7) with its non-fluorinated analogue (Fig. A2.7). For convenience, the protons are labelled in Fig. A2.7. The methyl and methylene protons on carbon atoms not bonded to oxygen atoms have signals at $\delta < 1.75$ ppm. The signal at 1.67 ppm for the non-fluorinated analogue is from the four protons on the carbon atoms in the middle of the spacer, and is not present in G45 since these protons are substituted for fluorine atoms. The hydroxyl protons are again identified by adding D_2O (Fig. A8.7 and A8.8), and are at approximately the same shift for both compounds ($\delta \sim 2.5 - 2.6$). The protons on the asymmetric carbon atom also have approximately the same shift (δ 3.95) and their signal (2H) for G45 overlaps the signal of the protons in the spacer (4H). The position of the latter can be verified by comparison with the corresponding diglycidylether (G37 - Fig.

A8.4). The multiplet at δ 3.5 (8H) is from the protons on the carbon atoms on either side of the oxygen atoms that connect the long chains to the rest of the structure, and the remaining four protons show up at δ 3.7 ppm.

With additional C_2F_4 units (G50 and G52), we only notice a very small shift downfield for the signals at \sim 4 ppm due to the increased number of fluorine atoms exerting their electron withdrawing effect.

Dimeric Surfactants (Ia-c)

We again compare these dimeric surfactants with their non-fluorinated analogues (Fig. A8.11 and A2.15). For convenience, the protons in Fig. A8.11 are labelled. The signals from H_a , H_b , and H_c have the same chemical shifts (δ 0.85, 1.25 and 1.48 ppm) for both compounds, as could reasonably be expected. The only difference is that the signal at δ 1.48 ppm integrates to four protons for the fluorinated surfactant, but to eight protons for the non-fluorinated analogue, because it includes the signals of the four protons on the two carbon atoms in the middle of the spacer. We can also easily identify the protons on the asymmetric carbon atom (H_d) at δ 4.2 ppm, because this is the only signal with an area corresponding to two protons, and it was previously rationalized that these protons would have the largest chemical shift (p. 196). The triplet at δ 3.95 ppm for **Ia** is also readily identified; it originates from the four H_e protons, and is split because of the nearby fluorine atoms (this signal was also identified as such in the long chain diol G45). The signal integrating to four protons at δ 3.35 for **Ia** can be assigned to the H_d protons; this signal is also present in the non-fluorinated analogue, but accounts there for eight protons

because there is also a contribution from the four protons in the spacer on the carbon atoms adjacent to the oxygen atoms. The signal at δ 3.45 ppm is also present in both compounds, but again accounts for four protons in **1a** ($H_{c,d}$) and eight protons in its non-fluorinated analogue. The other four protons ($H_{i,j}$) are shifted further downfield to δ 3.70. Extending the spacer with extra C_2F_4 units (**1b** and **1c**) shifts the signals of the H_k protons further downfield, so that they merge with the H_e signals for **1c**. This change is larger than was seen for the fluorinated diols, but this could be due to the different solvent (DMSO- d_6 vs. $CDCl_3$). There is also a minor shift downfield for the $H_{i,j}$ protons.

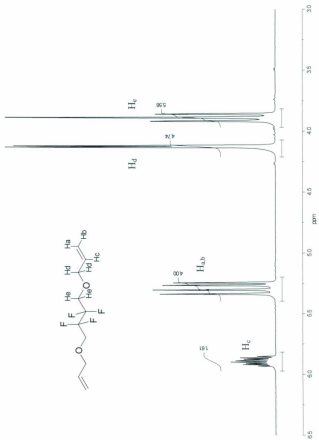


Fig. A8.1: ¹H-NMR of G44 in CDCl₃.

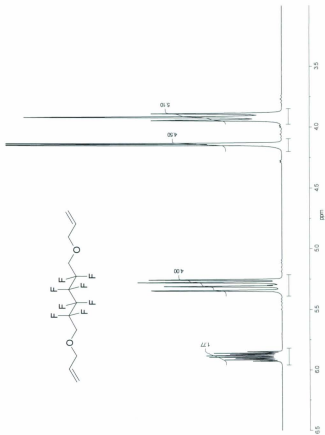


Fig. A8.2: $^1\text{H-NMR}$ of G39 in CDCl_3 .

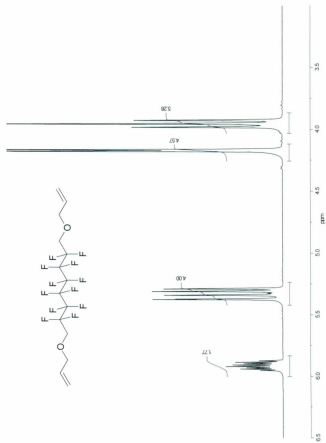


Fig. A8.3: $^1\text{H-NMR}$ of G42 in CDCl_3 .

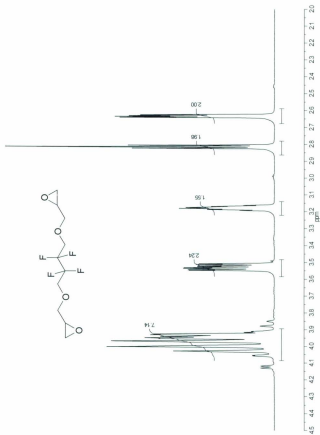


Fig. A8.4: $^1\text{H-NMR}$ of G37 in CDCl_3 .

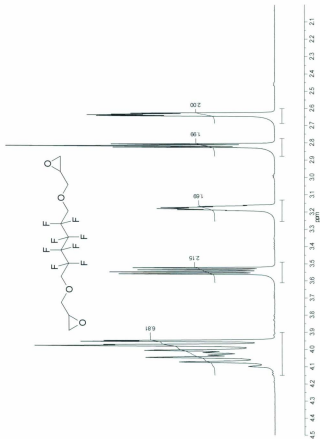


Fig. A8.5: $^1\text{H-NMR}$ of G40 in CDCl_3 .

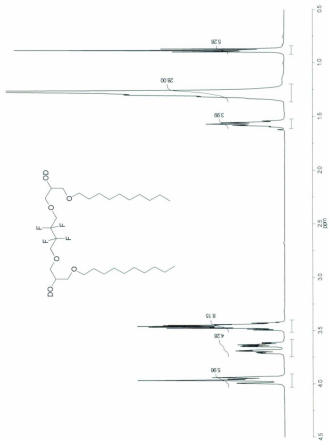


Fig. A8.8: $^1\text{H-NMR}$ of G45 in CDCl_3 after the addition of D_2O .

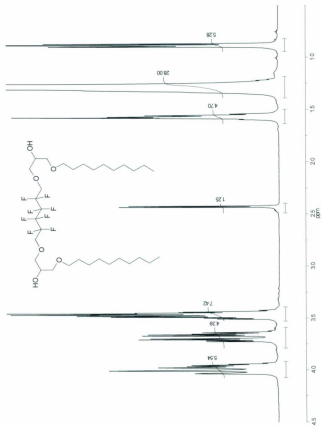


Fig. A8.9. $^1\text{H-NMR}$ of G50 in CDCl_3 .

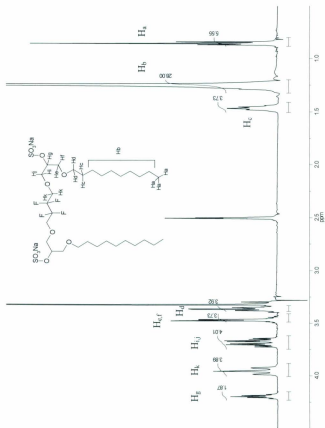


Fig. A8.11: $^1\text{H-NMR}$ of Ia (G46) in $\text{DMSO-}d_6$.

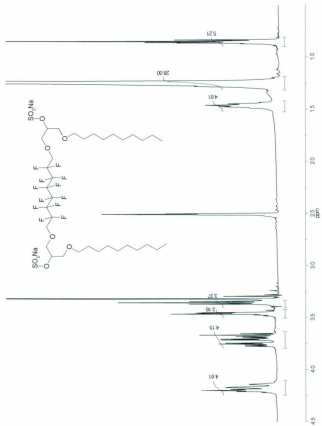


Fig. A8.13: $^1\text{H-NMR}$ of 653 in $\text{DMSO-}d_6$.

Appendix 9

Negative ESI-MS of dimeric surfactants of Chapter 5

Acquisition Parameters:

Mass Range Mode:	Std/Normal
Ion Polarity:	Negative
Ion Source Type:	ESI
Dry Temp (Set):	350 °C
Nebulizer (Set):	60.00 psi
Dry Gas (Set):	11.00 L/min
Trap Drive:	71.5
Octopole RF Amplitude:	200.0 Vpp
Capillary Exit:	-136.0 V (-166.0 V for II)
Skimmer:	-40.0 V
Oct 1 DC:	-12.00 V
Oct 2 DC:	-1.74 V (-2.70 V for II)
Scan Begin:	100 m/z
Scan End:	1000 m/z (1500 for II)
Averages:	7 Spectra
Max. Accu Time:	200000 µs
ICC Target:	10000
Charge Control:	On

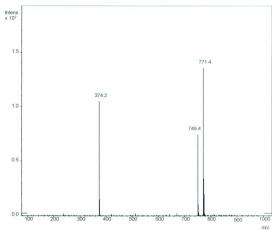


Fig. A9.1: Neg. ESI-MS of dimeric surfactant **1a** (Chapter 5)

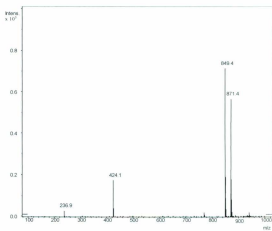


Fig. A9.2: Neg. ESI-MS of dimeric surfactant **1b** (Chapter 5)

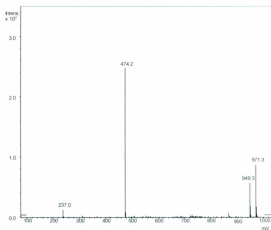


Fig. A9.3: Neg. ESI-MS of dimeric surfactant Ie (Chapter 5)

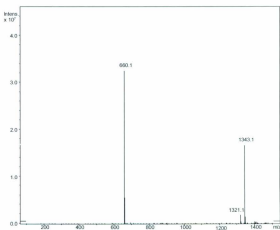


Fig. A9.4: Neg. ESI-MS of dimeric surfactant II (Chapter 5)

Appendix 10

CMC determinations of dimeric surfactants of Chapter 5

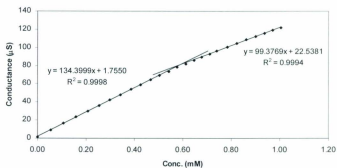


Fig. A10.1: Conductance vs. concentration plot for the determination of the CMC of dimeric surfactant **Ia** (CMC = 0.58 mM)

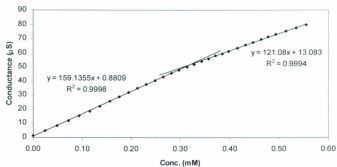


Fig. A10.2: Conductance vs. concentration plot for the determination of the CMC of dimeric surfactant **Ib** (CMC = 0.32 mM)

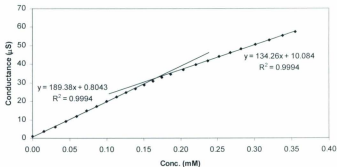


Fig. A10.3: Conductance vs. concentration plot for the determination of the CMC of dimeric surfactant **Ic** (CMC = 0.17 mM)

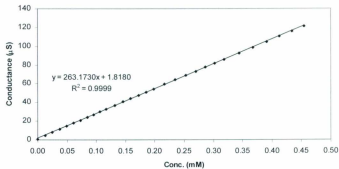


Fig. A10.4: Conductance vs. concentration plot for the determination of the CMC of dimeric surfactant **II**; no breakpoint is detected.

Appendix 11

System constants of PSPs

Table A11.1. Unadjusted and normalized system constants compiled by Fuguet et al.¹ (PSPs 1-55), and supplemented with data for 11 dimeric surfactants (56-66). The key to the identity of the PSPs is given in Table A11.2.

PSP	unadjusted system constants					normalized system constants				
	ρ	σ	a	b	v	ρ	σ	a	b	v
1	0.560	-0.600	-0.270	-1.670	2.720	0.169	-0.181	-0.062	-0.505	0.823
2	0.320	-0.240	0.000	-1.600	2.690	0.101	-0.076	0.000	-0.507	0.853
3	0.450	-0.310	-0.120	-1.870	2.850	0.130	-0.090	-0.035	-0.541	0.825
4	0.330	-0.420	-0.020	-1.780	2.840	0.087	-0.124	-0.008	-0.524	0.837
5	0.150	-0.390	0.230	-1.770	2.960	0.043	-0.112	0.066	-0.508	0.850
6	0.240	-0.550	0.150	-2.000	3.010	0.065	-0.150	0.041	-0.545	0.821
7	0.420	-0.610	0.110	-2.380	2.940	0.109	-0.158	0.029	-0.617	0.782
8	0.410	-0.370	0.100	-2.390	2.960	0.107	-0.096	0.026	-0.621	0.770
9	0.570	-0.660	-0.330	-1.560	2.560	0.182	-0.210	-0.105	-0.497	0.815
10	0.590	-0.600	-0.320	-1.570	2.610	0.186	-0.189	-0.101	-0.494	0.822
11	0.270	-0.420	-0.270	-1.880	3.020	0.075	-0.117	-0.075	-0.522	0.838
12	0.350	-0.510	-0.260	-1.920	3.050	0.095	-0.139	-0.071	-0.524	0.832
13	0.510	-0.350	0.390	-2.370	2.880	0.134	-0.092	0.103	-0.624	0.788
14	0.440	-0.370	0.490	-2.410	2.920	0.114	-0.096	0.127	-0.624	0.756
15	0.440	-0.390	0.450	-2.320	2.920	0.116	-0.103	0.118	-0.610	0.768
16	0.420	-0.450	0.480	-2.580	3.110	0.102	-0.109	0.117	-0.627	0.786
17	0.340	-0.430	0.020	-3.020	3.090	0.078	-0.099	0.005	-0.693	0.709
18	-0.110	-0.240	-0.880	-0.460	1.970	-0.050	-0.108	-0.396	-0.207	0.887
19	0.690	-0.690	0.120	-1.940	2.270	0.219	-0.219	0.038	-0.617	0.732
20	0.930	-0.870	0.070	-1.790	2.420	0.284	-0.266	0.021	-0.548	0.740
21	-0.530	-0.920	0.000	-2.500	3.100	-0.129	-0.223	0.000	-0.607	0.752
22	0.600	-0.340	0.000	-2.060	2.430	0.184	-0.104	0.000	-0.632	0.746
23	0.670	-0.450	0.000	-2.170	2.620	0.182	-0.129	0.000	-0.621	0.749
24	-0.600	-1.030	0.000	-1.990	2.780	-0.166	-0.284	0.000	-0.550	0.768
25	1.110	-0.760	0.820	-2.440	2.710	0.279	-0.191	0.206	-0.614	0.682
26	0.900	-0.620	0.770	-2.410	2.630	0.236	-0.163	0.202	-0.633	0.690
27	0.750	-0.430	0.870	-2.670	2.820	0.184	-0.106	0.214	-0.656	0.692
28	1.460	-0.590	1.340	-4.380	4.010	0.232	-0.094	0.213	-0.697	0.638
29	0.280	-0.690	-0.060	-2.810	3.050	0.066	-0.164	-0.014	-0.667	0.724
30	0.540	-0.650	0.320	-3.120	3.010	0.122	-0.147	0.172	-0.705	0.680
31	0.450	-0.440	0.710	-3.230	3.130	0.088	-0.096	0.154	-0.703	0.681
32	0.420	-0.650	0.470	-3.270	3.580	0.085	-0.132	0.089	-0.684	0.727
33	0.530	-0.770	0.430	-3.290	3.360	0.110	-0.160	0.089	-0.684	0.697
34	0.260	-0.160	-0.270	-1.050	2.110	0.109	-0.067	-0.113	-0.439	0.882
35	0.180	0.450	-0.150	-1.180	1.640	0.086	0.216	-0.072	-0.566	0.787
36	0.220	0.280	-0.140	-1.150	2.250	0.086	0.102	-0.045	-0.450	0.881
37	0.480	0.080	-0.190	-1.500	2.910	0.145	0.024	-0.045	-0.453	0.878
38	0.520	-0.040	-0.140	-1.640	2.950	0.152	-0.012	-0.041	-0.480	0.863
39	0.690	-0.190	-0.100	-1.770	3.180	0.186	-0.051	-0.027	-0.477	0.857
40	0.760	-0.070	0.450	-1.830	2.070	0.256	-0.024	0.152	-0.651	0.666
41	0.710	-1.080	0.110	-2.290	2.060	0.212	-0.323	0.033	-0.685	0.616

Table A11.1 (continued)

42	0.590	-0.780	0.230	-2.420	2.390	0.166	-0.220	0.065	-0.682	0.674
43	0.630	-1.140	0.330	-2.640	2.510	0.162	-0.294	0.085	-0.680	0.646
44	0.460	-0.430	0.270	-2.460	2.720	0.123	-0.115	0.072	-0.659	0.729
45	0.360	-0.190	0.070	-1.880	2.050	0.128	-0.068	0.025	-0.669	0.729
46	0.470	-0.600	-0.410	-3.750	3.560	0.090	-0.114	-0.078	-0.715	0.679
47	0.440	-0.670	-0.270	-3.700	3.650	0.084	-0.127	-0.051	-0.703	0.693
48	0.650	-0.850	-0.500	-3.830	3.780	0.118	-0.154	-0.091	-0.695	0.686
49	0.390	-0.400	-0.020	-3.520	3.580	0.077	-0.079	-0.004	-0.697	0.709
50	0.370	-0.320	0.250	-2.450	2.880	0.097	-0.084	0.065	-0.641	0.754
51	0.420	-0.530	-0.190	-3.050	3.390	0.091	-0.115	-0.041	-0.661	0.735
52	0.610	-0.600	-0.040	-2.580	2.910	0.153	-0.151	-0.010	-0.648	0.731
53	0.650	-0.460	0.240	-3.210	3.400	0.137	-0.097	0.051	-0.676	0.716
54	0.500	-0.400	0.230	-3.190	3.150	0.110	-0.088	0.051	-0.703	0.695
55	0.330	-0.440	0.430	-3.220	3.360	0.070	-0.093	0.091	-0.684	0.714
56	0.600	-0.500	0.070	-2.410	2.670	0.163	-0.136	0.019	-0.655	0.725
57	0.640	-0.490	0.130	-2.520	2.650	0.171	-0.131	0.035	-0.673	0.707
58	0.660	-0.470	0.160	-2.620	2.660	0.173	-0.123	0.042	-0.685	0.696
59	0.660	-0.440	0.210	-2.710	2.660	0.170	-0.113	0.054	-0.698	0.685
60	0.660	-0.430	0.240	-2.770	2.680	0.167	-0.109	0.061	-0.703	0.680
61	0.640	-0.550	0.100	-2.280	2.610	0.179	-0.154	0.028	-0.639	0.731
62	0.650	-0.560	0.080	-2.280	2.600	0.182	-0.157	0.022	-0.640	0.730
63	0.600	-0.540	0.040	-2.210	2.580	0.172	-0.155	0.011	-0.633	0.739
64	0.480	-0.460	-0.160	-2.230	2.600	0.137	-0.132	-0.046	-0.638	0.744
65	0.430	-0.480	-0.230	-2.180	2.640	0.123	-0.137	-0.066	-0.624	0.756
66	0.400	-0.490	-0.260	-2.190	2.660	0.114	-0.139	-0.074	-0.623	0.757

Table A11.2: Monomeric and polymeric PSPs corresponding to Fig. 6.1

1	Sodium dodecylsulfate (SDS)
2	Sodium decylsulfate (SdecS)
3	Sodium octylsulfate (SOS)
4	Sodium dodecylsulfonate (SDSu)
5	Sodium dodecylcarboxylate (SDCar)
6	Sodium dodecylfosfate (SDP)
7	Sodium dodecyl carbonyl valine (SDCV)
8	Sodium dodecyl sulfoacetate (SLSA)
9	Tris(hydroxymethyl)aminomethane dodecyl sulfate (THADS)
10	Lithium dodecylsulfate (LDS)
11	Magnesium dodecylsulfate (Mg(DS) ₂)
12	Copper dodecylsulfate (Cu(DS) ₂)
13	Sodium N-lauroyl-N-methyltaurate
14	Sodium N-lauroyl-N-methyl-β-alaninate (ALE)
15	Sodium N-lauroylsarcosinate (SLN)
16	Sodium N-parmitoylsarcosinate (SPN)
17	Bis (2-ethylhexyl) sodium sulfosuccinate (AOT)
18	Lithium perfluorooctanesulfonate (LPFOS)
19	Sodium cholate (SC)
20	Sodium deoxycholate (SDC)
21	Potassium deoxycholate (KDC)
22	Sodium taurocholate (STC)
23	Sodium taurodeoxycholate (STDC)
24	3-β-glucopyranosyl-5β-cholane-12α-hydroxy-24-oic acid
25	Hexadecyltrimethylammonium bromide (HTAB)
26	Tetradecyltrimethylammonium bromide (TTAB)
27	Dodecyltrimethylammonium chloride (DTAC)
28	Dihexadecyldimethylammonium bromide (DHAB)
29	Microemulsion (1.4% SDS, 6.49% 1-butanol, 0.82% heptane)
30	Dipalmitoylphosphatidyl glycerol (DPPG) : dipalmitoylphosphatidyl choline (DPPC) : cholesterol (Chol) 24:46:30
31	DPPG:DPPC 30:70
32	Dihexadecylfosfate (DHP)
33	DHP + Chol
34	Poly(sodium 11-acrylamidoundecanoate) (PAAU)
35	Poly(sodium 10-undecylenate) (PSUA)
36	Poly(sodium 7-octenylsulfate) (Poly-(SoeS))
37	Poly(sodium 8-nonenylsulfate) (Poly-(SNoS))
38	Poly(sodium 9-decenylysulfate) (Poly-(SDeS))
39	Poly(sodium 10-undecenylysulfate) (Poly-(SUS))
40	Ally glycidylether N-methyltaurine siloxane (AGENT)
41	Octane AGENT (25% C ₈) (OAGENT)
42	Dodecane AGENT (20% C ₁₂) (DAGENT)
43	Steryl AGENT (20% C ₁₈) (SAGENT)
44	Dodecane allylglycidylether sulfite-modified siloxane (AGESS)
45	Poly(methyl methacrylate - ethyl acrylate - methacrylic acid (Elvacite 2669)
46	poly(AMPS-sodium octyl methacrylate-21) (pOMAt-21-Na) ¹

Table A11.2: (continued)

47	poly(AMPS-sodium lauryl methacrylate-15) (pLMAI-15-Na)
48	poly(AMPS-sodium stearyl methacrylate-16) (pSMAI-16-Na)
49	poly(AMPS-sodium lauryl acrylate-13) (pAt-13-Na)
50	poly(AMPS-sodium lauryl methacrylamide-19) (pLMAM-19-Na)
51	poly(AMPS-sodium stearyl acrylamide-28) (pSAm-28-Na)
52	poly(AMPS-sodium dihydrocholesteryl acrylate-2) (pDHCHAI-2-Na)
53	poly(AMPS-triethylamine dihydrocholesteryl acrylate-33) (pDHCHAI-33-TEA)
54	poly(AMPS-triethylamine lauryl acrylate-9.2) (pLAt-9.2-TEA)
55	poly(AMPS-sodium tertiary octyl acrylamide-49) (pTOAm-49-Na)
56	G18 (IIIa Chapter 3)
57	G12 (IIIb Chapter 3)
58	G15 (IIIc Chapter 3)
59	G16 (IIIe Chapter 3)
60	G31 (IIIb Chapter 4)
61	G32 (IIIc Chapter 4)
62	G33 (IIId Chapter 4)
63	G36 (IIIe Chapter 4)
64	G46 (Ia Chapter 5)
65	G51 (Ib Chapter 5)
66	G53 (Ic Chapter 5)

¹ AMPS is 2-acrylamide-2-methyl-1-propanesulfonic acid; number refers to percentage of hydrophobic polymer



